UNIVERSIDAD
POLITÉCNICA
DE VALENCIA

Analysis and Enhancement of Multiactuator Panels for Wave Field Synthesis Reproduction

TESIS DOCTORAL

Autor:
Basilio Pueo Ortega

Director:
Dr. José Javier López Monfort

Valencia,
Julio 2008

A mis nenas
Leticia y Cristina

Abstract

This thesis addresses the development and enhancement of Multiactuator Panels (MAPs) with emphasis on the application to Wave Field Synthesis (WFS) reproduction. MAPs can be used alternatively to dynamic loudspeaker arrays for WFS with added benefits. However, since MAPs are panels of finite extent, excited mechanically on several points, there are structural and geometric issues that must be addressed to guarantee that all exciters are acting evenly to form an effective loudspeaker array for WFS. This aim is addressed by means of a methodology for the analysis of sound field radiation in the space-time domain that has been proposed and validated in this thesis. This research has produced a number of key conclusions. The proposed method analyzes aliasing artifacts in a graphical representation showing the distribution of radiated energy over space. In a comparative study between MAPs of different dimensions and dynamic loudspeaker arrays, the main conclusion, with significant practical consequences, is that the wave field created by large panels contains less artifacts than that of equivalent small panels. The effect of panel boundaries on the quality of the wave field has also been addressed by comparing several edge boundary conditions with multiple elastic materials. The main conclusion drawn from this study is the convenience of using elastic boundary conditions that can form a viable technology for a MAP frame while showing a proper acoustic radiation. Boundaries also affect the response of exciters near edges that must conveniently be equalized for a response similar to that of middle exciters. To that end, an efficient equalization filtering process has been introduced that takes into account the particular exciter distribution on a panel for considerably reducing the measurement points. Finally, an optimized large MAP has been designed and tested, incorporating the enhancements previously discussed and facilitating the combination of WFS with video projection for immersive multimedia applications.

Keywords: Multiactuator Panel, Wave Field Synthesis, Distributed Mode Loudspeaker, Wavenumber Domain, Loudspeaker, Boundary Condition, Filtering.

Resumen

Esta tesis aborda el desarrollo y mejora de los altavoces de panel multiexcitados (MAPs) con particular importancia en su aplicación para la reproducción de síntesis de campo (WFS). Los altavoces MAPs pueden usarse como alternativa a las agrupaciones de altavoces dinámicos para WFS con ventajas adicionales. Sin embargo, puesto que los altavoces MAPs son paneles finitos que se excitan en varios puntos de su superficie, existen cuestiones estructurales y geométricas que deben ser tratadas para garantizar que todos los excitadores actúan uniformemente para crear una agrupación de altavoces válida para WFS. Este objetivo se acomete a través de un método para el análisis de la radiación del campo sonoro en el dominio espacio-temporal que ha sido propuesto y validado en esta tesis. De la presente investigación se desprenden diversas conclusiones. El método propuesto analiza las imperfecciones del campo sonoro por el submuestreo espacial en una representación gráfica que muestra la distribución de energía radiada en el espacio. Mediante un estudio comparativo entre altavoces MAPs de diferentes tamaños y agrupaciones de altavoces dinámicos, la principal conclusión que se desprende, con implicaciones prácticas, es que el campo creado por paneles de grandes dimensiones presenta menos imperfecciones que el de paneles pequeños equivalentes. El efecto del contorno del panel en la calidad del campo creado también se ha considerado al comparar varias condiciones de contorno con diversos materiales elásticos. La conclusión principal es la conveniencia de usar condiciones elásticas que pueden crear una tecnología viable de sujeción de paneles y que presentan una radiación acústica adecuada. Los bordes también afectan a la respuesta de los excitadores cercanos, que debe ser convenientemente ecualizada para obtener una respuesta similar a la de los excitadores centrales. Para ello, se propone un filtrado eficiente que considera la distribución de los excitadores en un panel para reducir considerablemente los puntos de medida. Finalmente, se ha diseñado y probado un altavoz MAP optimizado de grandes dimensiones, que incorpora las mejoras propuestas anteriormente y permite la combinación de WFS con videoproyección para aplicaciones multimedia.

Palabras Clave: Panel multiexcitado, Síntesis de campo, Altavoz de modos distribuidos, Dominio transformado de número de onda, Altavoz, Condiciones de contorno, Filtrado.

Resum

Esta tesi aborda el desenvolupament i millora dels altaveus de panell multiexcitats (MAPs) amb particular importància en l'aplicació per a la reproducció de síntesi de camp (WFS). Els altaveus MAPs es poden usar com a alternativa a les agrupacions d'altaveus dinàmics per a WFS amb avantatges addicionals. No obstant això, ja que els altaveus MAPs són panells finits que s'exciten en diversos punts de la seua superfície, hi ha qüestions estructurals i geomètriques que han de ser tractades per a garantir que tots els excitadors actuen uniformement per a crear una agrupació d'altaveus vàlida per a WFS. Este objectiu s'escomet a través d'un mètode per a l'anàlisi de la radiació del camp sonor en el domini espai-temporal que ha sigut proposat i validat en esta tesi. De la present investigació es desprenen diverses conclusions. El mètode proposat analitza les imperfeccions del camp sonor causades pel submostratge espacial mitjançant una representació gràfica que mostra la distribució d'energia radiada en l'espai. Per mitjà d'un estudi comparatiu entre altaveus MAPs de diferents grandàries i agrupacions d'altaveus dinàmics, la principal conclusió que es desprén, amb implicacions pràctiques, és que el camp creat per panells de grans dimensions presenta menys imperfeccions que el de panells xicotets equivalents. L'efecte del contorn del panell en la qualitat del camp creat també s'ha considerat mitjançant la comparació de diverses condicions de contorn amb diversos materials elàstics. La conclusió principal és la conveniència d'usar condicions elàstiques que poden crear una tecnologia viable de subjecció de panells i que presenten una radiació acústica adequada. Els contorns també afecten la resposta dels excitadors pròxims, la qual ha de ser convenientment equalitzada per a obtindre una resposta semblant a la dels excitadors centrals. Per fer això, es proposa un filtratge eficient que considera la distribució dels excitadors en un panell per a reduir considerablement els punts de mesura. Finalment, s'ha dissenyat i provat un altaveu MAP optimitzat de grans dimensions, que incorpora les millores proposades anteriorment i permet la combinació de WFS amb videoprojecció per a aplicacions multimèdia.

Paraules Clau: Panell multiexcitat, Síntesi de camp, Altaveu de modes distribuïts, Domini transformat de nombre d'ona, Altaveu, Condicions de contorn, Filtratge.

No queda más remedio que jugar la partida
con las cartas que el burlón Destino
te pone en las manos,
aunque éstas sean pésimas

El Capitán Alatriste,
Arturo Pérez Reverte

Acknowledgements

Completing a PhD is truly a marathon event, and I would not have been able to complete this journey without the aid and support of countless people over the past years. It is difficult to recall every person that has assisted, contributed or more importantly encouraged me to pursue these studies, from the early B.Sc. Telecommunication Eng. to this doctoral thesis. Although perhaps not listed here, I hope they will know who they are and what they mean to me.

I would like to thank, first and foremost, my supervisor, Dr. José Javier López. He allowed me complete freedom in my choice of topic for this project and has trusted in me since the beginning, in a friendly and supportive relationship. I am proud to consider him more than an academic supervisor, but also a good friend. Thanks JJ.

I am also deeply indebted to my other traveling companion, my friend José Escolano, a.k.a. Josele. His insights and comments have been invaluable over the years, helping us to become mutually motivated, which we needed frequently in the "dark" moments. Josele, we have done it! I sincerely hope I continue collaborating with José Javier and Josele for the rest of my research career.

Special thanks go to the members of my committee, Dr. Felipe Orduña, of the National Autonomous University of Mexico, for his fruitful suggestions on this manuscript, Dr. Enrique Alexandre, of the University of Alcalá, Spain, and Dr. Diemer de Vries, of TU Delft, The Netherlands, who all made a long trip for my defense.

I have been fortunate to interact with many people who have influenced me greatly. At the University of Alicante, I am very grateful to my colleagues and friends Juanma López, Tomás Martínez, Miguel Romá, David Ballester, Jesús Selva, and Enrique Martín for providing technical means and personal assistance throughout these last years. I would like to thank Sergio Bleda and David Gil for their support. I also benefited greatly from my many colleagues at the Technical University of Valencia,

Dr. Alberto González, Dr. Germán Ramos, Máximo Cobos and Laura Fuster. I enjoyed the atmosphere, their friendship, and their support every time I visited them at the Institute of Telecommunications and Multimedia Applications.

I must also acknowledge Dr. Ramón Irles for his helpful advice on the theory of plates, Dr. José M. Martín for his suggestions on the rheological behavior of materials used for the elastic boundaries, and Dra. María José Muñoz for her tests of such elastic materials at the Thermomechanical Analysis Laboratory. I would also like to convey my thanks to Dr. Neil Harris from NXT plc for providing the mutual agreement to experiment with the distribute mode technology and for his suggestions on the introductory chapter.

A special word of appreciation goes to Dr. Marinus Boone and Lars Hörchens, from TU Delft, The Netherlands, Dr. Etienne Corteel from IRCAM, Paris and Sonic Emotion, Switzerland, and Dr. Rudolf Rabenstein from the University of Erlangen-Nuremberg, Germany. The discussions with all of them have contributed substantially to this thesis.

Thank you to everyone for letting me see a little further as I have stood on the shoulders of Giants.

I am very grateful to my friend Paquito, who encouraged me to start studying at University many years ago. Many thanks to Juanmi and David Cervera, my study companions in the B.Sc. Telecommunication Eng. studies at the Polytechnic School of Gandía. Also thanks to Josep and Remi, my laboratory colleagues during my first stage at the Technical University of Valencia, two oases in the desert. Thanks to Javi Carretero for your friendship, support and all the good times we had during our M.Sc. Telecommunication Eng. studies. Special thanks to Arturo Pérez Reverte for letting me use the above epigraph.

I would also like to thank all my friends Jarabo, Pedrito, Primo, Alfonso, Miñana, and many others at the rowing club. I will always treasure the wonderful moments we spent rowing together or just fooling around and for sharing some of the best times of our lives.

Needless to say, this entire exercise would be at most a dream were it not for my loving family. Thanks to both my family and my in-laws for their unending support. Kisses to my nieces Ainara, Moni and my smiling little nephew David. To my cousin Jordi and his partner Rosana, you are wonderful. I am particularly grateful to my brother Esteban and his partner Rosa, who are making their debut as parents soon. A warm embrace to my

next nephew too. I also dedicate this thesis to the loving memory of my aunt Carmen. I am deeply indebted to my dear parents, Javier and Rosi, for the unconditional support they have provided me with throughout my entire life. Thanks for giving me solid roots from which I could grow. All my family have always helped me to keep my life in context. I love you all.

Finally, I would like to express my gratitude and love to my wife Leticia and my charming three-year-old daughter, Cristina, who have always been there for me throughout my good and bad times, always encouraging me and for making me who I am. I could not have done this without you. You are the sunshine of my life.

Basilio Pueo
July 2008

Contents

List of Figures

List of symbols

β	Angle in the $k_x - k$ representation related to θ
δ	Dirac delta function
Δt	Temporal sampling period
Δx	Spatial sampling period
Δx_m	Microphone array spacing
Δx_l	Loudspeaker array spacing
Δx_p	Panel array spacing
θ	Plane wave angle of arrival
λ	Wavelength
$\sigma_{\log}$	Logarithmic Standard Deviation
ω	Angular frequency
III	Comb function
a	Piston model radius
c	Speed of sound
f	Linear frequency
f_{al}	Spatial aliasing frequency
$f(t)$	Time function
$f(x)$	Space function
$F(\omega)$	Temporal Fourier transform of $f(t)$
$\tilde{F}(k_x)$	Spatial Fourier transform of $f(x)$
H_f	Filter transfer function
H_l	Loudspeaker transfer function
H_t	Target transfer function
j	Complex number, $j^2 = -1$
k	Wavenumber
k_x	Spatial frequency
$p(x,t)$	Unidimensional pressure wave
$\tilde{P}(k_x,k)$	Temporal and spatial Fourier transform of $p(x,t)$
t	Continuous time

Abbreviations and Acronyms

ABX	Blind Listening Test
C	Clamped Boundary Condition
DML	Distributed Mode Loudspeaker
DSP	Digital Signal Processor
EB1	Elastic Boundary Type 1
EB2	Elastic Boundary Type 2
EB3	Elastic Boundary Type 3
EPDM	Ethylene Propylene Diene Monomer Rubber
EVA	Ethylene Vinyl Acetate
F	Free Boundary Condition
FIR	Finite Impulse Response Filter
IIR	Infinite Impulse Response Filter
LDPE	Low-density Polyethylene Foam
MAP	Multiactuator Panel
MAP3	MAP with 3 Exciters
MAP5	MAP with 5 Exciters
MDF	Medium-Density Fiberboard
MIMO	Multiple Input Multiple Output Filter
MLS	Maximum Length Sequence
LMAP	Large MAP with 13 Exciters
PC	Polycarbonate
PVC	Polyvinyl Chloride
SS	Simply Supported Boundary Condition
SOS	Second Order Section
TMA	Thermomechanical Analysis
WFS	Wave Field Synthesis

1 Introduction and Scope

Introduction and Scope 1

1.1 Background

Since the invention of the phonograph, sound recording and reproduction techniques have been continuously evolving. One of the important topics of research has always been to the preserve the spatial and temporal characteristics of recorded sound events. First, two-channel stereo systems were only introduced to the market in 1960s, for the first time adding the spatial dimension to sound reproduction technology at consumer level. The next major advancement was the step towards sound field reproduction, which attempts to recreate the pressure variations that allows a listener to perceive the position of sound sources as coming from arbitrary locations in three-dimensional space.

Sound field reproduction can be generated in essentially two ways. First, by providing signals directly to the ears, which are similar to those which would have occurred if there had been real sound sources in the intended positions. This approach is known as binaural or transaural reproduction. Second, by recreating the sound field over a more extended region of space, which will be interpreted by the listener as being in the environment intended to be simulated. This second approach is a holo-

graphic based reproduction. In this thesis, the latter approach of reproducing a sound field over a region of space is considered. One of the first holographic systems encoding height information was proposed by Gerzon [Gerzon, 1973] and was later developed as the Ambisonics system. Another alternative approach to holographic reproduction is known as Wave Field Synthesis (WFS), which is described as follows.

WFS is a spatial sound rendering technique that generates a true sound field using loudspeaker arrays [Berkhout et al., 1993]. Wave fields are synthesized based on virtual sound sources at some position in the sound stage behind the loudspeakers or even inside the listening area. When using sound reproduction based on WFS, sound fields can be generated in a spatially and temporally correct way. Therefore, listeners experience the feeling that the origin of the sound is actually in the position of the virtual sources. Furthermore, the synthesized wave field is correct for an extended listening area, with much larger dimensions than the "sweet spot" of the current surround systems, such as the commercial 5.1 channel surround.

Most WFS prototypes employ arrays of dynamic loudspeaker drivers. However, a main disadvantage of these drivers is that they need a housing with a relatively large volume to avoid the additional stiffness of the back-volume. Also, due to the piston-like motion of their diaphragms, they exhibit strong and narrow lobes around their main axis at high frequencies.

Therefore, efforts have been made to find alternatives that are as omnidirectional as possible, and easy to mount directly onto the wall surface. This prompted the idea of investigating the applicability of Distributed Mode Loudspeaker (DML) that combines these advantages. A DML essentially consists of a thin, stiff panel that needs only a small back-volume and vibrates in a complex pattern over its entire surface by means of an electro-mechanic transducer called an exciter [Harris and Hawksford, 1997]. The exciter is normally a moving coil device, which is carefully positioned and designed to excite the natural resonant modal structure of the panel optimally.

In 2000, Boone and de Brujin, encouraged by the positive results on sound localization, tested for the first time the applicability of DMLs for WFS reproduction [Boone and de Brujin, 2000] with a linear array of nine small single excited DMLs. Although this study confirmed that DMLs could be used with success for WFS, small panels posed problems with sound quality since they have a poor low-frequency response due to the

lack of excited modes in that frequency region. However, these results were promising enough to extend the DML technology to a panel with multiple exciters, each driven with a different signal [Boone, 2004]. A single panel driven by multiple exciters is called a Multiactuator Panel or MAP. With a proper selection of panel material, a MAP can act as a WFS array because every exciter on the panel excites only a small part of the panel around the exciter position [Kuster et al., 2006].

There are some benefits for MAPs to be used in WFS reproduction. MAPs are flat structures whose vibration is low enough to be imperceptible to the human eye. This property can be exploited by integrating them into a room interior and simultaneously using them as projection screens. In this way, image and sound are fully integrated for multimedia applications. Furthermore, the diffuse radiation of MAPs produces room reflections that are less correlated to the direct sound than those radiated from piston sources and thus, constructive and destructive interference of sound is minimized [Harris et al., 1998a]. This property is beneficial for WFS since the individual components can merge correctly into the desired wavefront for a wider area. Also, the sensation of spaciousness is better than that of dynamic loudspeakers, which enhances the recreation of sources far behind the panels. Moreover, for extending the synthesized wave field, the pressure level decay for MAPs as planar transducers is less pronounced with distance in comparison with conventional loudspeakers.

1.2 Motivation

The use of MAPs, however, poses some problems when synthesizing a wave field by means of WFS. These problems, which will be discussed throughout this thesis in detail, are addressed briefly as follows.

The practical application of WFS forces the theoretical continuous source distribution to be discretized, which causes a *Limited Spatial Resolution*. As a consequence, the wave field is correctly synthesized up to a limiting frequency, known as aliasing frequency. This is one of the main theoretical constraints of WFS, although not restricted to this particular audio reproduction system. The region above aliasing frequency is characterized by oscillations both in frequency and space. These interference patterns, although not pronounced, can be experienced when moving the head or

walking within the listening area. The diffuse behavior of MAPs helps in diminishing the effects of spatial color fluctuations. For that reason, an analysis of the aliasing artifacts and the geometric parameters of MAPs that modify them would be of great interest. For example, a WFS array can either be assembled by a large panel with many exciters or by small panels accommodating a lesser number of exciters per panel. Although having the same transducer spacing, the structural behavior of MAPs with different sizes must have consequences on their spatial resolution capability. Moreover, the vibration mode pattern varies with geometry, which also affects the spectrum of the wave field.

The vibration pattern of a panel is also a function of the *Driving Points*. In a single panel exciter, the optimal positions, usually four in the center area of the panel, are chosen to excite the maximum number of vibration modes. This results in an even distribution of modes and a higher modal density, which is more noticeable in the low frequency region [Angus, 2000b]. Also, the mechanical impedance at those points is seen as infinite and thus, there are virtually no reflected flexural waves. For WFS operation, such golden points cannot be observed since the vibration positions are the direct secondary sources of the WFS algorithm. Away from the optimal points, there is no guarantee of a proper distribution of modes. Moreover, the exciter spacing in a MAP is often an integer fraction of the panel width to allow panels to be put next to each other in landscape orientation. With such a configuration, the first and last exciters on a panel are attached in such a way as to have a continuous distribution of exciters evenly spaced. However, the number of excited vibration modes for the edge exciters is lower than for the middle exciters. This configuration poses problems with both the resulting frequency response and the effect that the edge boundary conditions may have on the exciter movement.

Boundary Conditions have a profound impact on the radiation characteristics of MAPs. In the technical literature, DMLs and MAPs have been presented with simply supported edges, or combined with free edges. Nevertheless, both free and simply supported edge conditions have disadvantages to form a viable technology for a MAP frame. On the one hand, the free condition causes a reduction of pressure in the plane of the panel due to the cancellation effect of acoustic radiation. On the other hand, simply supported conditions must contain a certain degree of frame grounding if the panel is to be held. Other kinds of practical boundary conditions

must be considered to form a viable MAP framework.

Another consequence of the modal vibration of MAPs is its inherent irregular frequency response. The MAP radiation is based on the excitation of modal frequencies to create a seamless modal density, yielding a continuous spectrum. However, there are moderate fluctuations which are determined by the vibration pattern of the panel. This response is a complex superposition of the bending wave excitations in the panel and can vary strongly with small changes in frequency. These irregularities will degrade the sound quality, making the use of MAPs less attractive compared with the use of conventional speakers. The uneven frequency response of MAPs will be experienced by the user as sound coloration. As a consequence, the typical MAP response needs to be equalized for a natural, uncolored response. For exciters near the edges that excite insufficient modes, a dedicated *Filtering Process* must be considered. Also, since WFS systems have become more popular in the past few years, an efficient filtering method to equalize exciters individually in large panels is advisable.

Large panels can also be integrated into room interiors because of their low visual profile. Furthermore, the vibration of their surface is almost negligible so that they can be used as projection screens. However, to obtain a better immersion for a large audience, the size of the screen must be moderately high. The purpose of the studies in the literature was not to cover a large listening area, but a small group of people in a teleconference. In this regard, a large MAP that truly integrates image and sound in multimedia applications is a very promising idea.

1.3 Scope of the Thesis

After introducing some of the open problems in MAPs as rendering systems of the WFS technique in the previous section, the main scope of this thesis is as follows:

To develop a method to analyze the radiation characteristics and spatial performance of loudspeaker arrays and to employ it for characterizing loudspeaker arrays' performance in the context of WFS, with emphasis on MAPs. To test and validate some practical edge boundary conditions to obtain a viable MAP frame using the proposed method, and to perform an efficient equalization to compensate for spectrum irregularities on MAPs' exciters.

With the gained knowledge, to design and build a large MAP prototype for WFS, incorporating the enhancements previously investigated.

Some particular aims emerge from this main scope, which are presented as follows:

- To draw a state of the art of flat panel loudspeaker systems based on distributed mode operation. This historic revision would introduce the early developments to achieve a single exciter panel loudspeaker, and the evolution to convert them into multiple exciter systems that can act as loudspeaker arrays for WFS systems.
- To study the spatial performance of loudspeaker arrays, paying attention to the theoretical constraints of WFS, which are related to the discreteness of the secondary sources. Additionally, to measure and characterize the spatial aliasing frequency and the related artifacts in practical loudspeaker setups.
- To analyze the role that edge boundary conditions have on the radiated wave field on MAPs. To that end, to experiment with different configurations and absorbing materials to achieve a practical solution to MAP frame manufacturing.
- To compensate for the characteristic uneven frequency response of MAPs in an efficient way, so that a large multichannel system can be equalized in real-time with minimum computational cost. For an optimized measuring and filtering process, to evaluate the perceptual impact on filter coefficient reduction and to reduce the number of measurement points by considering the geometrical distribution of driving points.
- To design, built and test an optimized MAP that includes the enhancements previously proposed, with emphasis on mixing the audio and video stimuli for an immersive multimedia environment.

1.4 Organization of the Thesis

The remainder of this thesis describes the research that has been undertaken to develop the aims stated above. The chapters are organized and presented as follows:

- Chapter 2: This chapter presents MAPs as an evolution of DMLs to fulfill the requirements of WFS systems. It addresses the bibliographic revision and the state of the art to which this thesis contributes. First, DMLs are introduced from early investigations that tried to explain the way of producing sound with vibrating panels. Some studies regarding DML characteristics, such as directivity, structural behavior or room interaction are addressed. The evolution from single to multiple exciter DMLs, later renamed as MAPs, is also discussed, paying attention to their structural and acoustical behavior. Since panel radiation depends strongly on the edge boundary conditions, a revision is presented with emphasis on practical application. Finally, the algorithms for compensating both, room effects and frequency response, are discussed.

- Chapter 3: This chapter presents a methodology for the analysis of the radiation characteristics and spatial performance of loudspeaker arrays for WFS reproduction, which is one of the main contributions of this thesis. The method provides measurement and analysis of the radiation performance, evaluation of the spatial aliasing frequency and associated sampling artifacts for linear loudspeaker arrays. A detailed description of the parameters that modify spatial aliasing artifacts, such as array directivity and truncation effects by geometry, is also discussed.

- Chapter 4: In this chapter, a study of the impact that the edge boundary conditions have on the radiated wave field for MAPs is presented as another contribution. The aim is to experiment with practical boundary conditions to obtain a viable technology for a MAP frame in WFS. Besides classical clamped and free boundary conditions, three types of elastic boundaries have been measured and validated as viable boundary conditions. Three elastic materials have been chosen as representative of soft, medium and hard types within the commercial range, to develop the elastic boundaries.

- Chapter 5: This chapter deals with an efficient filtering method for the equalization of MAPs. The method compensates for the MAP response in order to achieve a desired frequency response. The contribution of this chapter lies with the application of the method and further discussion regarding the equalization process for two MAP

prototypes comprising three and five exciters per panel. Both equalization for the panel as a single loudspeaker and dedicated exciter equalization are experimented, and their effects on the filtered responses are discussed. Additionally, a subjective assessment is carried out to test the influence of the filter order in the perceived quality of the equalization

- Chapter 6: In this chapter, a large MAP prototype is presented that has been designed and built to fulfill the requirements of immersive audio applications. It incorporates all the enhancements that were discussed over the previous chapters of this thesis. The panel size enhances its acoustic behavior in the low frequency range. Also, it can be employed for relatively large projection screens for videoconferencing.

- Chapter 7: Finally, conclusions obtained throughout this thesis are presented, including some guidelines for future research lines opened by this thesis. A list of published work related to this thesis is also given.

Additionally, an appendix has been added that includeS supplementary information without disrupting the development of the main argument. The appendix briefly reviews the theory and derivation behind the WFS rendering technique; from the Huygen's principle to a real-world configuration, with special attention to the associated errors introduced in the practical implementation.

2 Multiactuator Panels

Multiactuator Panels

2

In this chapter, MAPs are presented as an evolution of the DMLs to fulfill the requirements of multichannel audio reproduction. First, a brief historic revision shows the beginnings of the distributed mode operation and the progress made to understand such a new way of producing sound with vibrating panels. Some studies regarding DML characteristics, such as directivity, structural behavior and room interaction will be addressed. Multiexcited DMLs are discussed as a link between single-excited DMLs and what will be known as MAPs. Their structural and acoustical behavior was studied in the years following their introduction to observe if a single panel excited in many points behaves like independent loudspeakers in an array. In order to compensate for mutual reflections and room acoustics, some algorithms were proposed, in addition to smoothing filtering.

2.1 Introduction

Loudspeaker-based spatial audio systems allow listeners to perceive the position of sound sources, emanating from a static number of stationary loudspeakers, as coming from arbitrary locations in three-dimensional space. The sounds are actually created by the loudspeakers, but the listeners perception is that the sounds come from arbitrary points in space. These

systems can consist of a sufficient number of loudspeakers that surround a listener, in order to provide them with a greater sense of realism.

Multichannel sound reproduction requires arrays of loudspeakers in the reproduction room. Whereas in many applications arrays of piston-like dynamic loudspeakers are successfully employed for this purpose, their integration into a listening room is difficult because of their highly visual profile. Alternatively, DMLs are flat panel loudspeakers, whose transduction technology is based on the distributed mode operation. They can easily be integrated into a living room since they can be unnoticed by the audience. Furthermore, the vibration of their surface is almost negligible so that they can be used as projection screens.

2.2 Distributed Mode Loudspeakers

The DML essentially consists of a thin, stiff panel that vibrates in a complex pattern over its entire surface by means of an electro-mechanic transducer called an exciter. The exciter is normally a moving coil device, which is carefully positioned and designed to optimally excite the natural resonant modal structure of the panel. In Figure 2.1, a graphical representation of a DML is presented, which shows panel, exciter and housing.

This new class of acoustic radiator was discovered unexpectedly by Kenneth Heron at the Defense Evaluation and Research Agency (DERA) when he was working on composites as an alternative to the heavy materials for use in helicopters. Soon he realized that some panels re-radiated significant sound when excited, and patented his invention as a resonant "multi-modal radiator" that could be used as a loudspeaker [Heron, 1991]. In 1994 Verity Group plc, later known as NXT plc, negotiated a license from DERA to work on the theoretical and practical aspects and developed what is now known as DML. The first patents were filed in September 1996 [Azima et al., 1997], with a large group of patents following [Heron, 1998, 2000]. In [Borwick, 2001], a comprehensive historical background of DMLs is presented.

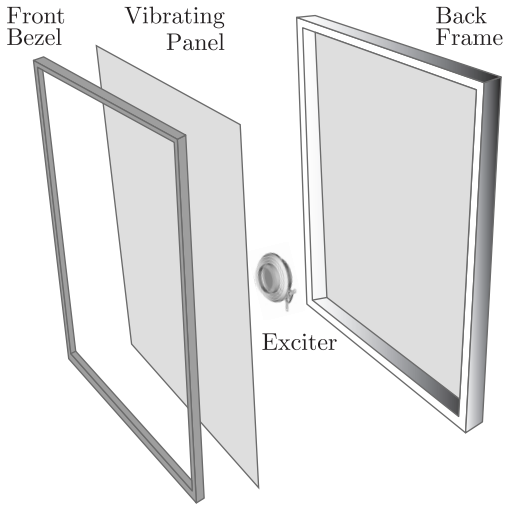

Figure 2.1. Graphical representation of a Distributed Mode Loudspeaker. Electric wiring is omitted for simplicity.

2.2.1 DML Model

DMLs are panels of finite extent deploying bending waves. The excitation of bending waves on panels results in sound radiation with distinct qualities with regard to the piston-like motion of typical dynamic loudspeakers. The theory involved in vibrational behavior of flat panels starts with expression of motion of an elementary section of a beam [Cremer et al., 2005] and its extension to describe a thin plate and its acoustic radiation due to structural waves on a vibrating panel [Fahy and Gardonio, 2007]. When considering the fourth order partial differential equation governing a thin plate, an important result is that phase velocity of the bending wave is frequency dependent.

In 1997, some publications modelled the DML as a panel with a velocity distribution of uniform magnitude but random phase, so a good approximation is to consider the panel as a random vibrating area [Harris and Hawksford, 1997],[Azima and Harris, 1997]. The velocity at any point on the panel is a sum of modal velocities or "modes" for short. The panel vibrates as a combination of its proper modes of vibration or eigen-modes, at its natural frequencies or eigen-frequencies, and at the driven frequencies, present in the external excitation signal, the driving signal in the context

of WFS. The resulting velocity profile may be considered as a sum of the mode-shapes, whose scaling will depend on both the driven frequency and the mode frequencies. This view should be considered as a mathematical approach to simplifying the simulation of a DML, rather than as a description of what is actually happening in the panel. The DML relies on the optimization of these modal frequencies to produce a modal density that is sufficiently high to obtain a continuous spectrum. Recently, a fully coupled model of the DML has been established for simulation in [Bai and Liu, 2004]. To obtain an optimal design, a Genetic Algorithm-based procedure has also been proposed.

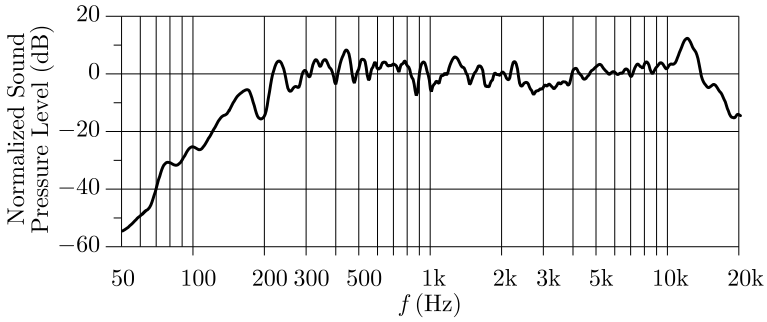

Figure 2.2. Measured pressure response of a medium-sized DML loudspeaker.

As with other finite vibrating panels, an analysis on the basis of eigenmodes can be carried out for two frequency bands: below and above the panel coincidence frequency [Angus, 1999], [Angus, 2000a]. The frequency where the wavelength is the same for the bending wave and for the sound wave in air is called coincidence frequency. At low frequencies, there are bending waves whose velocity is determined by the bending stiffness. In finite sandwich plates, the velocity is also determined by the shear modulus of the core and bending stiffness of skins. Above coincidence frequency, radiation is phase coherent and highly frequency dependent. For that reason, an appropriate choice of material properties is necessary to operate just below critical frequency. Except for high frequencies, panels will be operating with a subsonic flexural wave speed. Figure 2.2 shows a typical pressure response measurement of medium-sized DMLs.

2.2.2 Radiation Properties

The behavior of DMLs when radiating sound differs radically to that of piston-like motion loudspeakers. In a piston-like radiator, the transfer function changes slowly with position, hence there is a high degree of correlation between the responses at nearby positions. In a DML, the transfer functions include a component that can fluctuate rapidly with position, thereby reducing the correlation. It is this reduction of correlation between the transfer functions that is described as "diffuse".

With real loudspeakers, there are always components of both diffuse radiation and non-diffuse radiation. Typical cone-based loudspeakers are largely non-diffuse up to the frequencies where cone break-up begins. Typical DMLs have a relatively larger proportion of diffuse radiation, the proportion depending on the properties of the panel [Harris, 2001].

As a consequence, traditional measurement techniques that typified piston-like sources are no longer valid. Whereas DMLs give the listener the impression of a continuous spectrum, a single point measure indicates a fully modal, uncorrelated output [Gontcharov et al., 1999].

The polar response of a DML is again dependent on whether it is radiating below or above the coincide frequency, as stated in several studies [Bank, 1998], [Azima and Panzer, 1999], [Angus, 1999], [Gontcharov and Hill, 2000], [Bonhoff, 2005], which theoretical base can be found in [Fahy and Gardonio, 2007].

- Below coincidence frequency
  The polar pattern is an interference pattern for an odd and even mode strip radiator, which is orthogonal and thus the radiation pattern will swap from one to another. When many modes are excited, this summation of patterns gives a quasi-omnidirectional response but in reality, strong frequency variations are occurring at the listening point. For this region, the polar response of a DML is substantially independent of its size [Bank, 1998]. Figure 2.3 shows such a polar behavior up to 6 kHz, where coincidence occurs.

- Above coincidence frequency
  For this frequency band, the sound radiation is highly directive due to the occurring coincidence. The pattern is a combination of single lobes from forward and backward waves for each excited mode. As

frequency increases, such lobes become narrower and progressively move to the normal direction. As many modes are excited in a DML, the overall pattern is again a superposition of these lobes and would look omnidirectional. This would give the impression of increasing dispersion with frequency and thus diffuseness, as the radiation pattern becomes increasingly lobulated. With the exception of [Panzer and Harris, 1998], measured directivity patterns that would show the strong directional radiation for this frequency region, are not shown in technical publications. In Figure 2.3, the last two polar responses belong to the coincidence behavior of the panel.

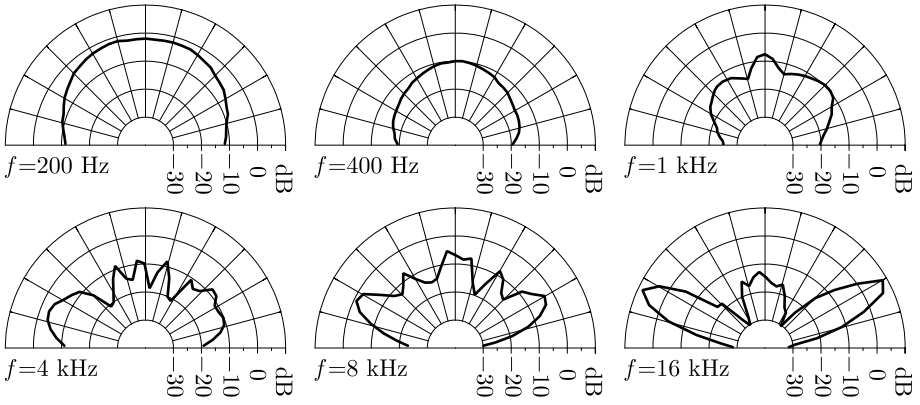

Figure 2.3. Measured polar response of a medium-sized DML loudspeaker.

Hence, although designers try to select the correct mechanical parameters to force a finite sized panel to radiate below coincidence, a DML loudspeaker makes use of both types of propagation, below and above coincidence, in order to achieve broadband transduction [Angus, 2000b]. Below coincidence the directivity is almost omnidirectional. At higher frequencies coincidence lobes start to form the typical radiation pattern of DMLs at and above coincidence.

2.2.3 Structural Behavior

The radiation of a DML is affected by its mechanical structure. In [Bai and Huang, 2001], a detailed study of structural and acoustic radiation was carried out. Later, it was shown that the proper placement of point-mass

discontinuities on infinite structures showed an increase in radiated power [Bonhoff, 2005]. However, for finite structures such as DMLs, which are already optimized for sound radiation, there is no gain in radiated power. Nonetheless, the added mass technique was soon reported to be effective in the modal behavior [Zhang et al., 2006]. They presented a model of a panel with attached mass and proposed a genetic algorithm to calculate where to put masses and exciters in an optimal manner. More recently, the problem of dispersion in plate-like structures has been addressed in [Hörchens and de Vries, 2007]. Dispersion causes resolution to fall with increasing distance from the vibration source, which can be problematic in large structures. To remove the effects of dispersion, a model function of the dispersion is obtained from measured data.

2.2.4 Housing

To prevent back to front cancellations, DMLs need to be mounted in a housing. The volume increase that absorption materials require in traditional loudspeaker cabinets is no longer needed for DMLs. In [Prokofieva et al., 2002b], an unbaffled and baffled panel with absorbing material were tested for on-axis frequency responses. The effect on the acoustic intensity was only pronounced in the low frequency range (100–1000 Hz). For mid and high frequencies, the effect of the absorber is minimal for both the baffled and unbaffled panel. Later, the same author addressed the changes caused on directivity with absorbing materials [Prokofieva, 2003]. The presence of an absorber in the vicinity of a DML panel generally results in a more uniform directivity pattern of the acoustic emission from a vibrating DML panel.

2.2.5 Room Interaction and Sound Localization

The reaction of diffuse sources, such as DMLs, to room boundaries is less severe than traditional piston loudspeakers. Harris studied the room interaction for a 2-D scheme in [Harris et al., 2000], extended to 3-D in [Harris and Hawksford, 2003], and introduced the concept of Correlation Maps in [Harris, 2004] to account for boundary reaction. DML sources produce room reflections that are less correlated to the direct sound than those radiated from piston sources and thus, constructive and destructive interference of sound is minimized.

Regarding the interaction with room modes, conventional loudspeakers are more susceptible to acoustic room modes and boundary interference [Azima and Harris, 1997], [Fazenda et al., 2002]. DMLs have a more even power distribution across a large listening area and over a wider frequency band. According to [Harris et al., 1998a], in a tentative way, and later proved in [Harris et al., 1998b], localization precision as a function of room acoustics is minimized by the use of diffuse acoustic radiators, such as DMLs. The proper sound localization by DMLs and the minimum degradation caused by room acoustics were of crucial importance in considering such radiators as alternatives to dynamic loudspeakers for multichannel systems, as will be explained in Section 2.3.

2.2.6 Other Applications

The radiation characteristics of DMLs lend themselves to use in other audio applications. In [Rumsey and Naqvi, 2001a],[Rumsey and Naqvi, 2001b], DMLs are embedded in deflector panels that surround a source loudspeaker and fulfil the fundamental requirements of an "active listening room": a critical listening environment where the key acoustic features of the room can be actively modified. This configuration has the potential to simulate the diffused nature of real room reflections. On the other hand, the effects of applying standard array technology, such as Bessel and Barker sequence modulation, to DMLs were addressed in [Copley et al., 2002]. However, the array response was not fully controlled because the individual DML elements themselves were not completely omnidirectional. Another study reported the applicability of DMLs for active noise control [Zhu et al., 2003]. Its effectiveness was moderate for feedback control, whereas for feedforward control, DMLs were proven to be very effective.

2.2.7 Array of Single Exciter Panels

In 2000, Boone and Brujin, encouraged by the positive results on sound localization, tested for the first time the applicability of DMLs for Wave Field Synthesis (WFS[1]) reproduction [Boone and de Brujin, 2000]. It was not evident from the beginning that the phase relationships between the secondary sources (loudspeakers) were not to be altered by these new radiators. A linear array of 9 rectangular single excited DMLs with radiating

[1] A comprehensive description of this multichannel technique is given in Appendix A.

surfaces of 0.18×0.125 m were essayed, confirming that DMLs could be used with success for WFS. Figure 2.4(a) shows a configuration similar to the one employed in this first prototype. The array of single excited panels was the predecessor of the current MAPs, which will be addressed in the next section.

2.3 Multiactuator Panels

The first publications on the viability of arrays of DMLs for multichannel reproduction pointed out that individual panels reconstruct the wave field correctly. However, the spacing of the secondary sources required by the WFS algorithm to acquire a reasonably useful bandwidth, forced the size of the panels to be very small. As a consequence, DMLs showed weak bass response due to the lack of excited modes in the low frequency region. As a reference, to achieve an aliasing frequency of 1 kHz, the distance between secondary sources must be approximately 17 cm. For that reason, it was decided to distribute the exciters over a single large panel and to study if exciters sharing the same vibrating surface were acting as individual secondary sources. Figure 2.4(b) depicts such a configuration in contrast to the single excited transduction.

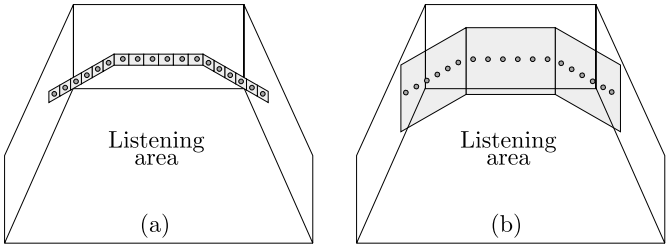

Figure 2.4. (a) Array of single-excited DMLs. (b) MAPs.

The development of MAPs was, in part, possible thanks to the European IST Project "Carrouso". This project started on January 1st, 2001 and lasted 30 months. Although the first paper announcing the project [Brix et al., 2001], did not include any reference to DMLs, they were soon part of the rendering systems objectives. The project objectives and list of participants can be found on the European Union, Information Society Technologies website [Carrouso, 2001].

As a result of the early investigations, the first MAP prototypes were shown at several conferences, such as the 19th AES International Conference in Elmau, June 2001 (see Figure 2.5), the IFA in Berlin in August 2001, and the IST event in December 2001 in Düsseldorf.

Figure 2.5. First MAP prototypes shown at the AES 19th Conference on Surround Sound, Elmau, Germany, June 2001.

2.3.1 From Single to Multi Exciter Panels

The evolution from arrays of single excited DMLs to MAPs and its validation started in 2001. Boone and others at Delft University conducted a series of experiments that ended with a prototype on which the Carrouso partners based the final design [Boone et al., 2001],[van Rooijen, 2001].

In single excited DMLs, they reported that the first wave front, related to the first part of the impulse response of the reproduction system, is as good as with conventional loudspeakers. However, small panels pose problems with sound quality since they have a poor low-frequency response. These results were promising enough to extend the DML technology to a panel with multiple exciters, each driven with a different signal. Such a configuration would act as a WFS array if every exciter on the panel would excite only a small part of the panel around the exciter position.

Since transducers must be spaced very close to reconstruct the wave form up to a reasonable frequency, a vibrating panel with low internal damping will result in cross-talk. For that reason, it is necessary to use panel material with high internal damping. This allows each exciter to act as a proper localized small individual loudspeaker. The counteraction is

that high internal damping causes a loss of efficiency, because part of the energy is dissipated within the panel and not radiated as acoustic energy.

At first, a polycarbonate resin (PC) panel, which has high internal damping, was built as a prototype with well defined source localization. However, the PC material had a very poor impulse response, with a lot of ringing. Foamboard arose as an alternative to PC panels which exhibited better impulse response and maintained the independent behavior of exciters for WFS. As with PC panels, FIR filtering was still necessary to obtain an adequate sound quality.

In [van Rooijen, 2001], three foamboards of 1×0.7 m and 0.5 cm width were mounted in a landscape orientation. They contained 20 exciters spaced 12.7 cm apart, six on the first and third panel and eight on the second panel. Whereas in the array of single excited panels, Peerless[2] 880101 25 mm exciters were used because of their small size and moderate power, in these foamboard panels, Elac Type G and D high power prototype exciters were employed. These 37 mm exciters evolved into the current models, such as the exciter 82073 type J. This concept was then referred to as a "single-panel, multi-exciter" array, a denomination which was employed in the following studies [Corteel et al., 2002], [Horbach et al., 2002].

On June 30th, 2003, the Carrouso Project ended with a multi-exciter DML jointly designed by some of the project partners. It was not until 2004 that such arrays appeared in the technical literature as "Multiactuator Panels or MAPs".

In the following, details on the technology that were published in the subsequent journals and conferences, are discussed. A new shortcoming in the WFS reproduction was that MAPs act as reflectors for acoustic waves which disturb the perception of the target soundfield. A room compensation technique that attenuates early reflections of MAPs by means of a mirror source algorithm was proposed in [van Zon et al., 2004]. In this same year there also appeared one of the most significant papers on MAPs [Boone, 2004]. It collected and discussed all the issues regarding the three years of investigation. This time, instead of using the early prototypes, Boone experimented with the new eight-exciter MAPs from the Carrouso Project. Two years later, another milestone in MAP development was the structural acoustic analysis by means of a laser Doppler vibrometer made by

[2]Peerless is now a partner of the Tymphany Corporation.

de Vries and other researchers at TU Delft [Kuster et al., 2006]. This study confirmed experimentally the basis on which MAPs relied since the first publications: acoustic radiation is generated almost entirely by the structural near field around the excitation point on the panel. The damping loss factor of the MAP material must be large to produce such an appropriate behavior. In addition, both, panel dimensions and exciter position, also played a role in the acoustic radiation of MAPs. It was then concluded that particular choices of panel size and damping loss factor were needed to meet the requirements of WFS in a single panel.

2.3.2 Current MAP Prototypes

As a result of the research undertaken in the Carrouso Project, some prototypes were designed and built, mostly intended for research purposes. The four MAP designs that have been employed in experimental setups in the technical literature are shown to scale in Figure 2.6.

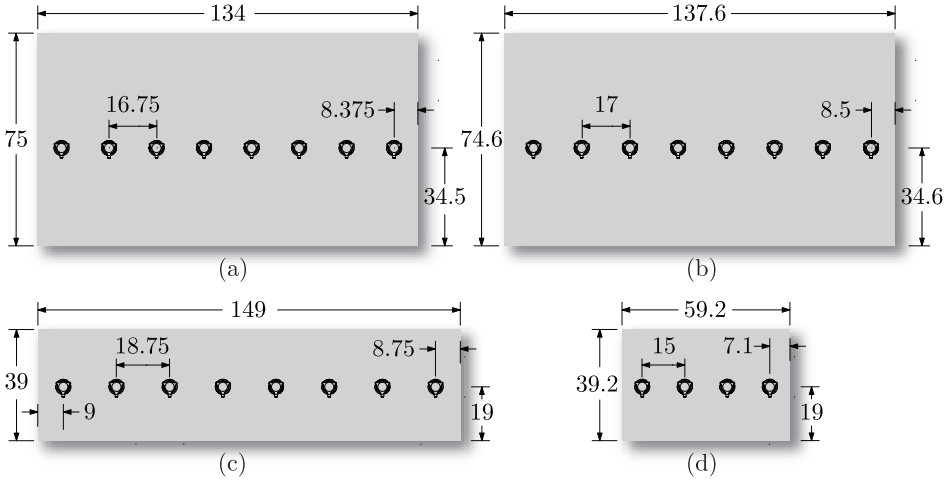

Figure 2.6. Geometric details on MAP prototypes developed by some of the Carrouso partners. (a) TU Delft. (b) University of Erlangen-Nuremberg. (c) and (d) IRCAM & Sonic Emotion AG. Dimensions in centimeters.

Laboratory of Acoustic Imaging and Sound Control, TU Delft

At the Laboratory of Acoustic Imaging and Sound Control at Delft University of Technology in The Netherlands, Dr. Boone and Dr. de Vries

experimented with the primitive single exciter panel and finally developed a MAP design that would appear in several publications [Boone et al., 2001],[van Rooijen, 2001], [Boone, 2004],[van Dorp, 2005],[van Dorp and de Vries, 2006], [Corteel, 2006a],[Kuster et al., 2006].

Figure 2.6(a) depicts the geometrical details of the design. It is a medium-sized panel of 134×75 cm with eight exciters spaced 16.75 cm apart. This spacing is an integer fraction of the panel width, in order to allow panels to be put next to each other in landscape orientation. With such a configuration, the first and last exciter on a panel is attached in such a way as to have a continuous distribution of exciters evenly spaced. As will be shown later, this technique is also used by the rest of the MAP designs. The line of exciters is slightly below the center of the panel to increase modal participation.

The material of the panel was 5-mm PVC foam board core with paper skins, which is sufficiently damped to let exciters generate the main contribution of energy in a region around them of 10 cm diameter. As suggested in past contributions, FIR filtering was still necessary to smooth the acoustic response. The selected exciters for this design were ELAC 82073, an 8 Ω exciter with a 37 mm diameter and a 20 W nominal power output. Figure 2.7 shows a picture of the MAP during a measurement session in the anechoic room.

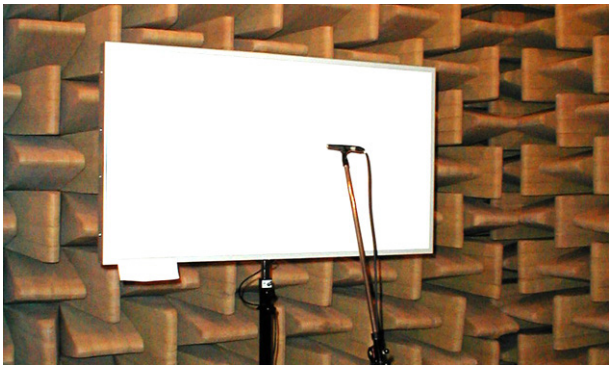

Figure 2.7. MAP prototype developed at the Laboratory of Acoustical Imaging and Sound Control, Delft University of Technology, The Netherlands.

Multimedia Communications & Signal Proc., University of Erlangen-Nuremberg

Dr. Rabenstein and others at the Laboratory of Multimedia Communications and Signal Processing at the University of Erlangen-Nuremberg in Germany developed an eight-exciter MAP, although it was named as Multi-exciter Panels or MEPs in the literature [Seuberth, 2003], [Spors et al., 2005b].

This model is virtually the same configuration as that in Delft, the difference being the slightly larger spacing of the exciters, as can be seen in Figure 2.6(b). It is a medium-sized panel of 137.6×74.6 cm with eight exciters spaced 17.1 cm apart. Since the transducer spacing is slightly larger, so should be the width of the panel, to maintain the functionality of attaching MAPs in landscape orientation. For this design, the panel material was also PVC foam and ELAC 82073 type J exciters were also used. Figure 2.8 presents a group of four of these MAPs in an open U configuration.

Figure 2.8. MAP prototype developed at the Laboratory of Multimedia Communications and Signal Processing, University of Erlangen-Nuremberg, Germany.

IRCAM Paris & Sonic Emotion AG

The collaboration carried out by Dr. Corteel at IRCAM in Paris and Dr. Pellegrini at Sonic Emotion AG in Switzerland led to the manufacture of two MAP designs, as shown in Figures 2.6(c) and (d). The latter has appeared in recent publications [Corteel et al., 2007],[Corteel, 2007]. Contrary to the preceding models, these panels are commercialized by Sonic Emotion under the name "M3S Panels" and have similar transducer spacing and exciter models. The innovation with respect to the latter designs is the use of high aspect ratios for the panel of Figure 2.6(c) and the introduction of

four-exciter small panels, shown in Figure 2.6(d). In addition to this, such panels are made of laminated honeycomb paper, which is more efficient than foam. An arrangement of eight panels in a 32-channel configuration is shown in Figure 2.9.

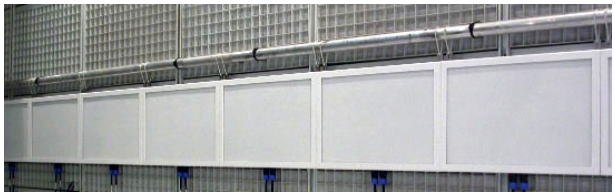

Figure 2.9. MAP prototype developed at IRCAM in Paris, France and Sonic Emotion AG in Oberglatt, Switzerland.

2.3.3 Spatial Frequency Response of MAPs

The diffuseness of the distributed mode operation in MAPs minimizes the drawbacks of room interaction, as with DMLs. On the one hand, MAPs radiate an even power distribution across a large listening area and, on the other hand, the reflections on the room boundaries are less correlated to the direct sound.

In the context of WFS, the region above aliasing frequency is characterized by oscillations both in frequency and space. These interference patterns can be experienced when moving the head or walking within the listening area. The diffuse behavior of MAPs helps in diminishing the effects of sound color variations. Corteel carried out a comparison between MAPs and dynamic cone loudspeakers on an objective and subjective level for WFS [Corteel et al., 2007]. Above the aliasing frequency, a diffuse filtering was used which consisted of time limited white noise, independently generated for each loudspeaker, to obtain uncorrelated outputs. The varying response through both frequency and space above the aliasing frequency is diffused with such a filtering technique and thus, their perceptual impact was minimized. This diffusion is introduced by natural properties of the MAP or by diffuse filtering both on MAPs and on dynamic loudspeakers. These results suggest that the aliasing artifacts start to appear at a certain frequency but increase in a progressive way rather than a sharp frequency caused by diffuseness. In addition to this, compared to dynamic transducers, the sensation of spaciousness is enhanced by means of the diffuse

radiation of MAPs. Therefore, a methodology for characterizing the spatial performance and the associated aliasing artifacts of loudspeaker arrays at the laboratory is very advisable.

2.3.4 Multimedia Applications

DMLs and MAPs are flat structures with vibrations low enough to be imperceptible to the human eye. This property can be exploited by integrating them into a room interior and simultaneously using them as projection screens. In this way, image and sound are fully integrated for multimedia applications. In [Chiao et al., 2000], this idea was first suggested as three single exciter DMLs for multiparticipant videoconferencing. Later, a combination of WFS with 2-D video projection was proposed [Boone et al., 2001],[de Brujin and Boone, 2003]. However, to obtain a better immersion for a large audience, the size of the screen must be moderately high. The purpose of the first study was not to cover a large listening area, but a small group of people in a videoconference. In the conference papers combining WFS with video projection, the panel itself was not the projection screen, but a dynamic loudspeaker array behind an acoustically transparent screen. The application with MAPs was only suggested.

2.4 Edge Panel Support

The panel of a MAP is a type of finite plate whose radiation is characterized by the superposition of waves travelling in opposite directions. These standing wave patterns are due to incident and reflected waves from the boundaries, allowing modal vibrations and radiation to appear. At subcritical frequencies, where the distributed mode operation works properly, boundary conditions have a profound impact on the radiation characteristics.

2.4.1 Influence of Boundary Conditions on Plate Radiation

As already pointed out in Section 2.2.2, sound radiation from finite plates are characterized by two frequency ranges: for frequencies above and below the critical frequency.

At high frequencies, in the coincidence region, the projection of the acoustic wavelength in air onto the panel, coincides with the bending wavelength. The coincidence effect consists of these wavelengths matching at a certain angle above the coincidence frequency. It has been shown that radiation resistance of a plate is not influenced by its boundary conditions [Renji et al., 1998],[Renji, 2001].

However, as stated in the above discussion, DMLs and MAPs are designed to operate at frequencies below coincidence, where edge boundary conditions shape the radiation characteristics [Angus, 1999]. In this region, the boundaries of any finite structure, locally suppress the interaction between waves travelling in opposite directions, which leads to sound radiation in general. Depending on the boundary condition considered, the interaction will be more or less pronounced, and thus, the efficiency of the panel radiation [Bonhoff, 2005]. For that reason, the radiation resistance is significantly influenced by the boundary conditions [Renji et al., 1998],[Renji, 2001].

MAPs have the disadvantage of placing exciters close to the edges in order to achieve a linear WFS secondary source distribution. In [Kuster et al., 2006], the radiation of the first exciter, which was only 80 mm from the edge, was studied in a eight-exciter MAP. The exciter performance showed some alteration with respect to the central ones, but the interference was smaller than expected.

2.4.2 Edge Boundary Conditions

In this section, the different ways of supporting the panel are discussed. Rectangular plates are generally classified in accordance with the type of support used [Timoshenko and Woinowsky-Krieger, 1959]. The three basic boundary conditions applied to a plate edge are Free, Clamped, and Simply Supported edges, also known as built-in plates. Figures 2.10(a) and (b) show a schematic view of the moments and forces governing the clamped and simply supported edge boundary conditions.

The ideal free condition implies that the structure is floating in the air without support of any kind. If such a condition is satisfied, no reaction forces arise along the edges: there are no bending or twisting moments, and also no vertical shearing forces. At the other extreme, the clamped condition is achieved by grounding the structure with well-tightened de-

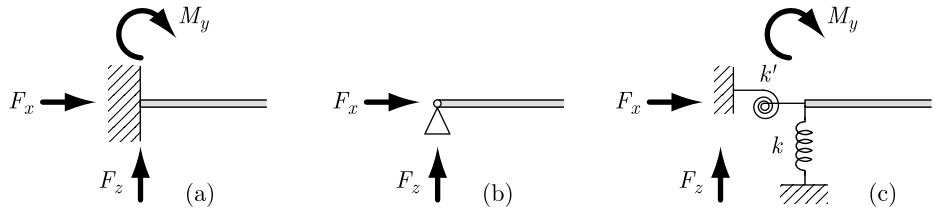

Figure 2.10. Edge boundary conditions and their associated forces and moments. (a) Clamped. (b) Simply Supported. (c) Elastic Boundary.

vices that prevent the deflection of the structure at the supports. In this case, several reaction forces are created along the edges: two forces F_x and F_z, normal and perpendicular to the support direction respectively, and a bending moment perpendicular to the plane structure M_y. In between, there is the simply supported condition, which behaves as a clamped edge but without bending moments because edges can rotate freely with respect to the edge line.

In addition, other types of boundary conditions appear as a result of combining the above conditions [Ugural, 1999]. For example, the mixed supported conditions have clamped, simple supported and free at different edges. There is also the point support, which consists of a plate supported by intermediate points.

However, the boundary condition that involves some sort of elastic damping is known as Elastic Edge Support or Elastic Boundary. Plates on elastic boundaries are supported by elastic supports which resist certain types of bending [Leissa, 1999], as depicted in Figure 2.10(c). Its mechanical model is equivalent to a plate supported elastically by springs uniformly distributed along its edge. Hence, two reactions arise F_x and M_y. Firstly, deflection is opposed by linear springs with a certain degree of stiffness k. Secondly, edge rotation is opposed by spiral springs having a certain degree of rotational stiffness k'. Because of the flexible features on edges, elastic boundaries are suitable in DML loudspeakers for audio reproduction.

2.4.3 Practical Implementations

In the technical literature, DML and MAP models have been presented with simply supported edges: [Prokofieva et al., 2002a] (for the baffled

loudspeaker) [Bai and Liu, 2004] (adhesive tape to fix boundaries in the laboratory), [Zhang et al., 2006], or combined with free edges: [Prokofieva et al., 2002a] (for the unbaffled loudspeaker), [Bai and Huang, 2001].

Nevertheless, both free and simply supported edge conditions have disadvantages to present a viable technology for a MAP frame. On the one hand, the free condition can be approximated by supporting the structure on very flexible soft springs, which give rise to a free radiating panel in a full-space radiation. However, when observing the typical polar response of a free DML, a reduction of pressure in the plane of the panel is noticed, due to the cancellation effect of acoustic radiation at or near the edges. For that reason, the panel is usually placed in a baffle, where radiation due to the rear part of the panel becomes contained. On the other hand, simply supported conditions must contain a certain degree of frame grounding if the panel is to be held. This problem can be faced by diffusing pseudorandomly the boundaries between pure clamped and free, in a special type of Mixed Boundary Condition suggested by [Angus, 2000b]. Unfortunately, such a condition does not present a reliable fixing frame since part of the panel is suspended in the air.

2.5 Equalization

As stated previously, MAP radiation is based on the excitation of natural and proper modes of vibration to create a seamless modal density, yielding a continuous spectrum. However, there are moderate fluctuations which are determined by the vibration pattern of the panel. This response is a complex superposition of the bending wave excitations in the panel and can vary strongly with small changes in frequency. As a consequence, the typical MAP response is very poor and needs to be equalized for a natural, uncolored response.

In the context of WFS reproduction, two filtering processes have been proposed. First, in order to compensate for reflections of the room, multichannel inverse filtering techniques are employed, which have also been extended to account for panel reflections. Second, filters to compensate for uneven frequency responses, such as those of MAPs, are known as spectral smoothness equalization.

The use of these filtering approaches for WFS is restricted by one of the most important artifacts, the aliasing frequency. Multichannel techniques are not applied above aliasing frequency, because otherwise severe spatial dependent distortion of the wave field will be introduced. On the contrary, above that frequency, spectral smooth equalization is used [van Dorp and de Vries, 2006].

2.5.1 Reflection and Room Compensation for WFS

Multichannel inverse filtering techniques offer control of the sound field at a limited number of points in the listening space [Nelson et al., 1996]. A method based partly on multichannel inversion, that aimed at controlling the free-field radiation patterns of multiexciter distributed mode loudspeakers, was proposed by Corteel and others [Corteel et al., 2002], [Horbach et al., 2002]. This method was later extended to room compensation for WFS [Corteel and Nicol, 2003], [van Zon et al., 2004], where the solution produced by multichannel equalization techniques achieved both the synthesis of the reproduction objective and the compensation of reproduction artifacts in a unique process. The latter included the suppression of undesired reflections between MAPs, by constructing cancelling waves emitted by virtual mirror image sources.

A similar method for room compensation in WFS was presented by Spors and others [Spors et al., 2003], [Buchner et al., 2004]. It relies on circular microphone array measurements that are decomposed onto a plane wave or cylindrical harmonic basis [Hulsebos et al., 2002]. Multichannel inversion is then performed in this transformed domain. The control remains efficient inside the circular array, with which the sound field is sampled, but may suffer from artifacts linked to both microphone and rendering system limitations [Spors et al., 2005a].

Alternatively, another approach based on multichannel inversion of Multiple-Input and Multiple-Output (MIMO) systems was proposed as a possible practical solution to room compensation in an extended area for WFS reproduction systems [López et al., 2005],[Fuster et al., 2005b],[Fuster et al., 2005a]. To that end, the reproduction area is sampled with multiple microphones with which to calculate a bank of inversion filters applied just before the loudspeaker section.

In [Corteel, 2006b],[Corteel, 2007], a modified version of [Corteel and

Nicol, 2003] is presented. This new technique adds the compensation of WFS artifacts by filtering the loudspeaker driving signals for each virtual source.

Multichannel filtering techniques can be divided into two categories: methods that perform the inverse filtering in the time domain using the MFAP algorithm [Corteel et al., 2002], [Corteel and Nicol, 2003], [van Zon et al., 2004] [Corteel, 2006b], and methods based on frequency domain inversion [van Dorp, 2005], [van Dorp and de Vries, 2006]. To avoid instabilities, singularities in the inversion are regularized using a technique based on Singular Value Decomposition (SVD).

2.5.2 Spectral Smoothness Equalization

The typical frequency response of a MAP contains sharp nulls, which are audible and highly undesired. This is due to a superposition of temporarily and spatially arriving diffuse waves. The transient response of panels with distributed mode operation is characterized by a long impulse response tail, which, in the frequency domain means that modes exhibit a narrow bandwidth [Angus, 2000b]. Therefore, to compensate for the complex and random characteristics, some sort of filtering is compulsory.

A method that combines digital inverse FIR filtering by Linear Predictive Coding inverse for room mode correction and tunable Discrete Wavelet Transform octave-band equalization is presented in [Chiao et al., 2000]. The method proved to be appropriate for equalizing peaks in the response rather than dips. A similar procedure of FIR filtering by varying coefficients for active noise control can be found in [Zhu et al., 2003].

For WFS reproduction, above the aliasing frequency, [Horbach et al., 2002] and [Corteel et al., 2002] employ individual equalization of the drivers, combined with energy control to recover the sound field in a perceptually, not physically exact sense. Other studies reported experimentally that, in general the measured frequency response after applying the equalization filter was still not flat but it exhibited a more uniform shape [van Dorp, 2005],[van Dorp and de Vries, 2006].

2.6 Conclusions

This chapter has explored the state of the art on MAPs as a reproduction system for WFS, which will be the basis and context of this thesis. The evolution of the DML to the current MAPs has been presented in sequence, through bibliographic cites of literature on the audio field. This bibliographic revision has shown that there are still some open problems and possible enhancements in some of the aspects regarding MAPs' structural behavior and response. In particular, the size of the panel and the edge boundary conditions can be studied for minimizing their impact on the radiation. Additionally, an efficient filtering method can be applied for MAP systems with a large number of exciters. These issues will be addressed in detail in the following chapters.

Wavenumber Domain Analysis 3

Wavenumber Domain Analysis 3

In a theoretical WFS reproduction system the infinitely dense secondary source distribution surrounding a listening space completely recreates the wave field and preserves all temporal, spectral, and spatial information present in the original field. To achieve a real-world application of this concept, the continuous-space distribution must be implemented through a discretized array of spatial sampling points composed of loudspeaker transducers, which causes a limited spatial resolution. As a consequence, the wave field is correctly synthesized up to a limiting frequency, known as spatial aliasing frequency in the technical literature. The spatial discretization errors or aliasing artifacts are of great interest since they restrict the useful bandwidth in the practical implementation of WFS systems. The diffuse radiation of MAPs leads to a pressure distribution over space which differs from that of dynamic loudspeaker-based systems. In this chapter, the aliasing artifacts of both rendering systems is addressed by means of a proposed methodology based on the wavenumber domain.

3.1 Introduction

This chapter describes an analysis of the acoustic wave fields and their aliasing artifacts generated by MAPs in the context of WFS. For this purpose,

wave fields are interpreted in the wavenumber domain, where the source radiation is decomposed into plane waves for arbitrary angles of incidence. Such a transformation allows one to distinguish the loudspeaker periodic spatial spectra and then to use this information for analyzing the aliasing frequency, the sampling artifacts, and the truncation effects in a given reproduction area. Furthermore, the method provides useful information on angle-dependent radiation of transducers in an array.

The method is applied for both dynamic loudspeaker arrays and, particularly for MAPs, taking into account their characteristic geometry and radiation features. In this regard, a WFS array can either be assembled by a large panel with many exciters or by small panels accommodating a smaller number of exciters per panel. This different approach to achieve an equivalent array in terms of aliasing frequency leads to dissimilar spatial resolution capabilities.

The outline of the chapter is presented as follows. Section 3.2 describes the mathematics of time-space domain sampled signals and their transformation into a multidimensional frequency domain. Sampling artifacts are described and analyzed by a graphical representation proposed here. Section 3.4 presents simulations and experimental results of WFS virtual sources reproduced by MAPs and dynamic loudspeakers, according to the setup described in Section 3.3. Two MAP configurations and a dynamic loudspeaker array have been measured by using the proposed method. Since all arrays exhibit the same transducer spacing, a comparison in equivalent conditions has been performed. Finally, Section 3.5 concludes the chapter.

3.2 Analysis Method

3.2.1 Space-Time Transformations

The analysis in the wavenumber domain is an intuitive and physically appealing technique to study wave propagation and diffraction that was first developed in optics [Sherman, 1967], [Shewell and Wolf, 1968], and has been extended to other fields such as seismics [Berkhout, 1987], ultrasonics [Lerner and Waag, 1988] and audio engineering [Teutsch and Kellermann, 2006],[Rafaely, 2004]. Implementation of such plane wave decomposition-takes place in the wavenumber domain.

Therefore, an analysis in the space-time wavenumber domain can be a powerful and intuitive tool for understanding and analyzing the acoustic wavefield (see [Williams, 1999], [Rabenstein et al., 2006] for details). As it will be demonstrated later, this tool is very effective for analyzing the MAPs presented in the last section.

The transformation of multidimensional wave fields is achieved by means of fundamental concepts of signal theory. In the following, the Fourier Transform is defined for time and space variables [Rabenstein et al., 2006].

For a one-dimensional signal $f(t)$, the Fourier Transform is defined as

$$F(\omega) = \int_{-\infty}^{\infty} f(t) e^{-j\omega t} dt, \tag{3.1}$$

where ω is the angular frequency. In the same way, the Fourier Transform of a one-dimensional signal $f(x)$ with x as the space variable is defined by

$$\tilde{F}(k_x) = \int_{-\infty}^{\infty} f(x) e^{jk_x x} dx, \tag{3.2}$$

where k_x is the spatial frequency. For multidimensional signals, which depends on time and spatial coordinates, the application of the Fourier transforms give raise to

$$\tilde{F}(k_x, \omega) = \int_{-\infty}^{\infty} \int_{-\infty}^{\infty} f(x,t) e^{jk_x x} e^{-j\omega t} dx dt, \tag{3.3}$$

Consider now a bidimensional monochromatic pressure plane wave in a x, z coordinate plane at $y = 0$, propagating in the θ direction at speed c, as shown in Figure 3.1(a),

$$p(x, z, t) = A e^{j(\omega_0 t - k_{x_0} x - k_{z_0} z)}, \tag{3.4}$$

where A is an arbitrary constant, ω_0 is the plane wave angular frequency and $k_0 = \omega_0 / c$ is the wave number. With regard to the x axis, its phase term is simply $\omega_0 t - k_{x_0} x$, so the wavelength in such a direction is $\lambda_x = 2\pi / k_{x_0}$. The wave is travelling at a phase speed of $c_x = \omega / k_{x_0}$ in the x direction. Similar results are obtained for the z axis [Williams, 1999].

According to Figure 3.1(a), the projected wavelengths in the vertical and horizontal directions may not be equal but the important relationship

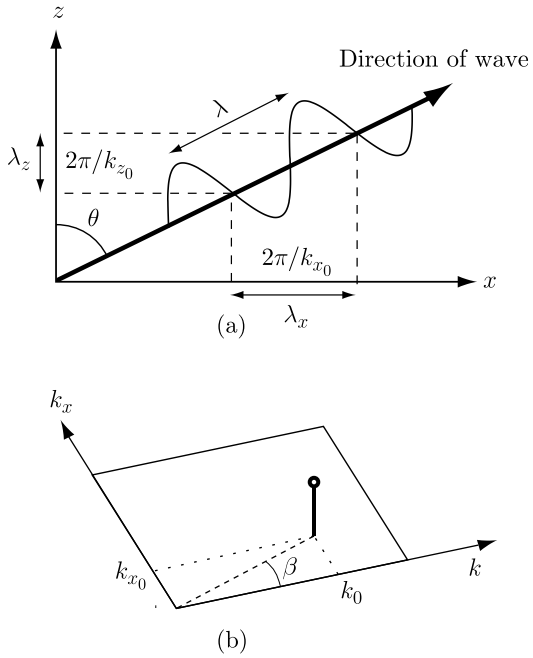

Figure 3.1. (a) Plane wave travelling with θ angle to the x axis in the $x-z$ domain. (b) In a $k_x - k$ representation, this wave appears as a delta in $k_x/k = \tan\beta$.

$k_0^2 = k_{x_0}^2 + k_{z_0}^2$ must be satisfied, which means that the wavenumbers are dependent of one another. In terms of the direction of wave θ, the spatial frequencies along the two axis are $k_{x_0} = k_0 \sin\theta$ and $k_{z_0} = k_0 \cos\theta$ and, similarly, the phase velocities must satisfy $c_x = c/\sin\theta$ and $c_z = c/\cos\theta$. Equation (3.4) can be written as

$$p(x,z,t) = p_0\left(t - \frac{x}{c_x} - \frac{z}{c_z}\right), \tag{3.5}$$

where p_0 is the wave form in the origin as $p(0,0,t) = p_0(t)$.

The Fourier transform with respect to time gives

$$\begin{aligned} P(x,z,\omega) &= \int_{-\infty}^{\infty} p_0\left(t - \frac{x}{c_x} - \frac{z}{c_z}\right) e^{-j\omega t} dt \\ &= P_0(\omega) e^{-j(k_{x_0}x + k_{z_0}z)}, \end{aligned} \tag{3.6}$$

where $P_0(\omega)$ is the Fourier Transform of $p_0(t)$. A second transform, this time with respect to the two spatial coordinates x and z results in

$$\tilde{P}(k_x, k_z, \omega) = \int_{-\infty}^{\infty}\int_{-\infty}^{\infty} P_0(\omega)e^{-j(k_{x_0}x+k_{z_0}z)}e^{jk_x x}e^{jk_z z}dxdz. \tag{3.7}$$

If the temporal frequency variable ω is expressed in terms of the wave number $k = \omega/c$, the multidimensional transform gives

$$\tilde{P}(k_x, k_z, k) = 4\pi^2 P_0(k)\delta(k_x - k_{x_0})\delta(k_z - k_{z_0}). \tag{3.8}$$

Now, consider a registration of the plane wave along the x axis alone, where $z = 0$. This is expressed by a simplified version of Equation (3.7):

$$\begin{aligned}\tilde{P}(k_x, k) = &\int_{-\infty}^{\infty} P_0(k)e^{jk_{x_0}x}e^{-jk_x x}dx \\ =&2\pi P_0(k)\delta(k_x - k_{x_0}) \\ =&2\pi P_0(k)\delta(k_x - k_0\sin\theta),\end{aligned} \tag{3.9}$$

where k_x is the spatial frequency along the registration axis and k_{x_0} is written as a function of the plane wave travelling direction θ.

The transformed monochromatic plane wave can be plotted in a $k_x - k$ diagram resulting in a delta pulse, as presented in Figure 3.1(b). The angle β where it appears is related to the angle θ by $\tan\beta = k_x/k = \sin\theta$.

Now, let us consider a broadband plane wave, which includes several frequency components. Then, the $k_x - k$ representation will exhibit a a single delta pulse for each frequency component. Since all the wavefronts are travelling at angle θ, the relation $\tan\beta = k_x/k$ must hold for all delta pulses, which makes them to distribute in a straight line with angle β.

According to this, a composition of two broadband plane waves with different travelling angles θ_1 and θ_2 will appear as two straight lines in this diagram, as shown in Figure 3.2 as β_1 and β_2, respectively. Consequently, an arbitrary wave field, which can be seen as a composition of plane waves will be represented as straight lines with different angles β. This means, in

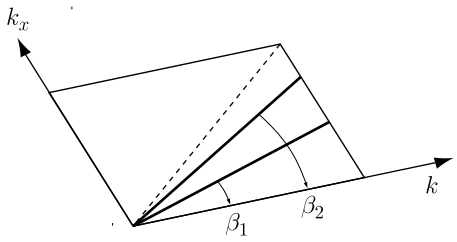

Figure 3.2. $k_x - k$ representation of a composition of two broadband plane waves.

turn, that each plane represents different spatial frequencies k_x. The extension of each line is related to the temporal frequency bandwidth that the wave has in this particular angle of incidence. As shown by the dashed line in Figure 3.2, the maximum angle β is 45° which correspond to a tangential incidence angle θ=90°. This multidimensional plot was first proposed for audio engineering in [Verheijen et al., 1995], [Start et al., 1995], [van Rooijen, 2001]. The enhancement proposed here is the further interpretation and information retrieval of spatial characteristics of practical loudspeaker arrays.

3.2.2 Sampling Artifacts

In the previous section, an acoustic wave field composed of plane waves has been considered. In order to generate such waves in a 2D space, a continuous infinite line source must ideally be employed. Analogously, in order to record the generated wave field to obtain the space time transformation as described in Equation (3.9), a continuous infinite line of receivers in the x axis must be also employed. Both requirements are not possible in practice which leads to the use of discrete alternatives.

In this case, three sampling processes arise: time sampling, spatial sampling in the reproduction stage and spatial sampling in the receiving stage. Assuming proper time sampling according to the Nyquist criteria, the two spatial aliasing artifacts are reviewed in the next subsections.

Reproduction Stage

Let us consider that a continuous distribution of sources is replaced by a set of aligned point sources at discrete positions (a loudspeaker array in

the context of this chapter, as depicted in Figure 3.4). As it is well known in time domain frequency analysis, for a given sampling period Δt, the maximum frequency that can be resolved is given by the Nyquist frequency $\omega_{\max} = \pi/\Delta t$. In analogy to time sampling, the Nyquist criterion [Proakis and Manolakis, 1998] can be modified for sampling in space, i.e., sampling along the x axis with a Δx interval, implies a spatial Nyquist frequency of $k_{x,\max} = \pi/\Delta x$. Assuming plane waves arriving at the x axis at angles up to $\theta = 90^{\text{o}}$ and a proper time sampling, there is a spatial aliasing which occurs above a certain temporal frequency, called *spatial aliasing frequency* [Berkhout et al., 1993],

$$f_{\text{al}} = \frac{c}{2\Delta x \sin\theta_{\max}}, \tag{3.10}$$

where the relation $k_{x,\max}/k_{\text{al}} = \sin\theta_{\max}$ has been used to derive the expression. Note that this equation is only valid if $\theta_{\min} = -\theta_{\max}$ is assumed.

The reproduced wave field for a spatially discrete secondary source distribution is a modified version of (3.9). Since a function is point sampled at Δx values when it is multiplied by the comb function $\text{III}(x/\Delta x)$, the spatially sampled wave field can be written as [Williams, 1999]

$$\begin{aligned}\tilde{P}_{\text{al}}(k_x, k) &= \int_{-\infty}^{\infty} P_0(k) e^{jk_{x_0}x}\, \text{III}\left(\frac{x}{\Delta x}\right) e^{-jk_x x} dx \\ &= \frac{\Delta x}{2\pi} P_0(k) e^{jk_{x_0}x} * \text{III}\left(\frac{k_x}{2\pi/\Delta x}\right).\end{aligned} \tag{3.11}$$

The comb function is a sequence of infinite delta pulses uniformly distributed, so its Fourier transform is another delta pulse sequence. As a consequence, the above convolution leads to

$$\tilde{P}_{\text{al}}(k_x, k) = \sum_{n=-\infty}^{\infty} 2\pi P_0(k)\delta\left(k_x - k\sin\theta - \frac{2\pi}{\Delta x}n\right), \tag{3.12}$$

which states that the ideal plane wave is repeated in the k_x axis at the n positions $k_x = k\sin\theta + 2\pi n/\Delta x$, each shifted by $2\pi/\Delta x$, as shown in Figure 3.3. The aliased contributions, which correspond to the infinite terms of the summation where $n \neq 0$, are a superposition of plane waves

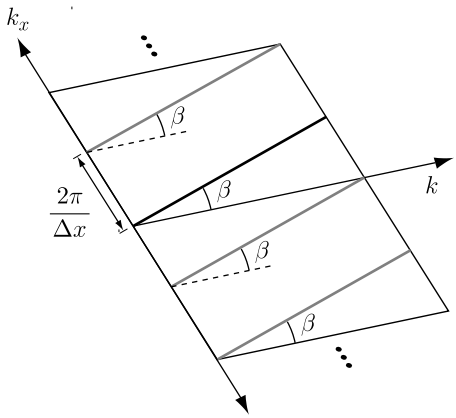

Figure 3.3. Aliasing effects in the $k_x - k$ representation of a plane wave generated by a discrete point source distribution due to sampling in the reproduction stage.

arriving at different angles with respect to the desired plane wave. In the following, the loudspeaker spacing will be denoted as Δx_l.

Receiving Stage

Let us now consider that a continuous distribution of receivers is replaced by a set of single receivers at discrete positions, which means, in practice, that a microphone linear array is used. As depicted in Figure 3.4, a microphone line array is placed in a line parallel to the main loudspeaker array. The microphone spacing is inversely proportional to the spatial resolution capacity of the recording array. If the microphone spacing Δx_m is smaller than the loudspeaker spacing in the array Δx_l, the recording setup will discriminate plane wave components with spatial frequency beyond that of the loudspeaker array. In that case, the loudspeaker wavenumber domain period will be visible within a $k_x - k$ representation, in which the spatial limiting interval is given by the microphone array spacing.

3.2.3 Space-Time Frequency Domain Analysis

The interpretation of the $k_x - k$ plot diagram when sampling is employed in both stages, is not straightforward. However, if the analysis is restricted to plane wave distributions, some interesting effects and characteristics are revealed. These are discussed below by using Figure 3.5(a) as a reference.

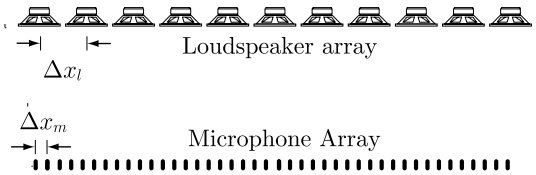

Figure 3.4. Loudspeaker and microphone array setup.

Limits and Areas

To start with, a deep insight into the plot limits and areas within a $k_x - k$ representation will be explained in the following. The spatial artifacts produced by the emitting and receiving stages will be addressed.

For illustration purposes, Figure 3.5(a) shows the $k_x - k$ diagram of an axial plane wave ($\theta = \beta = 0$) according to the setup of Figure 3.4. In such representation, apart from the main spectrum at $k_x = 0$, there are repetitions at $2\pi/\Delta_x$ positions, according to Equation (3.12). Let us define $k_{x,\max} = \pi/\Delta x$ as the limit value before entering into the aliased spectrum. For the loudspeaker array, such a limit is denoted as $k_{x,\max l}$ and, for the microphone array, as $k_{x,\max m}$.

First, the loudspeaker array effects can be analyzed by representing the wavenumber domain in the interval $[-k_{x,\max l}, k_{x,\max l}]$ –dark shaded triangle in Figure 3.5(a)–, in which only one spatial period is visible. Since the ratio between k_x and k is $\sin\theta$, where θ is the angle with which the plane wave is travelling, a wavenumber domain representation is zero everywhere except on a single line in k_x=0.

Second, the same $k_x - k$ representation can be used considering the limits imposed by the microphone array, which resolves higher spatial frequencies, and determines the highest frequency of the analysis. In this case, due to the periodicity in the k_x domain, a limit interval of $[-k_{x,\max m}, k_{x,\max m}]$ will include several spatial periods of the emitting wave, –light shaded triangle in Figure 3.5(a)–. For that reason, a single line on k_x=0 is now repeated for $\pm 2\pi/\Delta x_l, \pm 4\pi/\Delta x_l, \ldots$, according to the shifted delta function in Equation (3.12) and shown in Figure 3.5(a). In terms of the reproduced wave field, each line represents a series of plane waves arriving at decreasing angles with increasing frequency. When the plane wave contributions are merged, a superposition of plane waves of different angles at different

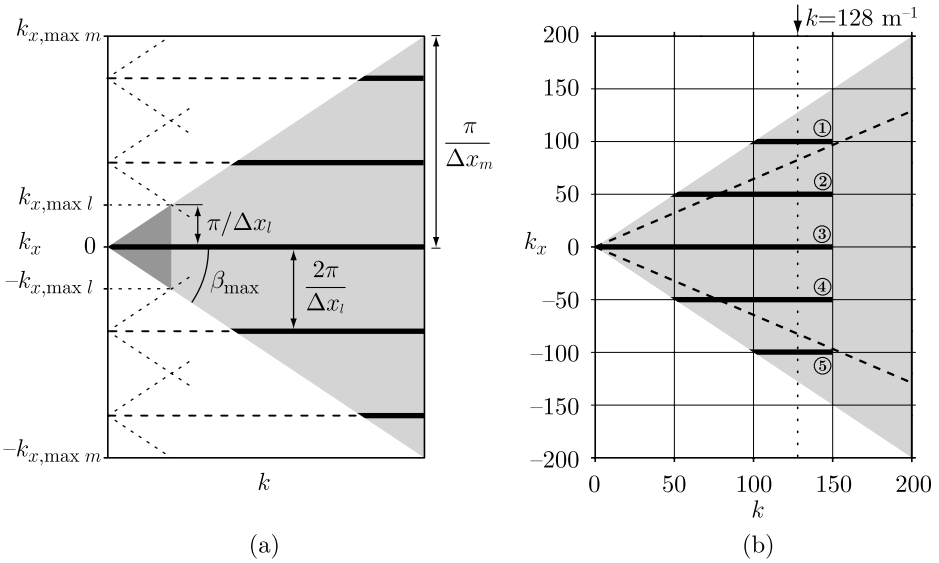

Figure 3.5. $k_x - k$ representation of a plane wave synthesized by a loudspeaker array and captured by a microphone array, both discrete. (a) Intervals of interest in the k_x domain. (b) Example plane wave, $\Delta x_l = 12.6$ cm, $\Delta x_m = 1.57$ cm and $f_s = 22$ kHz.

frequencies is created.

Evanescence Zone

The spatial resolution of the microphone array sets a light shadowed triangle area, whose aperture is determined by the maximum β. As shown in Figure 3.5(a), this triangle represents a visibility window which only allows display of spatial spectrum replicas in the high frequency range k. Out of this area, plane waves turn into evanescent waves since $k_x > k$ and thus, $k_z = \pm(k^2 - k_x^2)^{1/2} = \pm jk'_z$. As a result, the amplitude will decay exponentially in the z direction under the Sommerfeld radiation condition [Williams, 1999],

$$p(x, z, t) = Ae^{-k'_z z} e^{j(k_x x - \omega t)}, \tag{3.13}$$

which physically means that the projected trace velocity along the x axis is less than the speed of sound and no effective sensing occurs, due to the exponential decay of amplitude with $k'_z z > 0$.

Aliased Spectrum

If the reproduced wave field contains components at frequencies beyond the spatial aliasing frequency, Equation (3.10), sampling artifacts will be produced as new plane waves coming from different angles at different frequencies, according to Equation (3.12). The effects of such artifacts will start at a frequency k in which more than one spectral repetition is visible in the triangle of Figure 3.5(a). Then, all possible replicas that would cause aliasing must satisfy the condition:

$$\left| k_x - n\frac{2\pi}{\Delta x} \right| \leq k, \tag{3.14}$$

which is a modified version of the anti-evanescence condition. As a consequence, when the number of aliasing plane waves is known, and applying this condition for a given temporal frequency k, their incoming angles can be obtained as

$$\theta_{n(\mathrm{al})} = \arcsin \frac{k_x \pm n\frac{2\pi}{\Delta x}}{k}. \tag{3.15}$$

In section 3.2.4, an example with real values that illustrates this effect will be presented. If only a fixed temporal frequency is considered, a $k_x - k_y$ spatial frequency representation can be performed, as proposed in [Spors and Rabenstein, 2006]. It consists of a series of Dirac lines perpendicular to the k_y-axis that intersect with a circular Dirac pulse with radius k. This representation can be seen as a plane that intersects the $k_x - k$ representation of Figure 3.5(a) along a constant k line, where k is given by the Dirac pulse radius. Then, each plane wave inside the circular Dirac pulse or, alternatively, inside the triangle for the corresponding k can be understood as an aliasing contribution in both representations. The advantage in the representation proposed in this chapter is that it takes into account all temporal frequencies at a glance, thus allowing a frequency-dependent aliasing artifacts analysis.

Truncation Effects

In the preceding discussion, the limits of the gray triangle in Figure 3.5(a) are at an angle β of $\pm 45^{\mathrm{o}}$, which is equivalent to incident angles of $\theta = \pm 90^{\mathrm{o}}$. In order to generate such an extreme incidence angles, the length

of the emitting array must be infinite. However, in practice, arrays will be always of finite length, which introduces truncation effects that may modify the aliasing artifacts explained before. These effects can be considered by geometrical means, given that a plane wave will be reproduced only in a parallelepiped area in front of the array, whose width is the aperture of the array, height is infinite and inclination is the incidence angle of the plane wave, as described in [Spors and Rabenstein, 2006].

The effects of array truncation can be analyzed by means of the $k_x - k$ representation as it will be demonstrated below. Then, consider the geometry for an off-axis listener of Figure 3.6 and its corresponding representation. Accordingly, the maximum angle for a listener at a given position is calculated as $\theta = \arctan(l/d)$. Thus, aliasing plane waves whose incident angles are larger than the corresponding θ will be reproduced very faintly. In the representation, this behavior is observed in the decrease of β, which leaves certain spectra replicas out of the shaded triangle, in the evanescent zone. For the representation proposed in [Spors and Rabenstein, 2006], this limiting angle can be considered as to flatten the circular Dirac pulse horizontally so that the maximum α_{pw} is obtained as to reach the flat zone.

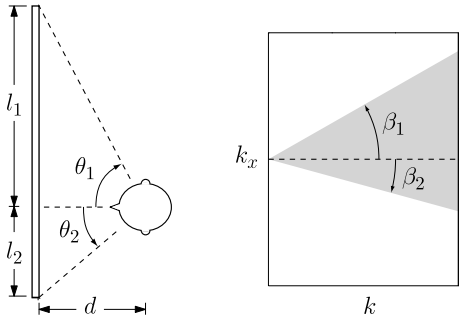

Figure 3.6. Geometry description of truncation and its effect in the $k_x - k$ representation for an off-axis listener.

The practical implication of this statement is that not all plane waves can be reproduced at any listener position, so truncation makes the aliasing effects depend on the listening point.

3.2.4 Example

In order to illustrate all the previous issues related to the interpretation of a $k_x - k$ representation, a numerical example with graphical interpretation is carried out. For this purpose, Figure 3.5(b) is discussed in comparison with Figure 3.5(a). In all the following figures, the wavenumber unit (m^{-1}) is dropped for simplicity.

Consider a plane wave that is bandlimited to 8.2 kHz and has been synthesized by a discrete loudspeaker linear array with $\Delta x_l = 12.6$ cm. The wave field arrives at normal incidence ($\theta = 0^{\mathrm{o}}$) to a linear microphone array of $\Delta x_m = 1.57$ cm. These two intervals will yield spatial Nyquist frequencies of $k_{x,\max l} = 25\ \mathrm{m}^{-1}$ and $k_{x,\max m} = 200\ \mathrm{m}^{-1}$ for the loudspeaker and microphone array respectively.

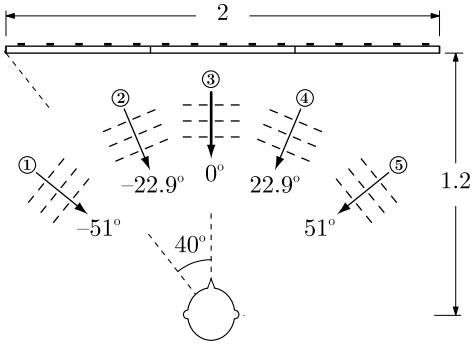

Figure 3.7. Desired and aliased plane wave angles for the example illustrated in Figure 3.5(b) at k=128 m^{-1}. For the depicted geometry, the only aliasing contributions are the ones labelled as "2" and "4". Dimensions in meters.

The example plane wave has been represented in a $k_x - k$ plot on Figure 3.5(b). A sampling frequency f_s =22 kHz was used so the maximum represented k is $2\pi f_s/(2c) \simeq 200\ \mathrm{m}^{-1}$. According to Equation (3.12), a series of replicas will be shifted $2\pi/0.126 = 50\ \mathrm{m}^{-1}$ with respect to the non-aliased spectrum at $k_x = 0$. Among the six possible replicas within the triangle representation, only four are visible because the signal is bandlimited to k =150 m^{-1} (8.2 kHz).

To illustrate that aliasing contributions consists of new plane waves with $\theta_{(\mathrm{al})}$ angles, according to Equation (3.15), that distort the desired wave field, let us consider a temporal frequency of 128 m^{-1} (7 kHz). As

indicated on Figure 3.5(b) in dotted line, at this particular frequency, four additional plane waves are reproduced, whose directions are $\pm 22.9^{\text{o}}$ and $\pm 51^{\text{o}}$, as depicted in Figure 3.7. This symmetry in the aliased angles is because an axial plane wave has been considered. Otherwise, symmetry is not maintained for aliased angles. For lower frequencies, for example f =3 kHz (k=55 m^{-1}), only two aliased contributions will be added to the desired wave field at $\theta_{(\text{al})} = \pm 65.1^{\text{o}}$. In the limit, for $k = 50$ m^{-1}, no aliasing occurs for this axial plane wave, although the limit for any incoming direction is set to the interval $\pm k_x = 25$ m^{-1}. In general, as the temporal frequency augments, the number of aliasing plane waves increases. Also, their aliasing angles $\theta_{(\text{al})}$ tend to narrow towards the desired angle, in this case, 0^{o}.

If the loudspeaker array comprises 15 transducers (total length 2 m) and the listening point is centered, 1.2 m in front of the array, truncation effects will modify the number of aliasing contributions. Now the listener point presents an angle of $\pm 40^{\text{o}}$ with respect to the array aperture, as shown in Figure 3.7, so a narrower triangle must be considered in the $k_x - k$ representation, as shown in dashed line in Figure 3.5(b). As a consequence to this limited reproduction area, the example plane wave discussed before ($k = 128$ m^{-1}, $f = 7$ kHz) will present only two aliasing contributions at $\pm 22.9^{\text{o}}$, since $\theta = \pm 51^{\text{o}}$ aliased contributions lays outside the dashed triangle. Figure 3.7 shows graphically how plane waves labelled as "1" and "5" point towards an empty reproduction area and thus, their energy will be low enough to be considered. For the second case study frequency ($k = 55$ m^{-1}, $f = 3$ kHz), no aliasing artifacts are present because the dashed line triangle in the $k_x - k$ representation does not include any spectrum replica. For this geometry, the aliasing frequency can be found as to apply $\theta_{\text{max}} = 40^{\text{o}}$ in Equation (3.10), resulting in 2.1 kHz. However, this increased f_{al} is associated with the lost of a wide range of incoming angles for virtual sources, from 40^{o} to the theoretical 90^{o}.

3.3 Experimental Setup

Once the fundamentals of the wavenumber domain representation have been presented, let us return to the study of MAPs, initiated in Chapter 2. For comparison purposes, three arrays have been built: firstly, an arrangement of three MAPs comprising 5 exciters each, secondly, a set of

five MAPs with 3 exciters per panel and, finally, a 5" dynamic loudspeaker array. Throughout this thesis, the panel with five exciters will be named as MAP5, whereas the panel with three exciters will be referred to as MAP3. Figure 3.8 shows the two MAPs used for the experiments.

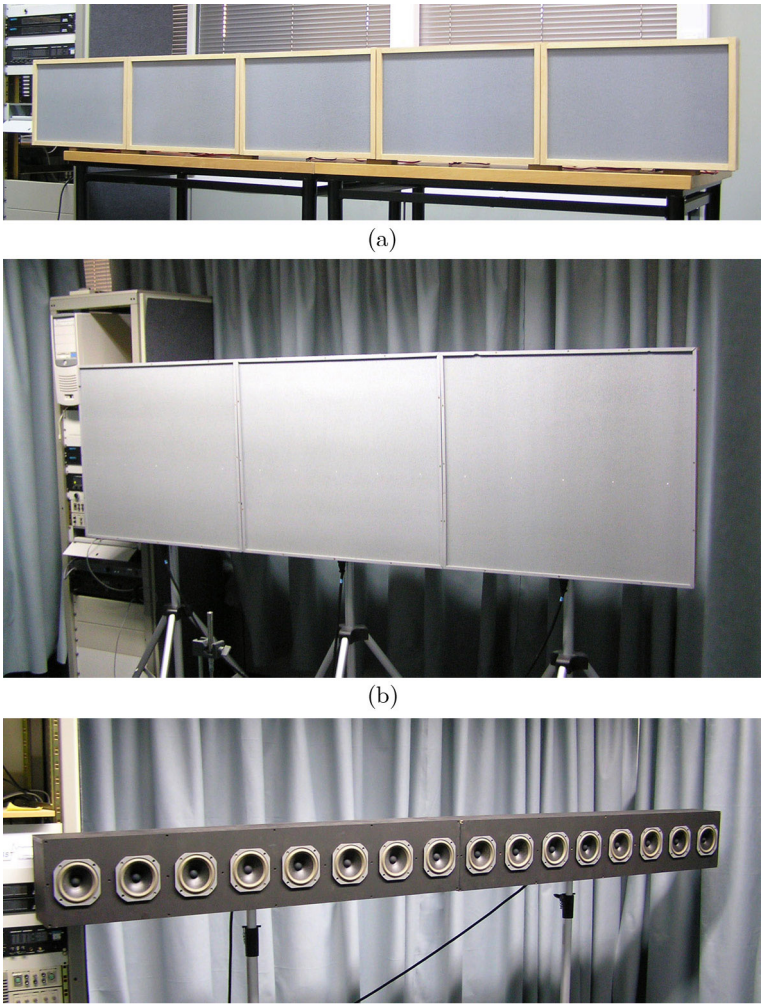

(a) (b) (c)

Figure 3.8. Picture of the MAP prototypes and the dynamic loudspeaker array. A total of 15 transducers are employed in all configurations. (a) Five MAP3. (b) Three MAP5. (c) Dynamic loudspeaker array.

All arrays present a transducer spacing of Δx =18 cm, thus the theoretical aliasing frequency is 950 Hz. In the following, the subscript l in Δx is dropped for simplicity.

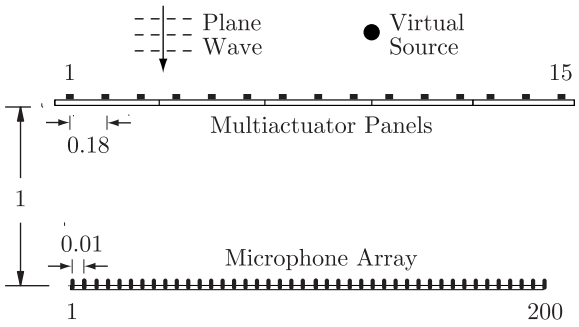

Figure 3.9. Experimental setup geometry for generating plane waves and WFS virtual sources. Dimensions in meters.

The MAPs used in this experiment present an outer skin thermoplastic material to a polycarbonate inner honeycomb core. The panel bending stiffness is 16.4 and 16 Nm in the x and y directions respectively and has an surface mass density of 0.89 kg/m^2.

Three experiments have been performed. In the first one, to study the transducer polar patterns, only the middle exciter/loudspeaker of the linear array reproduces a broadband signal. In the second one, the array generates spherical and plane waves at 0^o and 45^o using the WFS rendering algorithm. Finally, in the third experiment, the larger MAP5 are compared to the MAP3 small panels.

The recording stage consists of a 150 microphone array with 1 cm spacing that will sample the wave field on a parallel line according to the setup shown at Figure 3.9. For implementing such an array, a single 1/2" electrostatic microphone on a linear sliding table is used. This spacing allows a maximum recording frequency of 17 kHz (311 m^{-1}) without spatial aliasing. In all measurements, instead of generating an impulse signal directly, a MLS (Maximum Length Sequence) signal was used to minimize unwanted reflections [Vanderkooy, 1994]. Then, a two dimensional Fourier transformation was calculated on the microphone signals to obtain the wavenumber domain representation, as discussed in [Start et al., 1995].

3.4 Results and Discussion

In this section, the experiment results on MAPs and dynamic loudspeaker arrays are presented through the three case studies mentioned in the last section. In parallel with the experiments, simulations under the same conditions and geometry were made to gain knowledge on the fundamentals of the wavenumber domain representation.

3.4.1 Point Source from the Middle Exciter

As mentioned in the experimental setup, only the single central transducer is excited. Figure 3.10(b) shows the results of the simulation of an ideal point source located at the center of the loudspeaker array, according to geometry of Figure 3.10(a). At this distance, an omnidirectional point source radiation is recorded as a spherical wave. Since the wavenumber domain representation shows the temporal spectrum of each plane wave arriving at different angles, it is equivalent to a graphical plane wave decomposition. Hence, the $k_x - k$ representation of such a spherical wave is a dense distribution of lines corresponding to plane waves that starts at $k_x = k = 0$ and ends at the interval $k_x = [-198, 198]$. Such a limit is due to the geometry of the setup: a centered 1.5 m microphone array, away 20 cm from a single radiating source, captures plane wave components from $\theta = 0^{\text{o}}$ to the angle between the source and the first/last microphone. In this case, such an angle is $\theta_{\max} = \arctan(2.1/0.2) = 84.5^{\text{o}}$ and thus $\beta_{\max} = 44.8^{\text{o}}$, which corresponds to the sides of a triangle that goes from the origin to the $(\pm 198, 200)$ coordinates. For a geometry in which the maximum projected angle is 90^{o}, the energy will be contained in an isosceles triangle given by $k > |k_x|$. Out of this area, plane waves turn into evanescent waves and their amplitude decays exponentially, as stated in the introduction.

Figures 3.10(c) and 3.10(d) depicts the $k_x - k$ representation of a centered exciter on the MAP5 and a single dynamic loudspeaker that were used in the rest of the experiments. Since a single transducer does not create a sampled wave field, the variations in the gray level within the triangle are due only to the transducers directivity.

For the MAP5, there is an approximately constant level both in the k axis and in the k_x. Hence, the driven exciter generates a point source radiation and acts as a small loudspeaker, as shown by the aperture in the $k_x - k$ representation $k_x = [-185, 185]$, equivalent to a radiation aperture of $\pm 68^{\text{o}}$

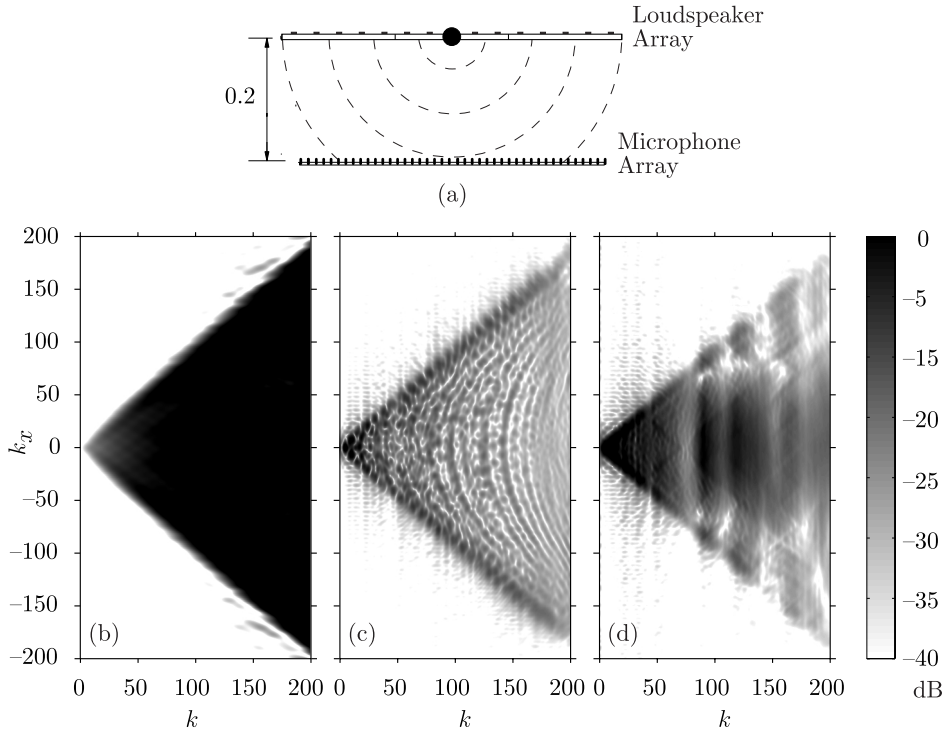

Figure 3.10. Wave field emitted by a single transducer in the $k - k_x$ representation. (a) Setup. (b) Simulation. (c) MAP5. (d) Dynamic loudspeaker. Dimensions in meters.

at 11 kHz. As a consequence, these panels do not exhibit a lobulate directivity, as seen on Figure 3.10(c), since waves travel in a distributed mode loudspeaker at a velocity below of that of the air [Angus, 2000a]. However, there are still some directional lobes in the response, as discussed in 2.2.2. In well designed MAPs, emitted and reflected waves are not correlated at the excitation points. For that reason, at these points, the panel is seen as infinite. However, the concentric pattern that is visible inside the triangle, and is repeated in the rest of the MAP measurements, may be a sign that the existing motion of the panel is not uncorrelated to the force applied by the exciters, and therefore it does not behave as an infinite plate.

For the dynamic array, energy is concentrated at the low end spectrum triangle since dynamic loudspeakers are mainly omnidirectional at these frequencies. As frequency increases some changes in the gray level can be

observed since the typical directivity of piston radiators is a lobulated pattern. If the piston on an infinite baffle model is considered [Beranek, 1954], omnidirectionality is maintained up to ka=3.83, where k is the temporal wavenumber and a is the radius of the piston. For higher values of ka, radiation consists of a main lobe and one or two side lobes that progressively narrow. The central black area represents such a main lobe and the spots above and below are the side lobes. The light gray that separates these areas is the first null of the Bessel function of the mentioned model and is located at $ka \sin\theta$=3.83. For frequencies above k=160 m^{-1}, the frequency response of the loudspeaker starts to roll off.

3.4.2 WFS Virtual Sources

Now, all transducers in the array are in operation, in order to apply the WFS algorithm for representing three different virtual sources: axial and 45^{o} plane waves, and an omnidirectional virtual source.

Axial Plane Wave

Axial plane waves are of great interest in this study as illustrated in the example of Section 3.2.4. Spatial periodicity in the $k_x - k$ domain can easily be observed if the reproduction stage emits broadband plane waves. For generating axial plane waves, all exciters/loudspeakers reproduce the same signal in the setup of Figure 3.11(a). The simulated wavenumber domain representation, and the measurements for both arrays emitting an axial plane wave are shown in Figures 3.11(b), 3.11(c) and 3.11(d). As expected, there are components at zero k_x in both arrays and these are repeated in the spatial axis with periods that depend on the spacing of the transducers in the array.

In the results for the MAP5, the repetition pattern is clearly seen. Several lines of constant spatial frequency appear at $k_x = \pm 34$, ± 68 and ± 102 m^{-1} as in the simulation. This is due to the fact that MAPs emits energy in a broad angle, quasi omnidirectional, which makes MAPs very suitable for WFS reproduction. This point source radiation has, however, some disadvantages when aliasing effects are considered: the aliased plane wave components, which introduces non desired waveforms, are reproduced up to high angles and frequencies. For example, if $f = 7$ kHz is considered again, the k =128 m^{-1} gray line of Figure 3.11(c) shows how two new plane waves arrive at 15.8^{o} and 32.9^{o} directions.

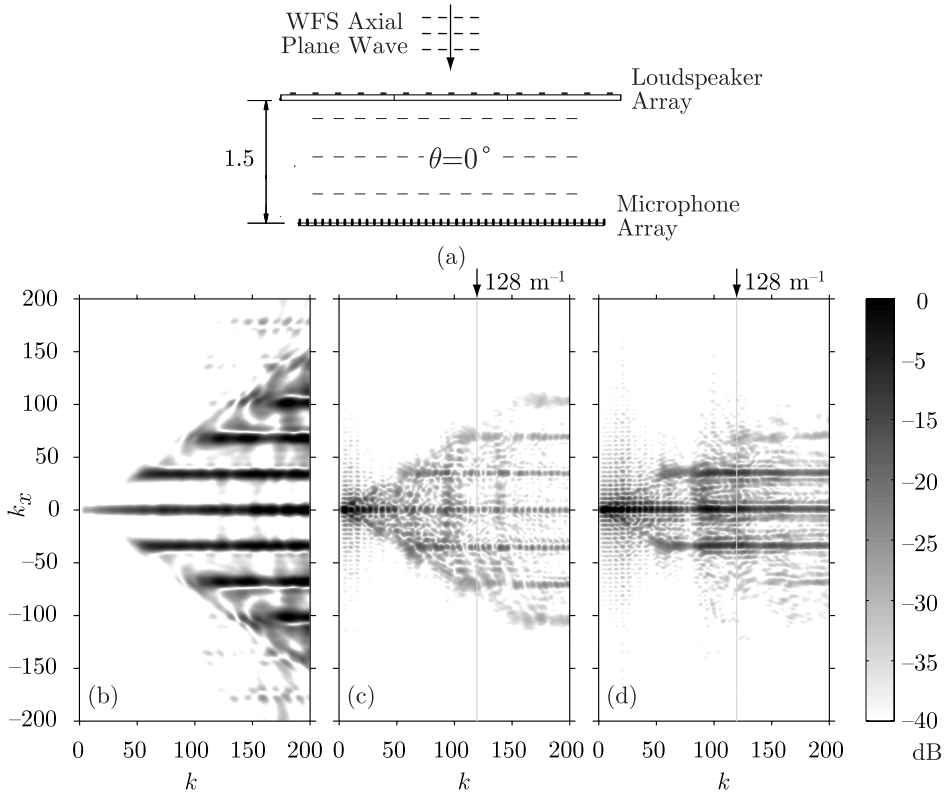

Figure 3.11. Wave field of an axial plane wave in the $k - k_x$ representation. (a) Setup. (b) Simulation. (c) MAP5. (d) Dynamic loudspeaker. Dimensions in meters.

For the dynamic loudspeaker array, only the first replica has considerable level, whereas the second is very faint, which means that directivity does not fulfill the point source radiation requirements but, in turn, there are few aliased components that contaminate the desired wave field.

Hence, aliasing artifacts can be affected by two characteristics.

1. First, as discussed before, by truncation effects, which are due to geometry, and limit the spatial resolution capacity of loudspeaker arrays.

2. Second, by transducer directivity, which restricts the listening area and thus, the incoming aliased waves.

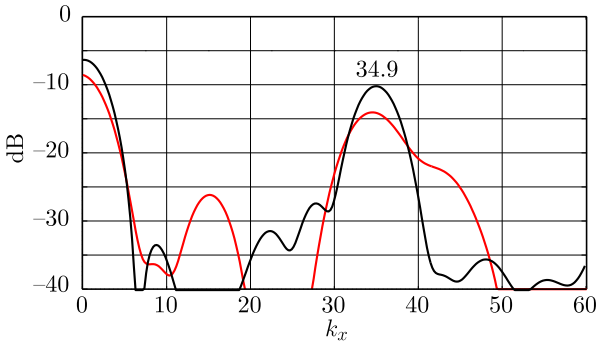

Figure 3.12. Representation of the positive spatial frequency k_x for a k =128 m^{-1} section of Figure 3.11 for MAP5 (black) and dynamic loudspeaker array (red).

The aliasing frequency for a given geometry can be obtained by analyzing the variation of the spatial frequency k_x for a given temporal frequency k. Now, let us study this variation by choosing a temporal frequency k and observing the changes in the spatial frequency k_x. Due to the vertical symmetry in the representation of Figure 3.11, only the positive axis is addressed. Then, Figure 3.12 shows the positive spatial frequency for $k = 128$ m^{-1} for the MAP5 and the dynamic loudspeaker array, where the first maximum is located near k_x=35 m^{-1}.

In terms of aliasing effects, the maximum spatial frequency that defines the aliasing frequency is simply half the distance between two consecutive spatial replicas ($\pi/\Delta x$). In this case, such a limit is approximately $k_{x,\max l}$ =17 m^{-1}, therefore, $f_{\text{al}} = ck_{x,\max l}/(2\pi)$ =950 Hz, which agrees with the result of Equation (3.10) when applying Δ_x=0.18 m in tangential incidence.

45º Plane Wave

The following experiment involves plane waves arriving at 45º. In general, the $k_x - k$ representation of a non sampled plane wave with direction θ is a single line that fulfills the relation $k_x = k \sin\theta$. Therefore, choosing any point on this line, it is a simple matter to calculate the direction of arrival of the plane wave from the two coordinates (k,k_x).

As discussed in previous sections, in an aliased reproduction, new plane waves distort the desired wave field. Figure 3.13 presents the setup, the simulated wavenumber domain representation and the measurements for

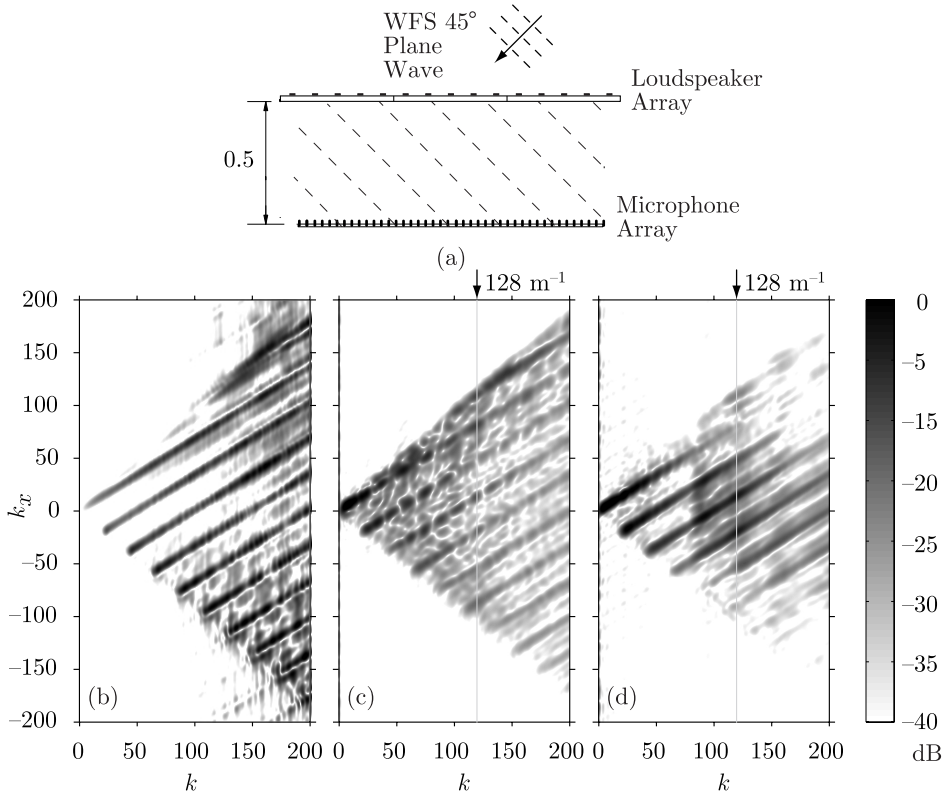

Figure 3.13. Wave field of plane wave arriving at 45° in the $k - k_x$ representation. (a) Setup. (b) Simulation. (c) MAP5. (d) Dynamic loudspeaker. Dimensions in meters.

the MAP and the dynamic loudspeaker array. Now, a tilted line pattern is observed as expected by the incident angle. For comparison, an analysis for both arrays is made again at 7 kHz, indicated in the figures by the k=128 m^{-1} gray line.

For the MAP5, seven new incoming plane waves, apart from the one desired, at 45°, are reproduced, according to the replicas in Figure 3.13(c) at k=128 m^{-1}. These are −67.8°, −40.8°, −22.4°, −6.3°, 9.4°, 25.8° and 78.3°. However, truncation effects caused by the geometry setup, will affect incoming angles greater than the angle between the axis and the array extremity, according to Figure 3.6. Since the measurement process involves the recording at different positions on a 1.5 m line, truncation effects are

given by the angle between the first loudspeaker and the last microphone. According to the experimental setup geometry of Figure 3.9, such an angle is directly arctan(2.1/0.5) =76.6°. Then, a graphical representation of the truncation effect for a single listener can be performed if the distance d is modified to account for a true 76.6° angle. Such an illustration is given in Figure 3.14, where the 78.3° plane wave, in dashed line, is not reproduced by truncation.

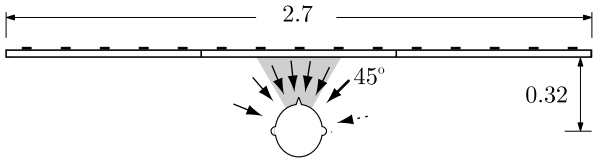

Figure 3.14. Desired and aliased plane wave angles for a 45° plane wave in Figure 3.13 at k=128 m^{-1}. For the measurement geometry, six aliasing components are present in the MAP5, while, in the dynamic loudspeaker array, directivity allows only to reproduce the four components in the gray wedge. Dimensions in meters.

Dynamic loudspeaker array presents, on the contrary, a strong on-axis directivity which restricts the number of aliased components. Moreover, directivity can even impede generation of the desired plane wave, but only aliased contributions. As shown as a gray line in Figure 3.13(d), the loudspeaker array spatial resolution for k=128 m^{-1} is k_x=±60 m^{-1} or, alternatively, ±30°. Then, at this frequency, only the four middle aliased angles −22.4° to 25.8° are reproduced, whereas the original 45° plane wave is not, since it is out of the angular range. In Figure 3.14, the gray wedge illustrates the loudspeaker directivity for a listener facing the center.

Thus, the restricted spatial resolution of directive arrays affects, together with truncation, the aliasing artifacts for a given listener position. This statement is also demonstrated in the case of axial plane waves reproduction, in the latter section.

Virtual Point Source

Now, a virtual point source 0.5 m behind the array is WFS rendered by means of MAPs and dynamic loudspeaker arrays. Figure 3.15 shows the setup and the wavenumber domain representation of the synthesized wave

field, both simulation and measurement.

In terms of phantom image rendering, both arrays work properly up to the theoretical aliasing frequency of $k = 17.4$ m^{-1}, but important differences in level are observed in the dynamic array from this point up to k=130 m^{-1} due to the array directivity, as discussed before.

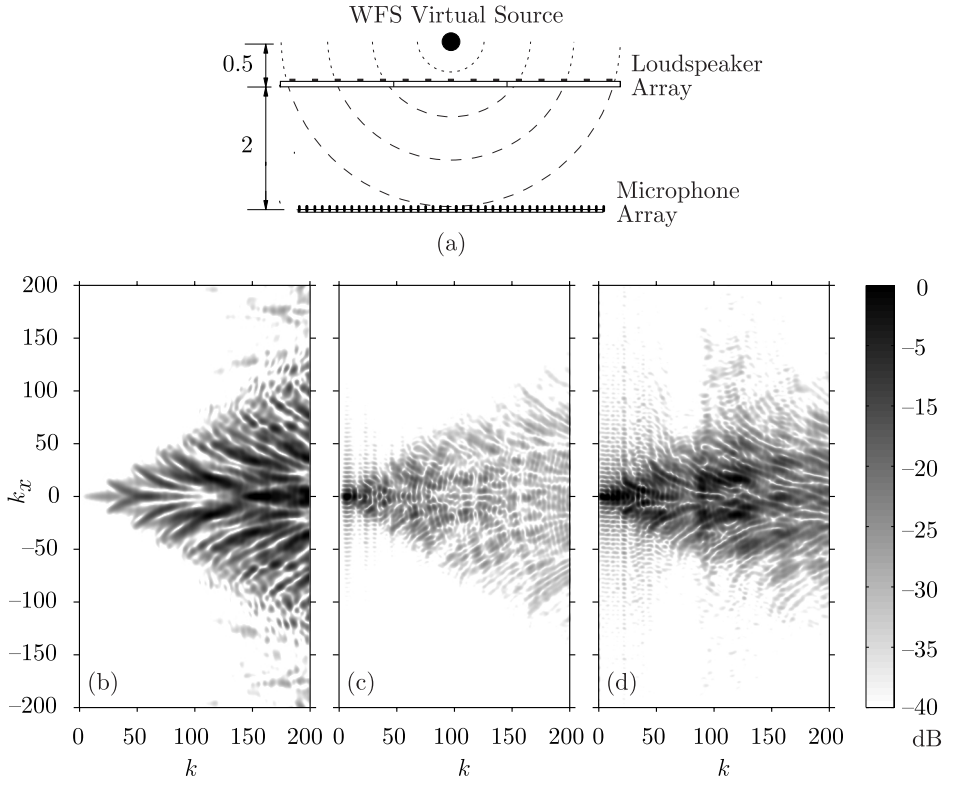

Figure 3.15. Wave field of a synthesized virtual source, centered 0.5 m behind the array, in the $k-k_x$ representation. (a) Setup. (b) Simulation. (c) MAP5. (d) Dynamic loudspeaker. Dimensions in meters.

Figure 3.15(a) shows a virtual source, centered, located 2.5 m far from the microphone array. According to this geometry, the angle between the first/last microphone and the source is 16.7° so the expected k_x interval at $k = 200$ m^{-1} would be $[-57, 57]$. Instead, the simulation shown in Figure 3.15(b) exhibits an interval of $[-145, 145]$. This is due to fact that energy displayed in a wavenumber domain representation is not related to

the virtual source angle, but to the angle between the first loudspeaker and the last microphone. For this setup, this is given by $\theta_{\max} = \arctan(2.1/2) = 46.4^{\circ}$, which corresponds to a maximum spatial frequency of 145 m^{-1}, as mentioned above.

With regard to MAPs, they exhibit a wide radiation as to judge by triangle aperture in Figure 3.15(c). Since a single exciter creates an omnidirectional radiation (see Figure 3.10(c)), when several are working to achieve a WFS image, there is no undesired interference that would contaminate the wave field. Then, driving signals are reproduced in such a way that the wave components are correctly merged to create a point source successfully.

On the other side, dynamic loudspeaker array representation starts to narrow in the high frequency end due to directivity, as shown in dark gray level in Figure 3.15(d). As a consequence, off-axis listeners would not perceive the centered source in a proper way, since there are components that do not merge into a unique wave front.

3.4.3 Comparison between MAPs

Over the past years, many MAP prototypes have been developed for WFS applications. Design parameters of MAPs are: panel dimensions, panel material, fixing points and mechanical boundary conditions. Regarding its use for WFS, exciter spacing was the key parameter since it sets the aliasing frequency, as with dynamic loudspeaker arrays. However, to the author knowledge, no analysis has been performed on the implications of splitting the panels into smaller pieces to accommodate less exciters per panel. This analysis is addressed in this section by considering another MAP prototype, different than the one used in the previous experiment, which exhibits the same transducer spacing but it is divided into five panels of three exciters each. The same experiments carried out with the MAP5 is now performed with the equivalent MAP3 arrangement.

Figure 3.16(a) shows the wave field emitted by a single centered exciter in a MAP3 at d=0.2 m. A rise in the on-axis directivity with respect to the MAPs of the preceding sections is observed for this small panel. However, the limits of the triangle set a $\theta_{\max} \simeq 84^{\circ}$, which is consistent with the geometric setup. Besides, a concentric circular pattern is observed again in the radiation in the same fashion as the same exciter on a larger

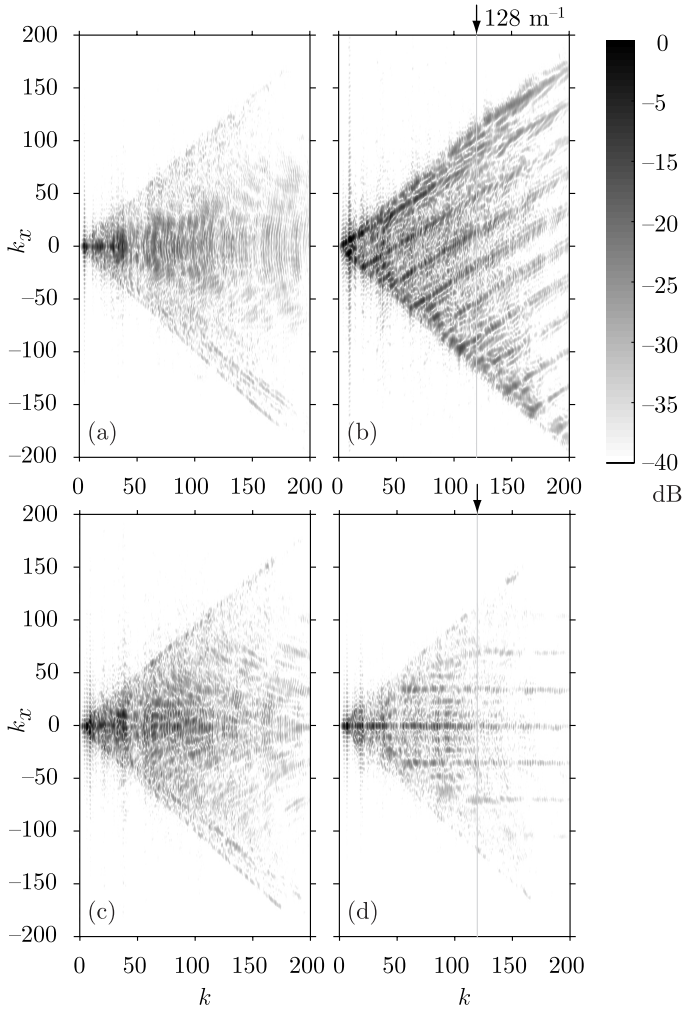

Figure 3.16. Wave field emitted by MAP3 in the $k - k_x$ representation. (a) Single transducer. (b) WFS 45° plane wave. (c) WFS omnidirectional virtual source. (d) WFS axial plane wave.

panel (see Figure 3.10(c)). In Figure 3.16(b), the wavenumber domain representation of a 45° plane wave reproduced by small MAP3 is presented. Almost imperceptible, the discussed spectral pattern also appears in this experiment in the same way that spectral replicas due to transducer spacing do.

Finally, a WFS centered virtual source is represented in the $k_x - k$ plot of Figure 3.16(c). From the gray level within the triangle, it can be concluded that the point source is not properly resolved due to specific MAP directivity.

Additional Aliasing Artifacts in Small Panels

With regard to the WFS axial plane wave, Figure 3.16(d) presents the results for a measuring distance of 0.5 m. Between the lines that already appear in the large MAPs of Figure 3.11(c) at spatial frequencies of k_x =0 and 34.9 m^{-1}, two new replicas are now noticeable. This pattern can be analyzed in detail if the variation in k_x is analyzed again for $k = 128$ m^{-1}, as shown in Figure 3.17. The peak at $k_x = \pm 34.9$ m^{-1} is the counterpart of that of the large MAP, as observed in continuous line in Figure 3.12. For the range plotted in the figure, new four maxima appear at spatial frequencies of k = 11.6, 23.3, 46.5 and 58.2 m^{-1}. The last two maxima present smaller amplitudes due to MAP directivity.

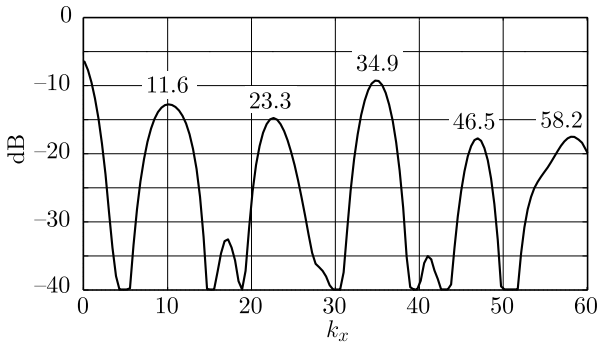

Figure 3.17. Representation of the positive spatial frequency k_x for a k =128 m^{-1} cut of Figure 3.16(d).

The reason of this new spatial pattern can be found in the MAPs boundary conditions. Although the total length of both MAPs coincides, clamped frames set now four zones in the exciter line that will not move, regardless of the input signal. Such boundary conditions play a role in both the lower vibration mode of the panel but also on the spatial sampling process of MAPs. This effect is not present in dynamic loudspeakers, where the housing is not moved by loudspeaker cones, thus no change in radiation is observed as a function of the number of transducers per array.

As observed in the wavenumber domain representation, these new spatial frequencies must be created by an additional spatial sampling. Figure 3.18 shows the origin of such new replicas in k_x: the panels themselves, as being clamped by their edges, are acting as sources. This creates a new sampling spacing of Δx_p, the distance between center panels. Since Δx_p is larger than the exciter spacing Δx_l, the spatial replicas are located at smaller values of k_x.

The geometry of MAPs in this chapter allows to join several panels while maintaining the transducer spacing because the first/last exciter is located at $\Delta x_l/2$ from the edge. As a consequence, both sampling distances are related in such a way that the peak at $k = 34$ m^{-1} is produced both by Δx_l and by Δx_p, as seen on Figure 3.18.

Although this behavior is expected for any reproduced wave field, it is more noticeable for axial plane wave radiation. In order to generate such plane waves, all transducers must act in phase. When all exciters move the panel with the same excitation signal, the panel acts as a whole vibrating surface, except for the points corresponding to the panel edges.

In the larger MAPs used before, there was also a sampling distance due to the panels, to be more precise, Δx_p =0.9 m. However, this spatial sampling creates a sequence of weak peaks separated 7 m^{-1}, which is interpreted as a constant background level in k_x. In general terms, the amplitude of each replica is related to the number of sampling points that creates it, as observed in Figure 3.18. For example, in the current MAP5, 15 contributions (exciters) form the spatial frequency series of $k_x = \pm 34$, ± 68 m^{-1} ..., whereas only 3 contributions (panels) do on the series of $k_x = \pm 7$, ± 14 m^{-1} .... This is the reason why the maximum at 34 m^{-1} in Figure 3.17 is several dB above the rest of aliased components.

The practical consideration of this additional sampling process has the consequence that new undesired plane waves will arise on the reproduced wave field. More precisely, between two consecutive replicas due to the transducer spacing, two other contribute to the wave field, as shown in Figure 3.19(b). Also, the temporal frequency at which they are reproduced is below the aliasing frequency due to Δx_l, Equation (3.10). To calculate the new f'_{al}, consider half of the first replica spatial frequency $k_{x,\max p}/2$:

$$f'_{\mathrm{al}} = \frac{c}{2\pi} \frac{k_{x,\max p}}{2}, \tag{3.16}$$

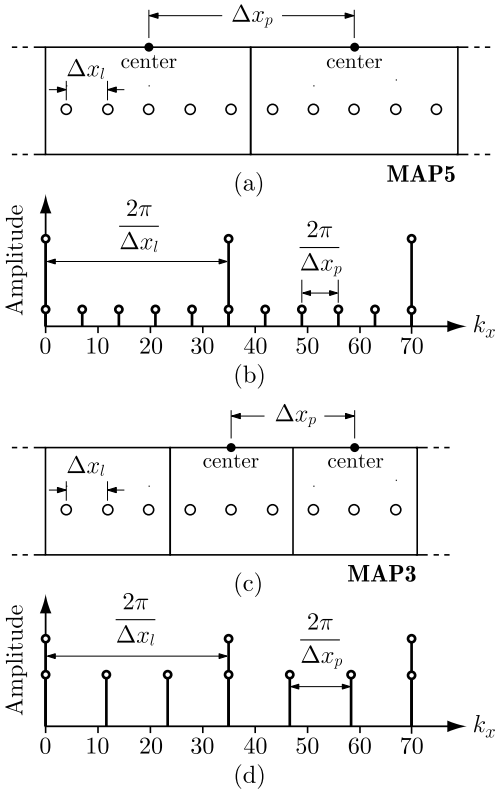

Figure 3.18. Sampling spacing of exciters and panels in a MAP arrangement. (a) Three MAP5 arrangement where Δx_p =0.90 m. (b) Graphical interpretation of the variation of k_x for large panels, measured in Figure 3.12. (c) Five MAP3 arrangement where Δx_p =0.54 m. (d) Graphical interpretation of the variation of k_x for small panels, measured in Figure 3.17. Both arrangements present an exciter spacing of Δx_l =0.18 m.

where $k_{x,\max p}$=11.6 m^{-1}, according to Figure 3.17 and, thus f'_{al}=316 Hz, which is substantially lower than 950 Hz. However, the psychoacoustic validity of this limiting frequency will depend on the energy that those new aliasing artifacts would present, which, in turn, depend on the rate between the total number of exciters and panels. For the above results, the spatial color fluctuations in the aliased wave field should be addressed by subjective experiments, in order to asses the perceptual consequences of aliasing.

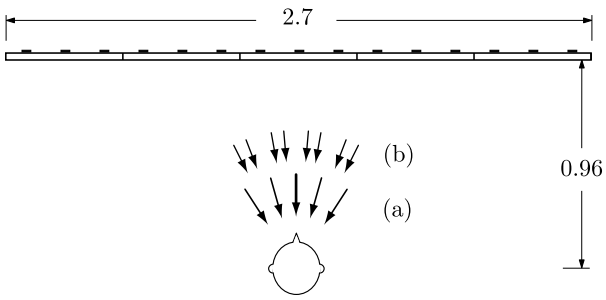

Figure 3.19. Effect of MAPs split on the number of aliased components. (a) Desired axial plane wave and four aliasing contributions at $\pm 15.8^{\circ}$, $\pm 32.9^{\circ}$. (b) Additional eight contributions at $\pm 5.2^{\circ}$, $\pm 10.4^{\circ}$, $\pm 21.3^{\circ}$ and $\pm 26.9^{\circ}$ due to splitting panels. For clarity, the angular range has been restricted to $\pm 35^{\circ}$. Dimensions in meters.

3.5 Conclusions

A methodology for the analysis of the radiation characteristics and spatial performance of loudspeaker arrays for WFS reproduction has been presented in this chapter. The analysis is performed in the space-time wavenumber domain, where the acoustic source radiation is interpreted as a multidimensional signal.

The effect that spatial sampling both in the reproduction and in the receiving stage has on the wave field was also addressed. For this purpose, the proposed method evaluates the spatial and temporal frequencies of the wave field via a linear array of microphones. The obtained multidimensional signal is plotted in a $k_x - k$ graphical representation, where limit spatial frequencies due to the reproduction and receiving sampling spacing can be observed. Moreover, the conditions for evanescent waves and the aliased spectrum can easily be analyzed. The sampling artifacts that spatial aliasing cause and the associated parameters that modify them were also studied. These are, mainly, truncation effects due to the geometric arrangement and transducer directivity, which restricts the listening area. To illustrate the potentials of the tool, a numerical example with graphical interpretation was carried out.

Once the methodology was established, several experiments were performed: first, dynamic loudspeaker arrays were compared with MAPs and,

next, large MAPs were compared with small MAPs in order to evaluate the effect of the panel size. In parallel, numerical simulations were made to clarify the experimental results. To that end, besides the dynamic loudspeaker array, two MAP arrangements have been design and built with similar characteristics as the current prototypes presented in Section 2.3.2. The panel was a sandwich of polyester film bonded to an polycarbonate inner honeycomb core; the same material as with Sonic Emotion panels, since a proper acoustical behavior was experienced in the preliminary tests.

As explained next, some valuable conclusions have been obtained. The reconstructed wave field presents spatial aliasing artifacts at high frequencies. In Section 2.3.3, it was reported that the region above aliasing frequency is characterized by oscillations both in frequency and space. The tool proposed in this chapter characterizes such aliasing artifacts as a superposition of undesired plane waves with different incidence angles at different frequencies. The number of such aliased contributions depends on two parameters when practical implementations are considered: on the one hand, by truncation effects due to the finiteness of the loudspeaker array, and, on the other hand, by array directivity, as experienced in dynamic loudspeaker arrays and small panels. Both parameters limitat the spatial resolution of the arrays.

The consequence of truncation effects and array directivity is to limit the reproduction area and thus, lead to a dependence of the aliasing artifacts on the listener position. Furthermore, the method provides useful information on angle-dependent radiation of transducers in an array and can confirm if each exciter on a MAP is acting as a single loudspeaker to correctly recreate the wave field. According to MAP historic evolution, as described in Section 2.3.1, independence between exciters on a single panel is essential to consider MAPs as an alternative to dynamic loudspeaker arrays.

Finally, as pointed out in Section 1.2, it has been demonstrated that the use of small panels that accommodate less exciters has implications on the reproduced wave field. Since the contour of panels present no motion when radiating, new aliasing artifacts at frequencies below those of larger panels or dynamic loudspeaker arrays will appear. Then, for WFS reproduction, it is more convenient to split the panels in the least sections possible in a given reproduction scene. Moreover, in large panels, vibration modes are present in high number, and they extend to the low end of the spectrum.

In terms of reproduced wave field, large MAPs are more suitable since the distance between panel centers does not cause noticeable aliasing artifacts at frequencies below that given by the exciter spacing.

4 Edge Boundary Conditions

4 Edge Boundary Conditions

The panel of a MAP vibrates in a complex pattern over its entire surface due to the mechanical excitations of many transducers. For a DML there are up to four optimal driving points in the central part of the panel that create an even distribution of modes and a high modal density. However, in MAPs such driving points are no longer located in optimal positions, but evenly distributed on a line to fulfill the requirements of the WFS algorithm. In terms of the independency between exciters to correctly reproduce a synthesized wave field, this setup poses no problem, as shown in the preceding chapter. However, MAPs are usually arranged in a landscape orientation to extend the listening area. With such a configuration, the first and last exciters on a panel are located very close to the panel edges in such a way as to have a continuous distribution of exciters evenly spaced. Furthermore, the excited vibration modes on the edge exciters is lower than on middle exciters. In this chapter, the influence of the edge boundary conditions on MAP radiation is addressed.

4.1 Introduction

This chapter deals with the impact of the edge boundary conditions on the radiated wave field by means of an empirical study. The aim is not

the underlying physics on plate theory, but to experiment with practical boundary conditions to form a viable technology for a MAP frame. Since the panel is usually placed in a baffle to avoid back to front cancellation, its edges must be supported in the frame in some boundary condition. Elastic boundaries are addressed for their flexible features. Three elastic materials have been used as representative of the range of available materials to support the panel. In addition, the classical clamped and free boundary conditions have also been tested in the laboratory for comparison purposes.

The outline of this chapter is presented as follows. Section 4.2 discusses the different ways of attaching the panel to the frame along the edges. Both pure boundary conditions, such as clamped or free, and three edge conditions based on elastic boundaries, are presented. The experimental setup is detailed in Section 4.3. Experimental results and discussion of MAPs when reproducing several stimuli are given in Section 4.4. On-axis and directivity responses are presented for single exciter operation. In addition, spherical and plane waves are measured in the wavenumber domain by a space and time sampling, according to the setup described in Section 4.3. Finally, Section 4.5 concludes the chapter.

4.2 Panel Edge Boundary Conditions

In this section, the different ways of supporting the panel is discussed. Rectangular plates are generally classified in accordance with the type of support used [Timoshenko and Woinowsky-Krieger, 1959]. The three basic boundary conditions applied to a plate edge are Free (F), Simply Supported (SS) and Clamped (C) edges, also known as built-in plates. The ideal free condition implies that the structure is floating in the air without support of any kind. If such a condition is satisfied, no reaction forces arise along the edges: there are no bending and twisting moments, and also no vertical shearing forces. At the other extreme, the clamped condition is achieved by grounding the structure with well-tightened devices that prevent the deflection of the structure at the supports. In this case, several reaction forces are created along edges: two forces, normal and perpendicular to the support direction, and a bending moment perpendicular to the plane structure. In between, there is the simply supported condition, which behaves as a clamped edge but without bending moments because edges can rotate freely with respect to the edge line.

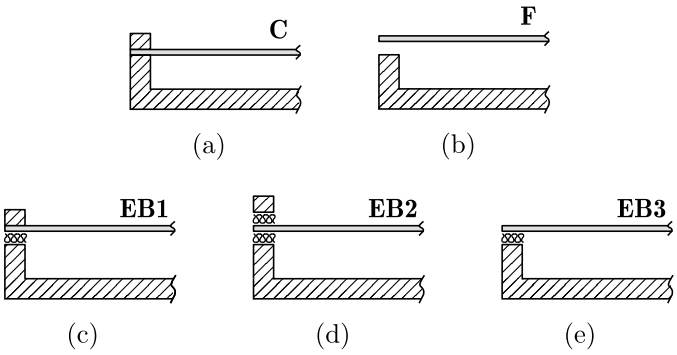

Figure 4.1. Section detail of the edge boundary conditions under test. (a) Clamped. (b) Free. (c) Elastic Boundary type 1. (d) Elastic Boundary type 2. (e) Elastic Boundary type 3.

In addition, other type of boundary conditions appear as a result of combining the above conditions [Ugural, 1999]. For example, the mixed supported conditions have clamped, simple supported and free at different edges. There are also the point supports, which consist of a plate supported by intermediate points.

However, the boundary condition that involves some sort of elastic damping is known as Elastic Boundary (EB). Plates on elastic boundaries are supported by elastic supports which resist certain type of bending [Leissa, 1999]. Its mechanical model is equivalent to a plate supported elastically by springs uniformly distributed along its edge. Hence, two reactions arise: deflection and edge rotation are opposed by linear and spiral springs having a certain degree of distributed stiffness. Because of the flexible features on edges, elastic boundaries are suitable in DML loudspeakers for audio reproduction.

In the technical literature, DML and MAP models have been presented with simply supported edges: [Prokofieva et al., 2002a] (for the baffled loudspeaker) [Bai and Liu, 2004] (adhesive tape to fix boundaries in the laboratory), [Zhang et al., 2006], or combined with free edges: [Prokofieva et al., 2002a] (for the unbaffled loudspeaker), [Bai and Huang, 2001].

Nevertheless, both free and simply supported edge conditions have disadvantages to form a viable technology for a MAP frame. On the one hand, the free condition can be approximated by supporting the structure on very flexible springs, which gives raise to a free radiating panel in a full-space

radiation. However, when observing the typical polar response of a free DML, a reduction of pressure in the plane of the panel is noticed, due to the cancellation effect of acoustic radiation at or near the edges. For that reason, the panel is usually placed in a baffle, where radiation due to the rear part of the panel becomes contained. On the other hand, simply supported conditions must contain a certain degree of frame grounding if the panel is to be held. This problem can be confronted by on pseudorandomly diffusing the boundaries between pure clamped and free, in a special type of Mixed Boundary Condition suggested by [Angus, 2000b]. Unfortunately, such a condition does not present a reliable fixing frame since part of the panel is suspended in the air.

Because of these practical drawbacks, this work is focused on the study of elastic boundaries as edge boundary conditions that can form the basis of a closed back MAP technology. For that purpose, three configurations are analyzed, covering the practical interactions between panel edges and housing. Elastic Boundary types 1 and 2 consist of a modification of the clamped conditions although including elastic materials in one or two sides of the panel. Elastic Boundary type 3 is formed by a simply supported edge but with an elastic material between panel and housing. In the following, elastic boundary types 1, 2 and 3 will be referred to as EB1, EB2 and EB3, respectively. Figure 4.1 shows a graphical representation of clamped, free and these elastic boundaries. For comparison purposes, two different elastic materials have been used, with enough elastic differences to become representative of hard and soft materials. Details on such elastic boundaries used in the experiments are addressed in the next section.

4.3 Experimental Setup

The impact of the edge boundary conditions on the radiation of MAPs is analyzed by considering an arrangement of MAPs in the laboratory which can change their supporting properties. Then, on-axis response and directivity measurements, and a space-time wavenumber domain analysis by sampling the created wave field, is performed. A detailed description of the experimental setup is given below.

4.3.1 MAPs

The emitting stage is composed of an arrangement of five MAP3, introduced in Section 3.3. With such a multiple small MAP configuration, it was intended to enhance the effect that different boundary conditions may have on the system. Alternatively, a larger MAP, including the same number of exciters would only have boundaries at the extent of the panel, far beyond the position of exciters, and their impact would be more difficult to detect. Details on the geometric description of the experimental setup are given in Figure 4.2.

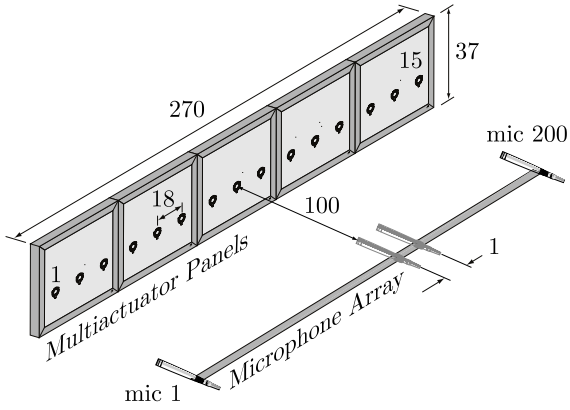

Figure 4.2. Experimental setup geometry for the analysis of the edge boundary conditions impact on the radiation. Dimensions in centimeters.

4.3.2 Assembling Edge Boundary Conditions

As stated previously, the edge boundary conditions based on elastic boundaries are of great interest to form a MAP frame technology. For comparison purposes, both clamped and free conditions have also been tested because of distinctive characteristics. Figure 4.3 shows a pictorial description of the experimental boundary conditions. Note that the MAPs in this experiment maintain the same sort of boundary condition along their four sides.

To achieve a clamped condition in the laboratory, no deflection must occur at any point along the boundary. If this requirement is not satisfied, a simply supported condition will arise instead. As a consequence, the portion of the panel to be clamped by the tight structure is more than twice

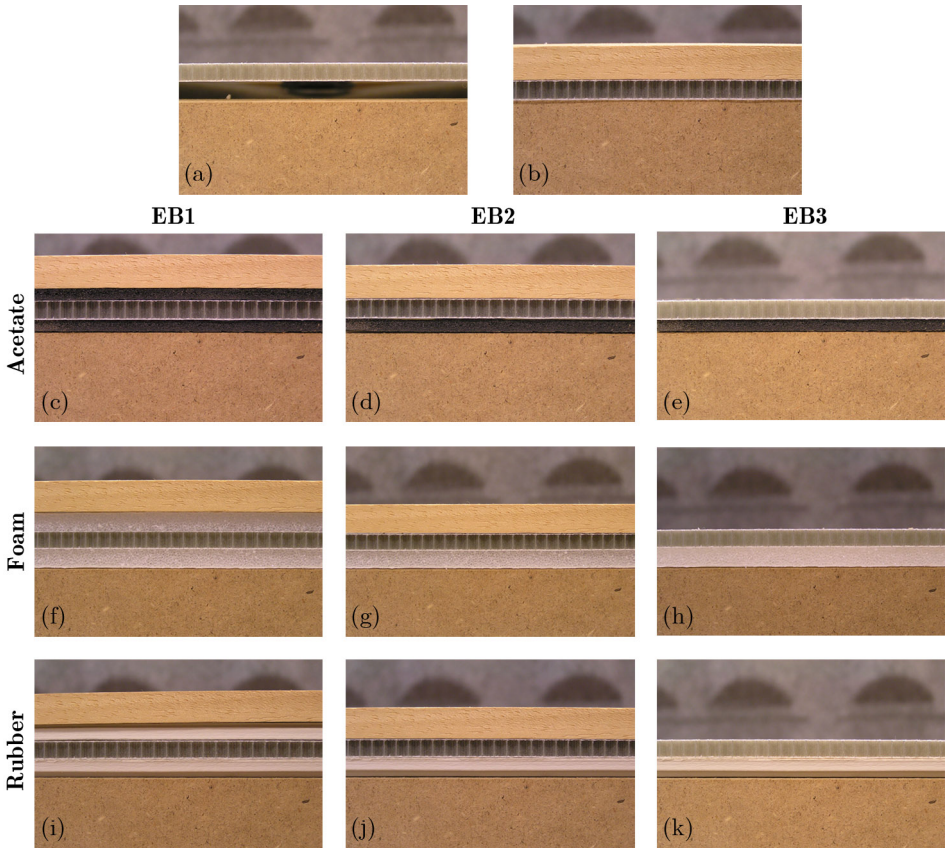

Figure 4.3. Pictorial description of the edge boundary conditions under test. (a) Free. (b) Clamped. Acetate in (c) EB1, (d) EB2, and (e) EB3. Foam in (f) EB1, (g) EB2, and (h) EB3. Rubber in (i) EB1, (j) EB2, and (k) EB3.

the width of the panel for the experiments. On the other hand, the free condition can be approximated by suspending the panel in the air with soft rubber bands, as suggested in [Hambric, 2006], [Raichel, 2006] and shown in Figure 4.4. This suspension in the air has been applied individually to each of the five MAPs under test, avoiding contact between adjacent sides. Additionally, for a proper comparison, the back housing that is present in the rest of boundary conditions, is also considered for the free condition. To that end, the housing is placed several millimeters below the panel to absorb the back radiation while allowing free movement at edges. Special

effort has been made to recreate such conditions in the laboratory so that presented measurements will reflect their impact on MAPs' radiation.

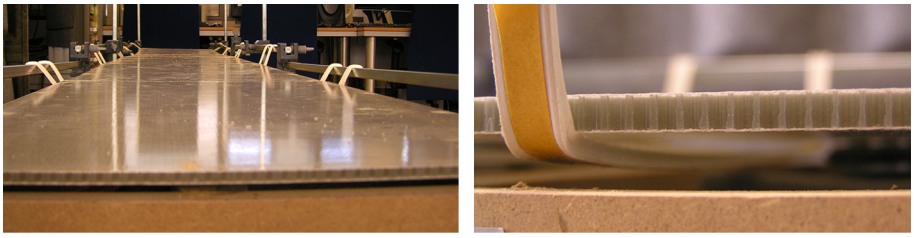

(a) (b)

Figure 4.4. (a) Approximate free condition by suspending the panel on air with soft rubber bands. (b) The housing is placed underneath the panel to absorb the back radiation.

4.3.3 Elastic Materials

Three types of elastic materials have been employed to develop the elastic boundaries. The first one is a Ethylene Vinyl Acetate foam (EVA), the second one is a Low Density Polyethylene foam (LDPE) and the third one is an Ethylene Propylene Diene Monomer rubber (EPDM), all of them widely available in the market under several commercial brands. In the following, EVA, LDPE and EPDM materials will be named with the simple tags "acetate", "foam" and "rubber" respectively, to avoid confusion with acronyms. For this experiment, all materials take the shape of a strip with a rectangular section (0.5×1 mm).

To characterize their elastic behavior with precision, they were tested in the laboratory by a thermomechanical analysis (TMA) at room temperature [Brown, 2001]. It was intended to measure the exact conditions with which they will be used, so values obtained in the material database were not valid since they did not account for the particular shape employed. For this reason, samples of elastic material which geometrical characteristic (width, length and depth) identical to those used in MAPs were essayed under compression for observing dimensional changes in the axis where forces are applied (see Figure 4.5). The elastic modulus for this particular case can be described as the ratio between stress and strain. Measurements with the TMA Analyzer provided values of $29.6{\cdot}10^6$ N/m^2 for acetate, $21.8{\cdot}10^6$ N/m^2 for foam and $191.4{\cdot}10^6$ N/m^2 for rubber, which means that foam is the most flexible material and rubber the most rigid.

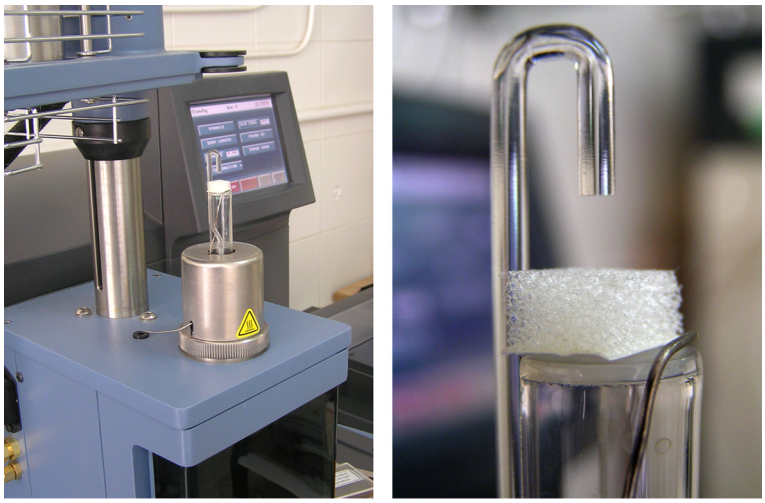

(a) (b)

Figure 4.5. Thermomechanical Analyzer with a sample of elastic material under test. (a) General view. (b) Detail of the probe.

4.3.4 Recording and Processing

At the first stage, directivity in the horizontal plane and on-axis frequency responses have been considered for a single MAP. They have been obtained by placing a 1/2" electrostatic microphone at 1 m and rotating the MAPs with a computer controlled rotating table. Secondly, space-time measurements are carried out by sampling a portion of the emitted wave field along a parallel line with respect to the MAPs (see Figure 4.2). This recording stage has consisted of a 200 microphone array with 1 cm spacing, which is sufficiently below the theoretical Nyquist sampling limit spacing of 9 cm (half the distance between exciters). For implementing such an array, a single 1/2" electrostatic microphone on a computer controlled linear sliding table has been used.

Three stimuli have been employed in the space-time measurements. Firstly, the middle exciter on the third of the five MAPs is excited to characterize the single-excited MAP operation when changing boundary conditions. Secondly, a synthesized point source is rendered by means of the WFS algorithm. Since additional drive points are excited with respect to the first stimulus, the impact of the boundary condition will be more

noticeable. Finally, an axial plane wave by means of WFS algorithm is reproduced by the MAPs. This configuration runs all the exciters with the same amplitude and phase signal, forcing vibration in areas near the boundaries.

Once the impulse responses have been recorded, an analysis of the acoustic wave fields is carried out in the space-time wavenumber domain, (see [Rabenstein et al., 2006]) where sampling artifacts, truncation effects and angle-dependent radiation are observed. To that end, the spatial and temporal frequencies are obtained with a double Fourier transformation on the microphone array signals. The obtained multidimensional signal is plotted in a spatial versus temporal wavenumber graphical representation ($k_x - k$ plot), where k_x and k are the spatial and temporal wavenumbers, respectively. For a detailed description of the tool and its interpretation, refer to the preceding Chapter 3.

4.4 Results and Discussion

In this section, measurements following the setup explained above are presented and commented upon. They include both elastic boundaries with acetate, foam and rubber and also clamped and free boundary conditions which, even though they do not employ such elastic materials, will be addressed as a basis with which to compare elastic boundaries. Firstly, in Section 4.4.1 on-axis frequency response and directivity is presented, and then, in Section 4.4.2, a wavenumber domain analysis is performed for three different stimuli.

4.4.1 On-axis Frequency Response and Directivity

On-axis frequency response and directivity can depict the influence that the boundary conditions may have on the vibration mode radiation of a single MAP. Figure 4.6 shows the results of eleven frequency response measurements combining the experimental conditions and the three elastic materials introduced in Section 4.3. Clamped and free are plotted in Figure 4.6(a) as reference responses. Figure 4.6(b), (c) and (d) depicts the three elastic boundary responses made with acetate, foam, and rubber material, respectively.

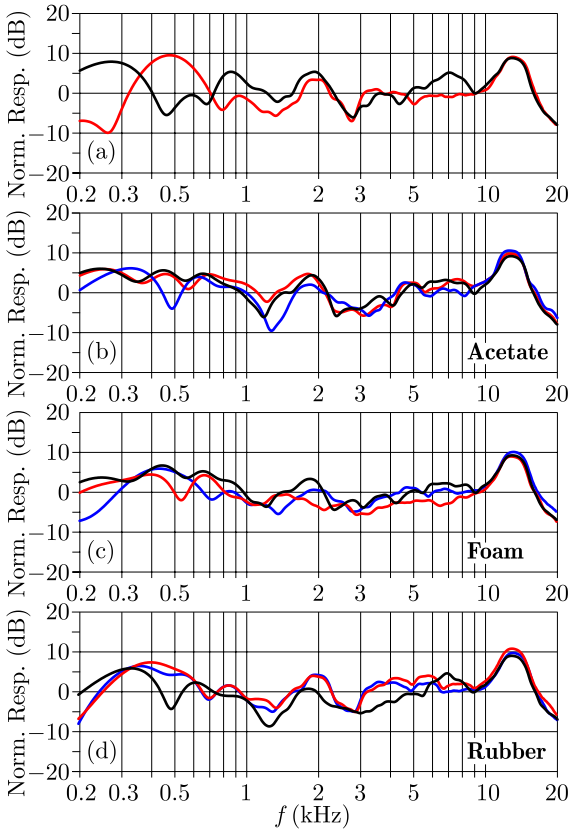

Figure 4.6. Normalized on-axis frequency response for (a) Clamped (black), Free (red) and Elastic boundaries EB1 (black), EB2 (red), EB3 (blue) for (b) Acetate, (c) Foam, (d) Rubber.

As shown in the responses, the main differences are observed in frequencies below 9 kHz, whereas no change is noticed for the rest of the high frequency band. This behavior is consistent with the radiation of bending wave plates. At low and mid frequencies, the edge radiation is predominant, so a change in its boundary conditions must alter their responses. On the contrary, for high frequencies, all the surface contributes to radiation, where the edge's effect is minimized.

Free and clamped conditions show very different responses up to 700 Hz due to their opposite behavior on edges, as depicted in Figure 4.6(a). The

responses with the acetate material are illustrated in Figure 4.6(b) for the three elastic boundaries. According to the measured elastic modulus, acetate and foam materials showed a similar elasticity, so their responses should also be similar. However, the on-axis responses are more irregular than foam and rubber. EB1 and EB2 show similar responses, which means that placing the elastic material in one or two sides does not play a role in the response. Regarding the foam material shown in Figure 4.6(c), the three elastic boundaries under test have similar on-axis responses. The flexibility of foam is high enough not to observe moderate differences between elastic boundaries having foam in one or two sides, even if these are not attached to the frame (EB3). Although EB3 response between 2 and 9 kHz is very smooth, there are moderate variations in low frequency. Hence, the most effective foam boundary condition is EB2, where the overall response is the smoothest one. With respect to rubber, Figure 4.6(d) illustrates that EB1 response exhibits several peaks and dips, as shown in the clamped condition of Figure 4.6(a). Since rubber is stiffer than foam and EB1 has only one side equipped with damping material, this resemblance makes sense. Although not as severe as EB1, EB2 also presents moderate variations in the on-axis response.

Comparing the four plots of Figure 4.6, a close resemblance in the low frequency responses of EB3 and free conditions can be observed. This is due to the similar behavior on edges of these two boundary conditions. For mid and high frequencies, both EB2 and EB3 are smoother than free. In general terms, free and clamped conditions give boost to bass power at the expense of smoothness compared to elastic boundaries.

Figure 4.7 depicts the directivity in the horizontal plane for clamped, free and elastic boundaries as an angle-frequency representation. This representation is useful to observe at a glance the pressure variations as a function of emitting angle for the audio frequency band under consideration.

As expected, since high frequencies are not controlled by panel edges, the directivity response is similar for all boundary conditions, regardless of the elastic material used. This similarity can be perceived in Figure 4.7 for frequencies above 9 kHz. The pattern that this region exhibits is the one of supersonic modes: forward and backward waves radiate in their direction of propagation producing two lobes pointing in opposite directions. Combined with the weaker main lobe, the overall radiation pattern is a three-lobe

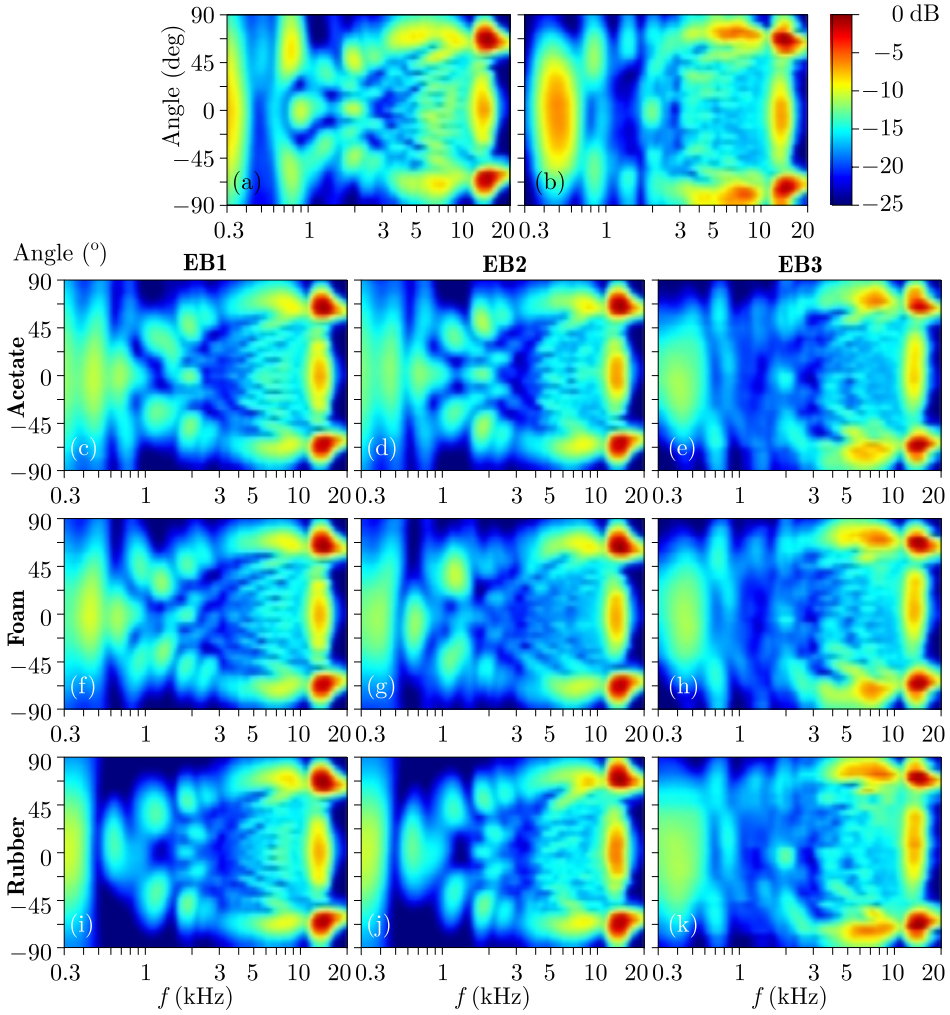

Figure 4.7. Horizontal plane directivity for (a) clamped and (b) free conditions, acetate for (c) EB1, (d) EB2, (e) EB3, foam for (f) EB1, (g) EB2, (h) EB3, rubber for (i) EB1, (j) EB2, (k) EB3.

broad angle response.

Clamped and free boundary conditions show opposite behavior for low frequencies. On the one hand, clamped is purely omnidirectional for frequencies up to 400 Hz, whereas free exhibits a broad main lobe. On the

other hand, between 1 and 2 kHz, the lobe pattern is different: clamped displays a three-lobe pattern, whereas free has only a centered lobe. In the frequency band of 3–9 kHz and for ±45 degrees, a grid area can be observed, not only for clamped and free but also for the rest of elastic boundaries. Although there is effective sound emission, moderate dips and peaks on varying direction are occurring. As regards elastic materials under test, responses with rubber are more directional than with acetate and foam. Figures 4.7(i) and (j) show opposite blue areas between 0.5 and 1 kHz, which means that a single main lobe is being emitted for rubber material in EB1 and EB2. The behavior in low and mid frequencies is similar for acetate and foam. If elastic boundaries are evaluated, it can be seen that EB1 and EB2 have virtually the same directivity responses, in spite of the elastic material employed. As with on-axis response, EB3 is very similar to free condition: energy fall at extreme angles in low frequency is observed as a white spot in both representations.

4.4.2 Space-Time Wavenumber Domain Analysis

Once the boundary conditions have been tested for their impact on the basic specifications on MAPs, in this subsection, a wavenumber domain analysis of the generated wave field for three different stimuli will be addressed. The three stimuli are designed to progressively increase the vibration of exciters near edges and thus, their influence on the type of edge boundary condition.

Point Source from the Middle Exciter

This configuration drives only one exciter on the third of the five MAPs, so their behavior will characterize the distributed mode loudspeaker operation when changing the boundary conditions. Also, the created wave field will help in comparing a synthesized version by running the WFS algorithm.

Figure 4.8 depicts the wavenumber domain representation for clamped and free conditions. Considering that the ideal situation is when several spatial components are emitted for different frequencies, a pure black triangle must be the basis to compare the rest of the responses. According to this, the clamped condition presents a rough distribution of energy within the theoretical triangle. When listening to such a wave field, strong pressure variations would be perceived both in frequency and on moving inside the listening area.

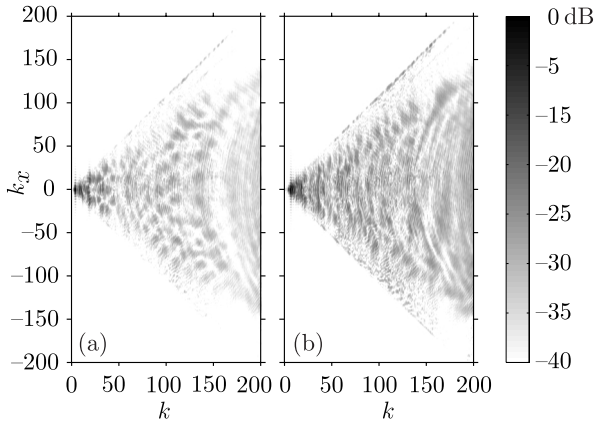

Figure 4.8. Wave field emitted by the central transducer in the $k_x - k$ representation for (a) clamped and (b) free boundary conditions.

Elastic boundaries show better responses in the $k_x - k$ representations than pure clamped and free (Figure 4.9). In order of smoothness, EB3 exhibits a moderate homogeneous response in the space-time frequency response for the three materials, Figures 4.9(c), (f) and (i). The ideal black triangle can be suggested in these responses with more clarity than with other elastic boundaries. As expected, EB2 shows a compromise between the commented EB3 and EB1. Some energy variations start to appear in EB2 and are enhanced for EB1, where a only half of the boundaries have elastic materials. Next, the free condition demonstrates a reasonable smoothness but a concentric circular pattern is visible as a superposition. This behavior is due to the modal nature of the panel, which effect is minimized in elastic boundaries. Finally, as discussed before, clamped shows both an inhomogeneous pattern and a circular pattern, which disturb the generated wave field to an extent.

Acetate, foam and rubber materials display noticeable differences for EB1 and EB2, where materials play a role on the emitted wave field. These dissimilarities are less evident for foam and acetate since their elasticities are similar. For EB3, since elastic materials serve as boundaries in which to support the panel, all responses have close resemblance. Rubber stiffness prevents movement on edges to some extent, as with clamped condition, which causes an inhomogeneous pattern.

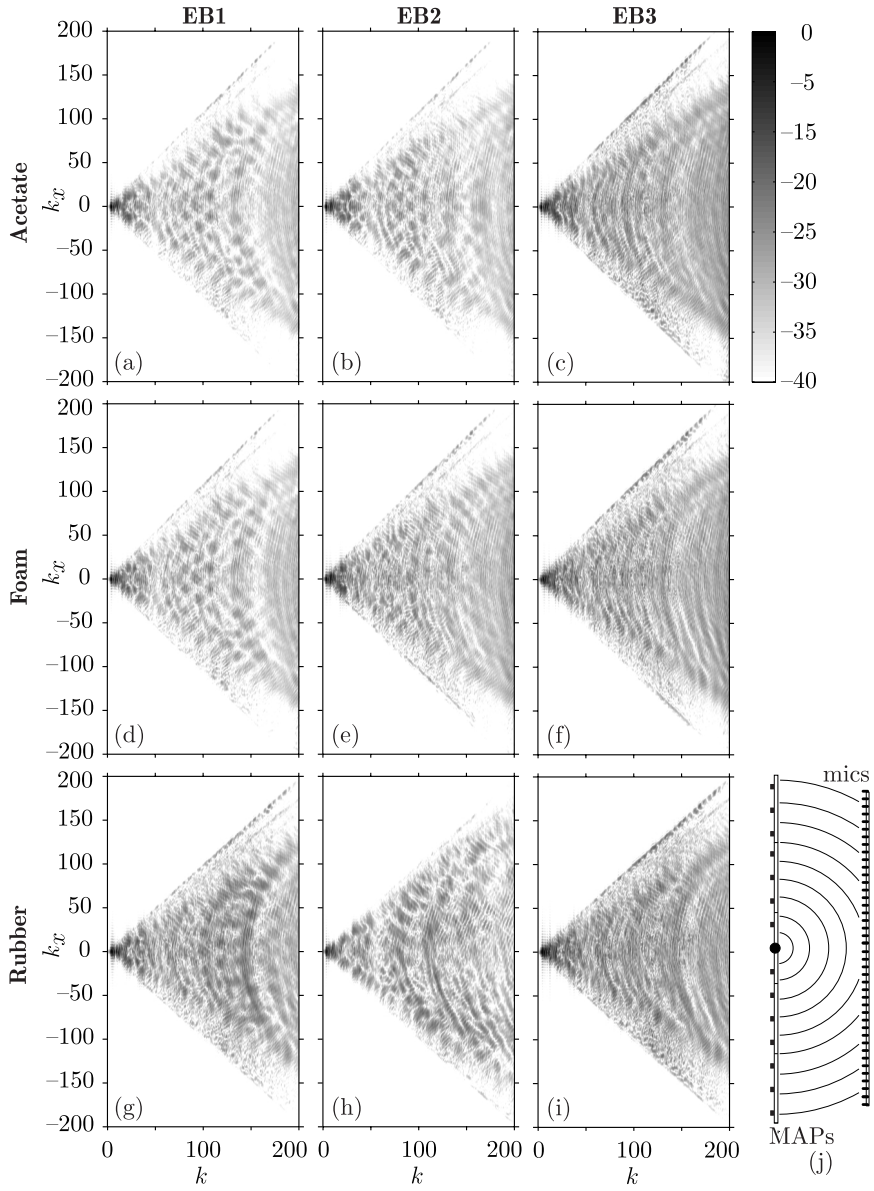

Figure 4.9. Wave field emitted by a single transducer in the $k_x - k$ representation. Elastic boundaries with acetate on (a) EB1, (b) EB2, (c) EB3, foam on (d) EB1, (e) EB2, (f) EB3, and rubber on (g) EB1, (h) EB2, (i) EB3. (g) Experiment graphical description.

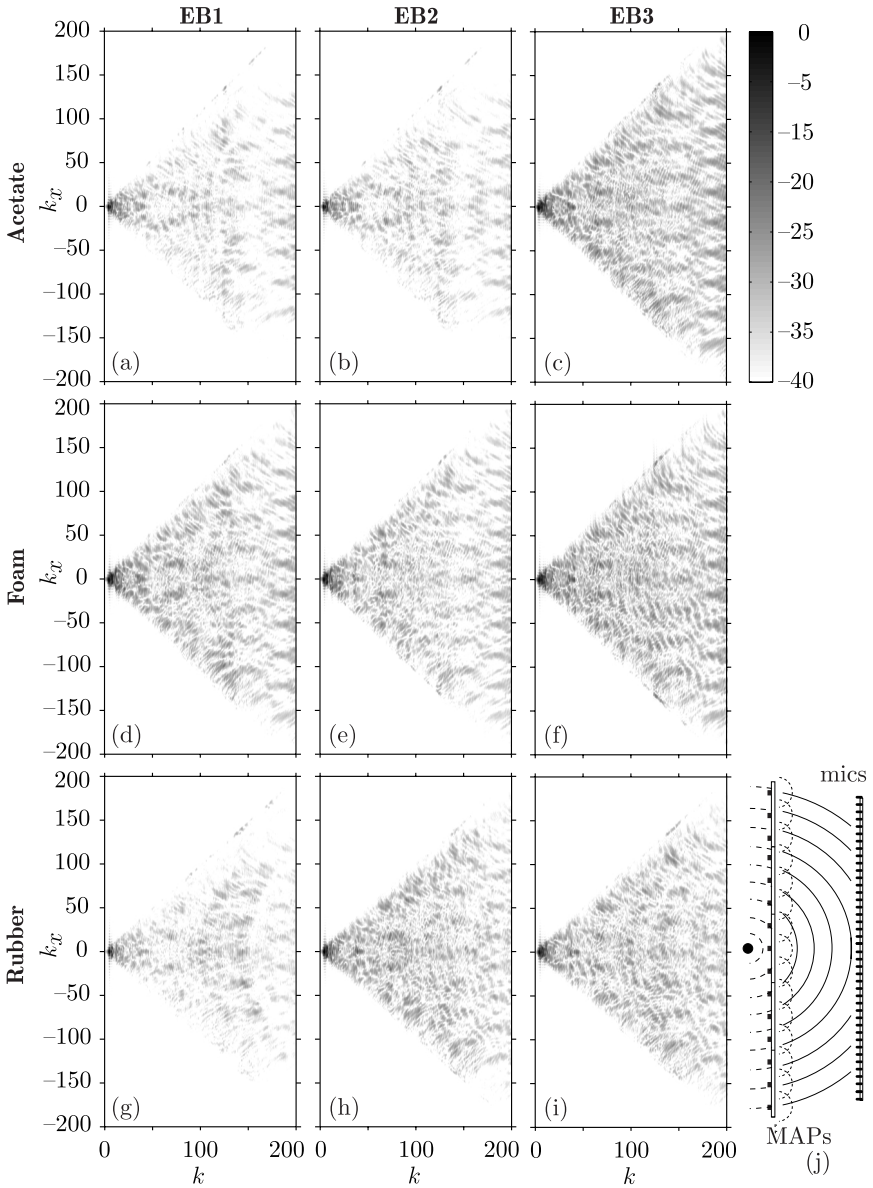

Figure 4.10. Wave field of a virtual point source centered 0.5 m behind the array, in the $k_x - k$ representation. Elastic boundaries with acetate on (a) EB1, (b) EB2, (c) EB3, foam on (d) EB1, (e) EB2, (f) EB3, and rubber on (g) EB1, (h) EB2, (i) EB3. (g) Experiment graphical description.

Virtual Point Source

In this case, from the center to the sides, driving signals' amplitude will decay progressively. For that reason, the impact of the boundary condition will be more noticeable considering that additional drive points are excited close to edges.

Figure 4.10 depicts the wave field representation of a virtual point source behind the MAP for elastic boundaries with acetate, foam and rubber. Again, rubber responses display moderate variations for EB1 and EB3, whereas EB2 does not show clear deviations with respect to foam. Regarding acetate and foam responses, no major differences between EB1 and EB2 are observed, as shown in Figures 4.10(a) and (b), and Figures 4.10(d) and (e), respectively.

Axial Plane Wave

Such a stimulus will drive all the exciters in MAPs with the same signal, amplitude and phase. Then, the area near the boundaries which is forced to vibrate is at maximum and the potential reflections on the edges will be visible.

Figure 4.11 shows an axial plane wave field for elastic boundaries with acetate, foam and rubber. Plane waves can give additional information to that of the previous sections. In a continuous panel that contains 15 exciters, edge boundary condition's impact on the panel movement is located before the first exciter and after the last one. In an arrangement of small MAPs that are attached to each other to maintain the transducer spacing, the horizontal extension of each MAP now creates four new areas in the exciter line that will behave according to their boundary conditions. The consequence of such a configuration is the appearance of new undesired replicas of the plane wave field. Therefore, to evaluate the impact of elastic boundaries on such an effect, and considering that the distance between the MAPs' centers is 0.54 m, two new replicas must be examined at $k_x = 2\pi/0.54 = 11.6$ m^{-1} and $4\pi/0.54 = 23.3$ m^{-1} that are located between the lines that an 18 cm exciter distance creates at spatial frequencies of $k_x = 0$ and 34.9 m^{-1}. The practical consideration of this additional sampling process is that new undesired plane waves will arise on the reproduced wave field.

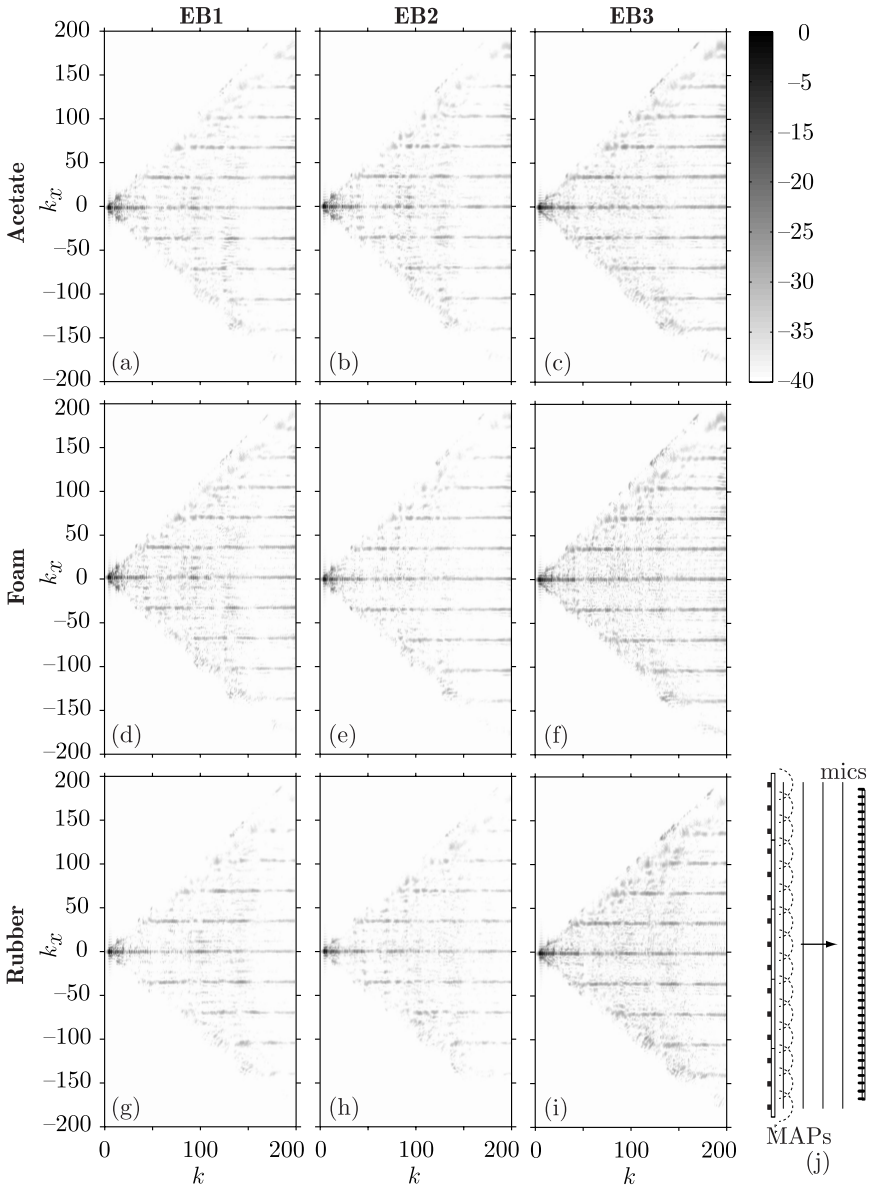

Figure 4.11. Wave field of an axial plane wave in the $k_x - k$ representation. Elastic boundaries with acetate on (a) EB1, (b) EB2, (c) EB3, foam on (d) EB1, (e) EB2, (f) EB3, and rubber on (g) EB1, (h) EB2, (i) EB3. (g) Experiment graphical description.

For EB1, both acetate, foam and rubber responses have replicas at 11.6 and 23.3 m^{-1}, as shown in Figures 4.11(a), (d) and (g). Regardless of the elasticity material under test, replicas are visible, which could be due to the panel area in contact with the frame, acting as clamped. When two elastic materials are used in EB2, unwanted lines are noticeable only for acetate and rubber in Figures 4.11(b) and (h). The use of two elastic sides and an improved elasticity can minimize the effect of new boundary conditions. Finally, EB3 being the closer to free, has no additional replicas. As a consequence, elastic boundaries can decrease the impact of edge boundary conditions on the reproduced replicas.

4.5 Conclusion

An empirical study of the impact that the edge boundary conditions have on the radiated wave field has been presented in this chapter. As an alternative to the DML and MAP boundary conditions depicted in Section 2.4.3, elastic boundaries have been addressed as practical boundary conditions that can form a viable technology for a MAP frame. Three elastic materials, representative of soft, medium and hard types within the commercial range, have been employed to produce the elastic boundaries. They were measured in the laboratory to recreate the exact conditions with which they were used in the prototypes.

The major changes have been observed at low and mid frequencies, where the edge radiation was predominant. In general terms, free and clamped conditions boost bass power, at the expense of smoothness compared to elastic boundaries. Wavenumber domain analysis has shown that strong pressure variations would be perceived, both in the frequency response, and and spatially on moving inside the listening area for these two conditions, this makes them inadvisable in multichannel audio reproduction.

Alternatively, elastic boundaries are a compromise between clamped and free, that can be realized with different elastic materials. For mid frequencies, on-axis responses were smoother for elastic boundaries than clamped and free edges, regardless of the elastic material employed. Moderate variations were found in directivity patterns on using clamped and free but not on elastic boundary types 1 and 2, where half or the entire part

of the support is filled with material. As a consequence, both boundary conditions can be used alternatively with similar results for elastic materials with proper flexibility. Elastic boundary type 3 is a modified version of simply supported, but including elastic material between panel and housing. According to the results, it has no primary advantages over the two other elastic boundaries. Therefore, its use is not recommended, considering the problems that will arise on manufacture in a real MAP frame, as mentioned in Section 1.2.

Finally, the appearance of new undesired replicas of the plane wave field that were drawn in Section 3.5, is minimized for elastic boundaries with flexible materials. As a consequence, with the proper selection of materials for elastic boundaries, the effect of edge boundary conditions on the reproduced replicas can be decreased to a minimum.

Results presented in this chapter may help as guidelines in the design and manufacture of new MAPs. They also confirm, together with laboratory measurements, the general trend of using elastic materials in panels design.

Efficient Equalization

5

5 Efficient Equalization

The MAP radiation yields to the excitation of modal frequencies, which are sufficiently dense and evenly spaced that an illusion of continuous spectrum is created on the listener. However, the vibration pattern of the panel causes a complex superposition of the bending wave excitations which vary strongly with frequency. This uneven response, with large dips and peaks, degrades the perceived sound quality and makes the use of MAPs less attractive compared with the use of conventional speakers. Therefore, the irregular MAP response needs to be equalized for a natural, uncolored response. This chapter addresses the equalization of the inherent uneven spectra of MAPs by applying an efficient filtering method.

5.1 Introduction

The irregular frequency response of MAPs can be compensated for by means of different digital filter topologies, such as Finite Impulse Response (FIR) or Infinite Impulse Response (IIR). For MAPs, which contain several exciters on a single panel, a dedicated filter must be applied to every exciter but the position where to measure and equalize is not straightforward. Moreover, if MAPs reproduce WFS sound scenes in a room, they also introduce unwanted echoes that will merge with direct signals coming

from the panels. This drawback can degrade the rendered wave field or even ruin the localization perception of the virtual sources. Moreover, the result of the mixture of direct and reflected signals is a colored spectrum that alters the timbre of sound sources. Therefore, the room effect has two drawbacks on the perceived sound: degradation of the sound field shape and spectrum timbre alteration.

For the first drawback, room compensation or reflection compensation algorithms apply multichannel FIR filters to the audio signals to minimize the unwanted effects of the room. For the second drawback, spectral equalization algorithms are employed to compensate for the uneven frequency response of loudspeakers. The use of these two filtering strategies for WFS is restricted by the aliasing frequency, which is one of the most important artifacts in WFS. Room compensation algorithms are only applied for frequencies below the aliasing frequency because for higher frequencies, severe spatial dependent distortion of the wave field will be introduced. For that high frequency region, spectral equalization is used to compensate spectra rather than wave fields, which is not possible.

The latter approach of spectral equalization is addressed here by an efficient algorithm. The method is oriented towards using a very low computational cost by means of an advantageous IIR scheme. Therefore, it can be employed for compensating the absolute value of the spectrum with application to spectrum equalization of the panel. However, it is not advisable for echo compensation since this application requires the use of non-minimum phase FIR filters. Therefore, this chapter addresses experimentally the compensation of irregularities in the spectrum of MAPs without considering the room effect. Nevertheless, it is straightforward to extend the presented scheme for compensating the room effect on the sound source timbre by means of a multichannel measurement and processing.

The chapter is outlined as follows: in Section 5.2 the equalization method is described, with a comparison to the current filtering strategies. Multi-exciter prototypes in which the equalization process will be applied and the measurement setup is given in Section 5.3. Results are presented in Section 5.4. According to the measurement procedures described in Section 5.3, both prototypes are equalized, which results are discussed in terms of sound quality and filter efficiency. To study the influence of the filter order in the perceived quality of the equalization, some subjective assessments are carried out. Finally, the chapter is concluded in Section 5.5.

5.2 Efficient MAP Equalization

5.2.1 WFS Filtering Strategies

In the context of WFS reproduction, different filtering strategies have been proposed, as stated in the introduction. On the one hand, room compensation algorithms apply multichannel inverse FIR filters to the audio signals such that the unwanted effects of the room are diminished. To that end, the wave field is sampled at several points in a room. There are two approaches for that purpose: first, Spors [Spors et al., 2007] proposed a decomposition of the wave field in a mixture of plane waves with all kinds of different angles. Then, the WFS driving signals are recalculated from the filtered decomposed plane waves. Second, there is the approach that consists of describing the multichannel sound reproduction system as a multi-input multi-output (MIMO) system and generating a bank of filters prior to the loudspeakers. Filters are designed so as to minimize the error between the synthesized sound field and a given target. This system was proposed in [López et al., 2005] and has been extended and improved in [Corteel, 2006a, 2007],[Gauthier and Berry, 2007]. On the other hand, spectral equalization was previously addressed by Corteel [Corteel et al., 2002] on employing individual equalization of the drivers, combined with energy control to recover the sound field in a perceptually, not physically exact sense. Other studies reported experimentally that, in general the measured frequency response after applying the equalization filter was still not flat but it exhibited a more uniform shape [van Dorp and de Vries, 2006]. The purpose of this chapter is not to deal with compensating for the reflections of the room, but to compensate efficiently the unnatural colored response of MAPs for WFS. In these applications, a large number of channels is used and the computational cost of the compensation filters increases linearly with channel numbers. Furthermore, in a MAP, the behavior of the exciters is a function of their position on the panel, so a filtering process must be considered for each exciter.

For compensating the room effect by means of a bank of MIMO filters, the phase of the computed filters is crucial, being usually of minimum phase. Hence, the FIR scheme is mandatory for this application. However, for only compensating the spectrum absolute value, i.e. the coloration, a IIR scheme can be employed, which requires a lower computational cost to achieve a proper equalization.

5.2.2 Filtering Design Methods

Equalization methods employing FIR filters are straightforward to design and implement, correcting magnitude and phase, if desired, simultaneously, and always guaranteeing the stability of the filter [Karjalainen et al., 1999]. Nevertheless if low frequencies need to be equalized with enough resolution, the order of the filter, its delay, and the computational costs increase excessively. Moreover, if linear phase response is required on the filter response, pre-echo could appear on the combined impulse response, being especially noticeable with transient stimuli. Alternatively, IIR filters in general need lower orders. However, their design is more difficult than that of FIR filters, and the stability of the solution is not always guaranteed. Another problem is the noise generated due to quantization effects, especially when low frequencies are filtered. To solve these well-known problems, different filter topologies and noise-shaping techniques have been developed to minimize this effect in [Zölzer, 1997],[Dattorro, 1989],[Wilson, 1993]. The designs of IIR filters can be carried out by means of different techniques in the time domain (Prony [Parks and Burrus, 1987], least mean squares, Steiglitz-McBride [Steiglitz and McBride, 1965]) or in frequency domain (Levi [Levi, 1959], Yule-Walker [Friedlander and Porat, 1984]). After an evaluation of such methodologies, IIR-based filtering is selected to develop an efficient equalization, which is explained in the next section.

5.2.3 SOS Filtering

This section briefly describes a successful technique of IIR design applied to audio systems that has been proposed recently in [Ramos and López, 2006]. This filter design method, differing from other IIR design methods, is characterized by the fact that the equalization structure is planned from the beginning as a chain of second order sections (SOS). An SOS chain is usually the way in which IIR filters are implemented later on a digital signal processor (DSP). As shown in Figure 5.1, the transfer function of the IIR equalization filter is structured as a chain of SOS, $H_f(z) = H_1(z) \cdot H_2(z) \cdots H_N(z)$, where z is the continuous complex variable of the z-transform. Each SOS section, illustrated as a gray box in the figure, has a transfer function that in general is defined by its five coefficients b_0, b_1, b_2, a_1, a_2, according to:

$$H(z) = \frac{b_0 + b_1 z^{-1} + b_2 z^{-2}}{1 + a_1 z^{-1} + a_2 z^{-2}}. \tag{5.1}$$

The point of this filtering structure is that instead of defining each SOS by its five coefficients, each section is set as a parametric peak filter, high-pass filter or low-pass filter defined by three parameters of acoustic significance: central frequency, gain and Q-factor. Therefore the parameters to be optimized fulfill a desired frequency response range from five coefficients by filter to only three. The mathematical proof of the relation between filter coefficients and acoustic parameters is beyond the scope of this chapter and can be found in [Zölzer, 1997]. In order to guarantee the final stability of the filter and a successful and controlled implementation of it on a DSP, each SOS will be restricted to being a minimum phase peak, low-pass, or high-pass filter. Moreover, this approach facilitates obtaining information about the influence of each SOS in frequency and magnitude on the final equalization.

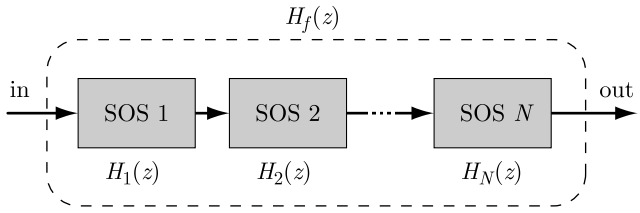

Figure 5.1. Filter implementation as a chain of SOS.

The frequency response of a loudspeaker could be considered as a deviation from a flat ideal response with peaks and dips over the ideal flatness. Figure 5.2(a) shows an example where several peaks and dips have been identified over the 0 dB level. Considering such a loudspeaker response, and using the proposed structure of the equalization filter $H_f(z)$, it is straightforward to compensate for the differences between the measured frequency response of the loudspeaker and the target frequency response $H_t(\omega)$ using peak filters, where ω is the frequency pulsation. In Figure 5.2(a), the red line represents the peak filter $H_1(e^{j\omega})$ attempting to compensate the largest peak A2, gray shaded, where $e^{j\omega}$ is the continuous complex variable of the Fourier transform. For a comprehensive description of these variables, refer to [Oppenheim et al., 1999]. In addition to the peak filters, which correct peaks and dips, low-pass and high-pass filters should be used to control the frequency band and to define a proper target response, shows as a green line in Figure 5.2(a). This target response should have bandpass characteristics to respect the bandpass behavior of the MAP. The values ω_i and ω_f

represent the initial and final frequencies when performing the equalization.

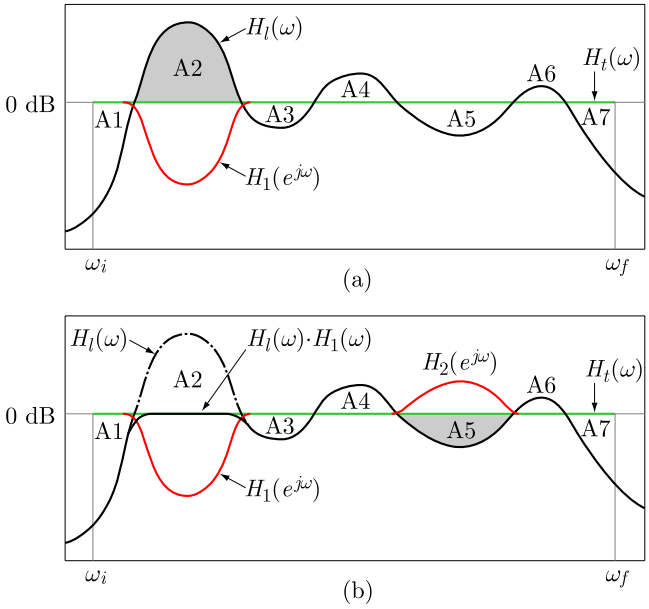

Figure 5.2. (a) Search of the largest error area and design of the first SOS. (b) Correction effect of the first SOS and search for the second SOS.

Instead of designing the digital equalizer $H_f(z)$ to minimize the error function, searching for the set of coefficients, it will be designed to look for the set of parameters of the filters (frequency, gain, and Q-factor). The algorithm is divided into two stages: first, a direct search for initial values of the parameters for each SOS filter is performed, aiming at compensating the largest irregularity in the response. In Figure 5.2(a), the most prominent irregularity is the peak A2 which will be compensated first. Next, a parametric optimization with constraints will be made in order to control the allowed ranges of these three parameters for obtaining a realizable final implementation. After the calculation of the first SOS, the frequency response is updated and the process is repeated, the peak A5 being the current largest of Figure 5.2(b). Among the possible optimization methods available for computing the three parameters, a heuristic approach is employed in this method. After the process completes N stages, the final filtered response is obtained as a combination of the N SOS.

This method outperforms, from a psychoacoustic point of view, all the well-known IIR filter design methods that have been discussed in the previous section, because it evaluates the error considering the double logarithmic behavior of human hearing, using a discrete and logarithmic frequency axis and a decibel magnitude axis. Moreover, there are two additional advantages of the method to be emphasized: first, the final solution is straightforward to post-modify without redesigning the filter again, just modifying the values of the parameters, and second, the solution is scalable because the SOS are designed in correction order, initially with those that correct the response more effectively.

5.2.4 Example of MAP Equalization

In order to test the behavior of the filtering method, a single-exciter MAP has been equalized using the IIR design method. To that end, the frequency response has been measured first and an IIR equalization filter has been computed using the proposed method. The measured frequency response is depicted in Figure 5.3(a) as a black line.

For comparison purposes, an FIR filter of high order has been calculated following the Kirkeby method [Kirkeby et al., 1998]. For both filters, the target response is set to a second-order high-pass Butterworth at 125 Hz, shown in Figure 5.3(a) as a red line. The results of the equalization with a 15 SOS IIR filter proposed here and with a 2048 taps FIR filter are depicted as a blue line in Figures 5.3(b) and (c), respectively. Although the order of the FIR filter is very high compared to the IIR method, both equalized responses are quite similar. The remaining irregularities of the IIR filtering are low enough to be unnoticed. However, the main drawback of the FIR filter can be found on observing the filter responses in red line in Figures 5.3(b) and (c). FIR filtering takes no control over filter gain leading to excessive peaks in the filter response of 20 dB, as shown in the low frequency response of Figure 5.3(c), which poses implementation problems on a DSP. Later in Section 5.4.4, a subjective assessment is carried out to demonstrate that these ripples are unnoticed by averaged listeners.

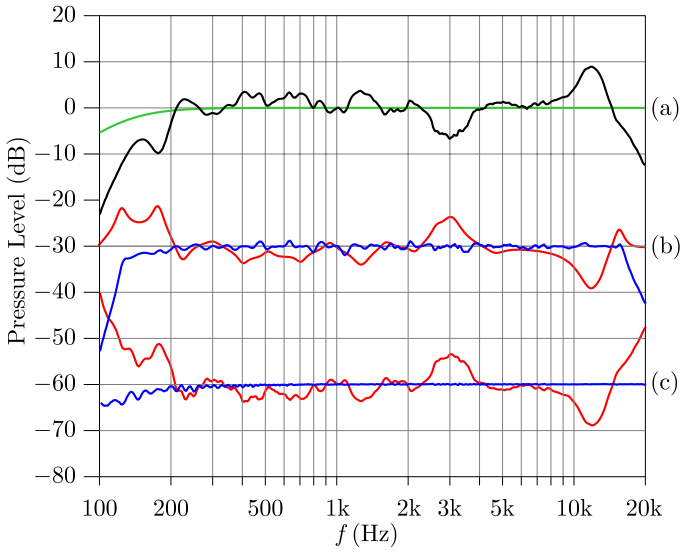

Figure 5.3. Exciter equalization comparison for FIR and the proposed IIR filtering. (a) Exciter measurement (black) and filter target (green). (b) 15 SOS IIR filter: exciter filtered response (blue), filter response (red). (c) 2048 taps FIR filter: exciter filtered response (blue), filter response (red). Representations are shifted 30 dB in order to maintain clarity.

5.3 Experimental Setup

The equalization process is executed for two MAP prototypes having different geometry: MAP3 and MAP5. This configuration is set to experiment the filters' performance in panels ranging from small to moderate size and their associated impact on attached exciters to the structural behavior of the panel.

On-axis frequency responses have been obtained by placing a 1/2" electrostatic microphone 1 meter from the panels. In all measurements, Maximum Length Sequences (MLS) were used as excitation signals in order to improve signal-to-noise ratio and minimize unwanted reflections [Vanderkooy, 1994].

According to the position of the microphone with respect to the panel, two kinds of measurements are experimented. On the one hand, considering the panel as a whole, the individual impulse responses are measured at

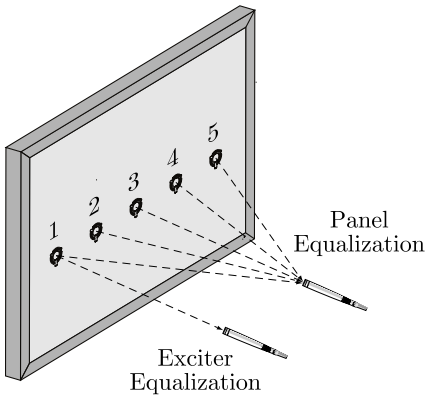

Figure 5.4. Impulse response measurement according to panel and exciter equalization. In the latter, only the first exciter measurement is represented to maintain clarity.

a middle position and an averaged impulse response is obtained. Then, every exciter on the panel is filtered according to the averaged response. This approach will be described as "Panel equalization". On the other hand, filters are based on the response of measurements taken in front of every individual exciter, which will be referred to as "Exciter equalization". Figure 5.4 shows a graphic representation of panel and exciter equalization for the MAP5. For the latter equalization, the measurement process will continue for exciters 2 to 5, obtaining a total of five impulse responses.

5.4 Results and Discussion

In this section, the above equalization approaches will be applied first to the MAP3 to explore the potential benefits of both methods. Then, the MAP5 will be equalized considering the symmetry in the exciter positions. Finally, in order to reduce the filter coefficients, a subjective assessment is carried out.

5.4.1 Exciter Equalization for the MAP3

The MAP3 is first measured for the *exciter equalization*. To that end, the microphone is located on the axis of every exciter, which gives three impulse response measurements. Figure 5.5 shows in black lines the three

corresponding frequency responses. For exciters 1 and 3, responses reach 0 dB approximately at 280 Hz and continue increasing to a large peak of 12 dB. For mid frequencies, a 3 dB dip at 3 kHz and a 5 dB peak between 5 and 8 kHz are observed. In the high frequency region, a peak resonance of 6 dB due to the coincidence effect is visible and will not change for the rest of the configurations. The frequency response of exciter 2 extends the low frequency region up to 180 Hz and presents another peak, slightly weaker (9 dB), that ends at 400 Hz. The mid and high frequency regions are similar to those of exciters 1 and 3. The loss of low frequency radiation of the edge exciters with respect to the middle exciter is consistent with the poor mode excitation at low frequency for driving points near edges.

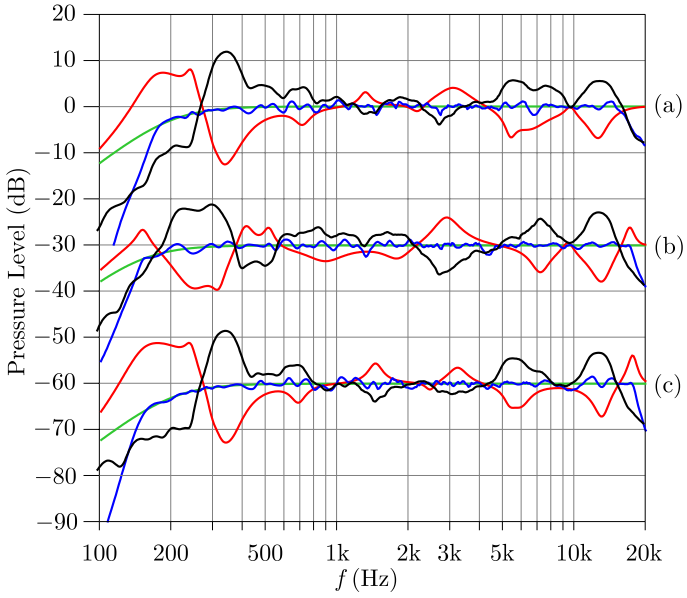

Figure 5.5. Frequency responses of the exciter equalization process for the MAP3. Exciter measurement (black), filter target (green), filter response (red), simulated exciter filtered response (blue). (a) Exciter 1. (b) Exciter 2. (c) Exciter 3. Representations are shifted 30 dB in order to maintain clarity.

Three filters are designed to compensate for the irregularities of each exciter above described. Due to the similarities in the response, exciters 1 and 3 are designed with the same target frequency response. As shown in the green lines in Figures 5.5(a) and (c), a second-order high-pass But-

terworth at 200 Hz is set to the desired target. Since the nature of the distributed mode loudspeaker causes a roll-off at high frequencies, no additional low-pass filtering is needed. For exciter 2, the same target applies but with low frequency cut at 150 Hz. Considering the target bandwidth and the irregularities on the responses, three filters are computed: for exciters 1 and 3, a structure of 14 SOS is used, whereas for exciter 2, 16 SOS are needed. The responses of these filters and the simulated exciter filtered responses are given in Figure 5.5 in red and blue lines respectively.

Filters are now applied to the MAP3 and the equalized frequency responses are measured in the laboratory. The resulting frequency responses and the original unfiltered responses are depicted in Figure 5.6. The graph shows that the equalized spectrum has improved considerably, being now almost flat. The irregularities that are still present and were not simulated in the responses of Figure 5.5 are due to physical constraints of the panels, counteracting the equalization process to a certain extent. However, the responses have been considerably improved with a very light filtering process.

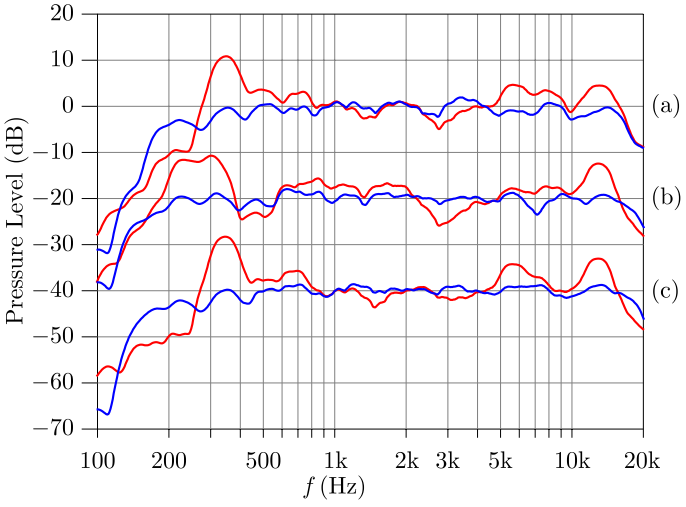

Figure 5.6. Equalization results of the MAP3. Filtered response (blue), original response (red), (a) Exciter 1. (b) Exciter 2. (c) Exciter 3. Representations are shifted 20 dB in order to maintain clarity.

In order to give an objective quality measurement of the flatness of responses, the logarithmic standard deviation can be used. For a discrete Fourier spectrum $P[k]$ with length L the logarithmic standard deviation is given by:

$$\sigma_{\log} = \sqrt{\frac{1}{L-1}\sum_{k=1}^{L}\{20\log|P[k]| - \overline{P_{\log}}\}^2} \tag{5.2}$$

where $P_{\log}$ is the mean value of $20\log|P[k]|$ for $1 \leq k \leq L$.

The logarithmic standard deviation allows one to compare multiple responses with different amplitudes since scale factors in the data are cancelled out. This measurement is also used by other authors for assessing the quality of MAPs [van Dorp and de Vries, 2006]. For a perfectly flat frequency response, the logarithmic standard deviation will be equal to 0 dB, which is the lower limit. The higher the value, the more irregular is the frequency response.

The computed logarithmic standard deviation values for the unfiltered responses were 4.22, 3.73 and 4.39 dB, whereas those of equalized responses have dropped to 1.49, 1.26 and 1.32 dB for the first, second and third exciter respectively. These values were calculated for the frequency band of each filter target response: 200 Hz to 20 kHz for exciters 1 and 3, and 150 Hz to 20 kHz for exciter 3.

From the above results, it can be concluded that the equalization process is very efficient for achieving a reasonable degree of flatness without expending too much computational cost. If a classic FIR filtering was used instead, a considerably higher order would have been necessary to obtain a bass response such as the one acquired here.

5.4.2 Panel Equalization for the MAP3

Once the exciter equalization is proved to be effective, this MAP3 is now measured for a *panel equalization* according to the procedure described in Section 5.3. The aim of this equalization was not to outperform the above results but to obtain similar performance with an additional saving of laboratory tasks. In a large scale production, a simplified equalizing procedure, whose measurements were taken at a fixed microphone position, looks promising enough to run some experiments.

Three impulse responses are now obtained at a single centered microphone position and are averaged to obtain the basis with which to design a unique filter. Figure 5.7 shows the individual frequency responses for the first (brown), second (magenta) and third (cyan) exciter and the averaged frequency response in black line.

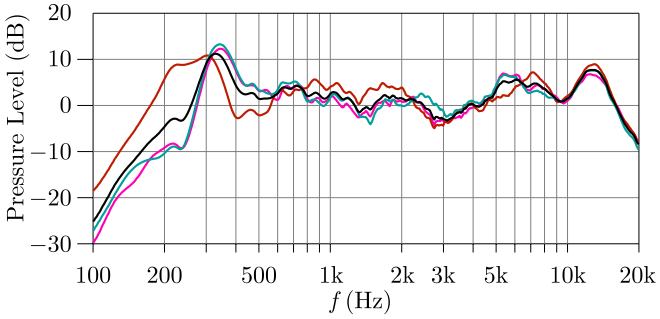

Figure 5.7. Individual frequency responses (brown, magenta and cyan) and the calculated average response (black) for a panel equalization of the MAP3.

Only one filter must be designed to compensate for peaks and dips that are present in the averaged response. Since the averaged response is similar to those of exciters 1 and 3, the filter is designed with the same parameters: target response of second-order high-pass Butterworth at 200 Hz with 14 SOS filter structure. The computed filter is applied to three exciters and their responses measured again, which results are presented in Figure 5.8.

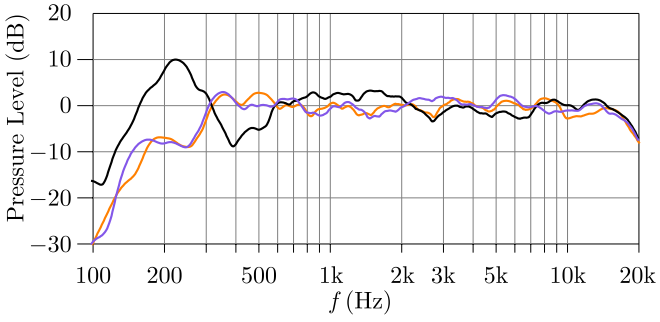

Figure 5.8. Measured frequency responses for the MAP3 with panel equalization. Exciter no. 1 (orange), Exciter no. 2 (black), Exciter no. 3 (violet).

The result of the equalization procedure is unsatisfactory for the middle exciter, which shows large irregularities of magnitude comparable to the unfiltered response. Although the spectral response for the edge exciters demonstrates a proper equalization, the poor performance for only one exciter invalidates the procedure. This dissimilarity in the filtered response is caused by the averaged response, which is very similar to that of exciters 1 and 3, and thus, it works effectively for those exciters.

The MAP3 filtered here is the simplest configuration to apply the panel equalization since it only accounts for three exciters, two of them being symmetrical. Considering that panel equalization has not given satisfactory results, it can be concluded that, for larger panels with more exciters involved, the panel equalization is not a proper method. As a consequence, in the following section, the exciter equalization will be applied to the MAP5.

5.4.3 Exciter Equalization for the MAP5

The exciter equalization that has given positive results is now applied for a larger MAP. The aim is to experiment with the equalization performance on panels with extended bass frequency response, where this method is particularly effective.

Each exciter was measured on its respective axis, resulting in a set of five frequency responses. Figures 5.9(a) and (b) show the spectra of the symmetric exciters 1–5 and 2–4, respectively. From the graphs, it can be seen that the measured frequency responses for exciter pairs have lots of similarities. These exciters are placed in a symmetrical position on the panel. Providing that the electromechanical characteristics are virtually the same for these two exciters, the only parameter that can change the radiation properties is the excitation mode pattern, which is a function of the driving point. For that reason, this similitude was as expected.

Since the behavior of the exciters positioned in symmetrical places at both ends of the panel is almost identical, it is feasible to measure for exciters 1 and 2, and assume that 4 and 5 will behave in a similar way. Therefore, filters will be designed for exciters 1 to 3 and will be replicated accordingly to account for the rest of the exciters. Figures 5.10(a), (b), and (c) show in black lines the frequency responses of the exciters 1, 2 and 3, respectively. Due to the proximity to the edge, exciter 1 has the worst

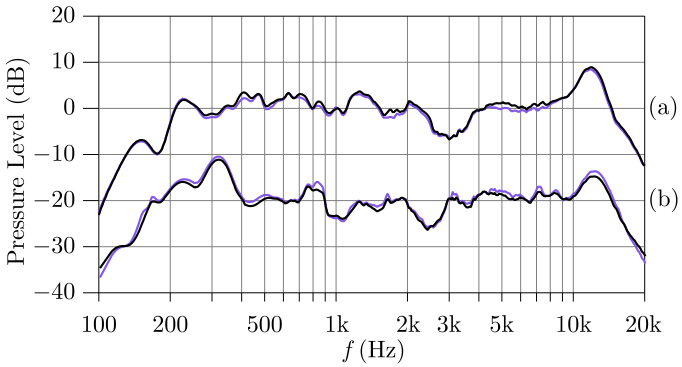

Figure 5.9. Similarity in frequency responses for symmetrical exciters. (a) Exciter 1 (black) and 5 (violet), (b) Exciter 2 (black) and 4 (violet). Representations are shifted 20 dB in order to maintain clarity.

low frequency response of the three. It reaches the mid frequency band at 200 Hz and presents a dip of 7 dB at 3 kHz. The spectra of exciters 2 and 3 broadens the low frequency region up to 170 Hz. For mid frequencies, a significant peak of 10 dB is observed in the region around 300 Hz and a weaker dip arises at 2.3 kHz. Again, the peak resonance caused by the coincidence effect is visible in these measurements at high frequencies.

The main difference with respect to the MAP3 is the extension in the low frequency radiation. Therefore, the filter is designed with a second-order high-pass Butterworth target at 175 Hz for exciter 1 and 125 Hz for exciters 2 and 3. Figure 5.10 shows in green lines the target responses for each exciter. For the three exciters, filters are then designed with a 15 SOS scheme. The responses of these filters and the simulated exciter filtered responses are shown in Figure 5.10 in red and blue lines respectively.

The measured equalized frequency responses after applying the designed filter are given in Figure 5.11 in blue lines, together with the original unfiltered responses in red lines. As with the small panel, the improvement of the frequency responses using the proposed filter is remarkable. Not only have the irregularities been flattened, but also an extension in low frequencies is observed for the first exciter. Therefore, all three exciters now share similar low cut off frequency, as can be noticed in Figure 5.11. The remaining variations in spectra that are not properly equalized are again due to the physical constraints of the panels.

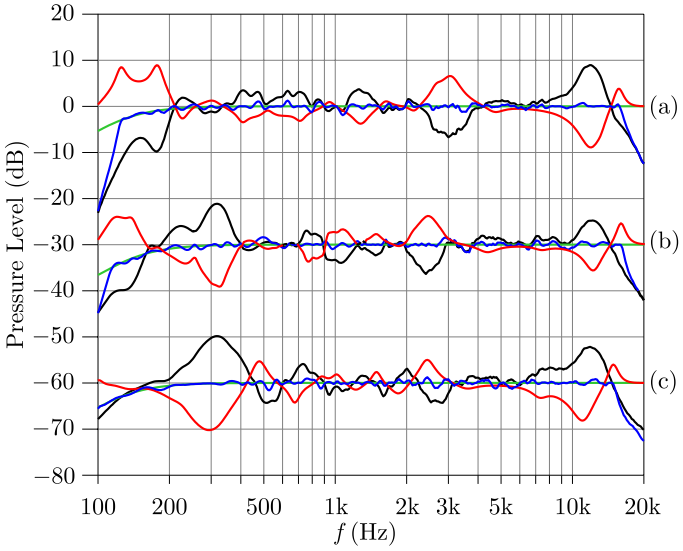

Figure 5.10. Frequency responses of the exciter equalization process for the first three exciters of the MAP5. Exciter measurement (black), filter target (green), filter response (red), simulated exciter filtered response (blue). (a) Exciter 1. (b) Exciter 2. (c) Exciter 3. Representations are shifted 30 dB in order to maintain clarity.

The logarithmic standard deviation values for this MAP5 are as follows: for the unfiltered responses $\sigma_{\log}$=3.64, 3.47, 3.16, 3.49 and 3.65 dB, whereas for equalized responses, $\sigma_{\log}$ has decreased to 1.04, 1.84, 1.37, 1.80 and 1.06 dB for the first to fifth exciter respectively. The frequency ranges employed to compute these values were those of the target frequency response.

From the above results, the similarities in the response of symmetrical exciters can lead to a reduction of the measurement points without sacrificing the filtering accuracy. From a practical point of view, this reduction has technological and economical benefits in a large scale production of such panels, where measurements are performed with time restrictions. In the next section, a further step towards a more efficient procedure is made by means of a reduction of filter coefficients.

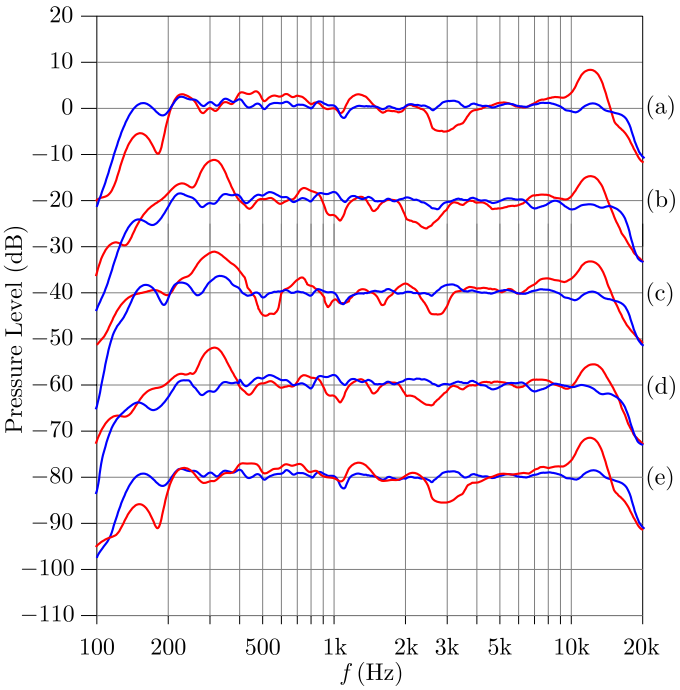

Figure 5.11. Equalization results of the MAP5. Filtered response (blue), original response (red), (a) Exciter 1. (b) Exciter 2. (c) Exciter 3. (d) Exciter 4. (e) Exciter 5. Representations are shifted 20 dB in order to maintain clarity.

5.4.4 Filter Order Reduction with Subjective Assessment

In Section 5.2.3 it was introduced that an SOS chain with enough order provides a high equalization quality with low computational cost, minimum objective error and a subjective quality similar to that of a high order FIR filter.

However, a further step can be made to optimize the method by reducing the number of stages in the SOS chain, that is, the number of coefficients, based on a subjective assessment. The objective is to study the influence of the order of the filter in the perceived quality of the equalization. To that end, a total of 20 listeners with normal hearing participated in a blind test. It consisted of a progressive decrement of the filter coefficients up to a point at which listeners would perceive a difference between two consecutive samples.

The test was carried out in two ways in order to obtain irrefutable conclusions. First, an ABX test was performed and second, a test based on the dynamic commutation of the bank of filters was made to prove if the listener could perceive any difference in the process. The description and results of both tests follows:

ABX Test

The ABX test protocol was proposed by Krueger and Muller in 1977 and first reported in [Clark, 1982]. In the ABX test there are two sources that are compared to determine if there are detectable differences between them, for example, two audio sources for a listening test or two pictures for a viewing test. ABX testing can prove to a certain level of confidence that one can, or cannot, distinguish between them. It is not proof of quality, but it is proof of equal or disparate quality. A key feature of this method is that the tests are performed "double blind", or without the listener's knowledge of what equalization is under test. The listener has full access to the two known equalizations, A and B, and to an equalization X that can be either A or B, but without knowing in advance which one of them it is. Just by listening to the equalization X, the listener must decide if it is A or B. This eliminates the placebo effect that is present on all sighted listening tests. To reduce the influence of chance on the results, multiple tests or trials are performed and a statistical analysis is made with the results to determine if the listener is really hearing a difference.

To perform the ABX test, a 20-people jury was employed. A particular pop music sample 20 second's long was chosen because of its broad spectrum and the high number of musical instruments. This fragment was filtered with different SOS filter orders. As a reference of a properly filtered spectrum, a 15 SOS filter was used and then, lower order filters were essayed in the range where differences were starting to be noticed. After some informal tests to explore the critical values, three filter banks were selected: 10, 8 and 7 SOS coefficients. Therefore, all the subjects performed three turns comparing 15 vs 10, 15 vs 8 and 15 vs 7. Table 5.1 shows the results of the ABX test, indicating the number of subjects that could or could not detect the differences.

As can be observed by the test results, between 15 and 10 SOS, no differences were found by any of the listeners, whereas between 15 and 8 SOS, only one listener could tell the difference. The limit is given for the

	Detectable differences	Non detectable differences
15 vs 10	0	20
15 vs 8	1	19
15 vs 7	18	2

Table 5.1. Results of the ABX test for reducing the number of SOS coefficients in the MAP5.

comparison between 15 and 7 SOS, in which almost all the participants could distinguish the differences between samples.

Dynamic Commutation Test

Although the above results are conclusive enough, it was intended to know if the listeners were able to notice a difference upon commuting the filter at any moment when the music was reproducing. This test was also performed in three turns but with a slight change in the procedure. It consisted of reproducing the music and progressively decrementing the filter coefficients in real time up to a point at which listeners would perceive a difference. In such a test, the subject will hear a musical passage with 10 changes of filtering with 15 SOS and n SOS, being $n < 15$, in a random distribution. If no difference is perceived, the number of coefficients n decreases and a new trial is run. The distribution of samples changes for every new trial. The subject undergoing the test does not know which sample is 15 or n SOS, so no user bias will exist. The person conducting the test notifies the subjects when a sample is going to change, so they can pay attention to the potential change.

A "Correct match" is achieved when a subject is able to distinguish the coefficient reduction. This happens if the subject only notices changes at the transitions from samples with a different filter. On the contrary, if no transition is occurring and a change is reported (false positive) or if nothing is pointed out when there is a change (false negative), these are marked as "Incorrect match". Figure 5.12 depicts the results of testing three comparison pairs.

As observed in the figure, the subjects were not able to distinguish between samples filtered with 15 SOS and filtered with 10 SOS. Therefore, some more tests were performed in a similar way to explore the limit at which listeners reported changes correctly. For the comparison between 15

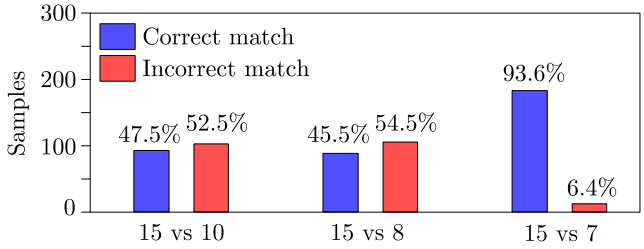

Figure 5.12. Results of the dynamic commutation test for reducing the number of SOS coefficients in the MAP5.

and 8 SOS, the balanced distribution of correct and incorrect answers still demonstrates that no difference is appreciable by listeners. The limiting reduction was found when switching from filters with 15 to 7 SOS. According to the results of Figure 5.12, 93.6% of the total transitions between samples were correctly perceived. As a consequence of both tests, from a perceptual point of view, the filtering process of the MAP5 can be applied with 8 SOS because no difference with respect to the original coefficients is reported. As expected, the objective measurements of the filtered response with 8 SOS show a more irregular pattern than with the initial 15 SOS, but these tests have demonstrated that the two responses are equivalent from a perceptual point of view.

5.5 Conclusion

Two MAP prototypes, MAP3 and MAP5, being representative of small and mid size panels, have been equalized with an efficient equalization method that requires a very low computational cost by means of an advantageous IIR scheme that outperforms the efficiency of FIR filtering approaches discussed in Section 2.5.2.

MAPs are flat loudspeakers comprising multiple drivers, so a methodology that applies filters to the panel as a whole has been tried in the small panel, but with discouraging results. Since the panel equalization of a MAP with only three exciters has resulted in faulty response for some of the exciters, the method is not advised for larger panels.

On the contrary, individual equalization of the drivers has been tested

with both small and mid size panels with satisfactory results. Although not completely flat, the improvement of the frequency responses using the proposed filter is remarkable. Not only have the irregularities been flattened, but also an extension in the response of low frequencies is observed for the edge exciters. This improvement helps in solving the problem of the dissimilar frequency response of an exciter near the panel boundaries that was mentioned in Section 1.2.

According to the two filtering frequency bands for WFS applications, this equalization method can be employed on the entire audio frequency band. At high frequencies, the equalization outperforms the efficiency of other methods. At low frequencies, below the aliasing frequency, the method can be employed as a pre-filtering for the room compensation algorithms.

Results have also confirmed that the similarities in the response of symmetrical exciters on a MAP can be used to considerably reduce the number of measurement points. Additionally, if several MAPs are manufactured maintaining exciter type and position, panel material and housing, their responses will be similar. Hence, for a complete reproduction setup with several MAP5, only three unique equalization filters must be designed, provided that exciters are symmetrically placed on the panels.

Finally, some subjective tests have confirmed that it is possible to reduce the order of the filter considerably without sacrificing the perceived quality of the equalization. As a consequence, from a perceptual point of view, the filtering process of the 5-Exciter MAP can be applied with 8 SOS because no difference with respect to the original coefficients is reported. The particular number of reduced coefficients must be tested for each application.

By taking advantage of this filter coefficient reduction, a very large WFS system driven by MAPs can be equalized individually with low hardware requirements.

6 Large Multiactuator Panel Prototype

Large Multiactuator Panel Prototype 6

MAPs ARE FLAT STRUCTURES that facilitate the integration of sound and image stimuli into a single device. To that end, MAPs present an advantageous screen shape in which to project images without blur because the vibration of the panel is low enough to be imperceptible to the human eye. In addition, MAPs can be integrated into room interiors because of their low visual profile, as part of the decoration or embedded into walls. However, the size of the screen must be moderately large for certain audiences, such as cinemas and conference rooms. Therefore, a large MAP prototype that fulfills the image and sound requirements above mentioned is presented in this chapter, incorporating all the enhancements that were discussed over the previous chapters of this thesis.

6.1 Introduction

MAPs enhance audiovisual immersion and provide integration with room interiors in a way that conventional loudspeaker arrays cannot perform. To that end, the size of the panels must be large to project moving or still images for large audiences. Also, regarding the quality of sound radiation, large panels are advisable since the lowest excitation modes can be excited, which determine the useful bandwidth at low frequencies. In

addition, the extra area of such large panels can be used to accommodate extra exciters with which to generate sound fields at other elevation levels. Figure 6.1 shows the amended concept of audiovisual immersion by means of an offset videoprojection onto a large MAP. In this setup, both image and multichannel audio reproduction is located on the panel of the MAP.

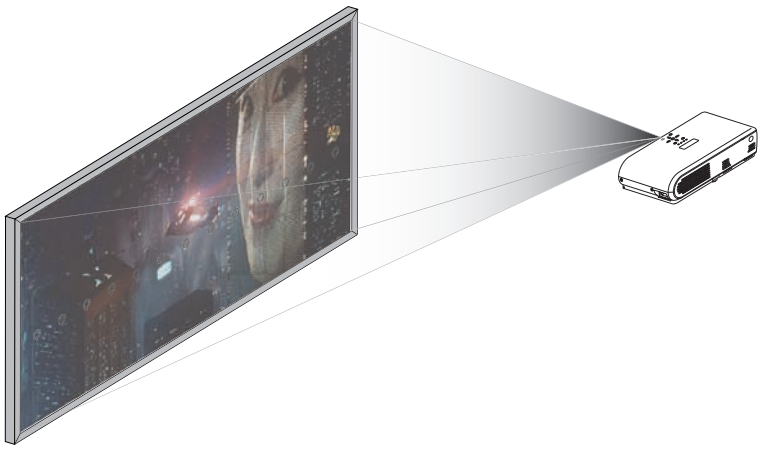

Figure 6.1. Audiovisual immersion concept in a large MAP.

In this chapter, the design process of a large MAP prototype is presented. The prototype has been designed and built to fulfill the requirements of immersive audio applications and utilizes the enhancements discussed in previous chapters. Due to the panel size, it gives a proper acoustic behavior in distributed mode operation since the low frequency range is correctly generated by vibrating modes.

The outline of the chapter is as follows: Section 6.2 describes the design of the large MAP prototype, including the filtering process and the boundary condition used. In Section 6.3, the performance of the large MAP is assessed and compared to smaller panels and dynamic loudspeaker arrays. Finally, Section 6.4 concludes the chapter.

6.2 Prototype Description

In this section the design, building and adjusting of the large MAP prototype is presented. Two subsections are devoted to the discussion of the

boundary conditions employed as part of the MAP frame and the filtering process to equalize the spectra of each exciter according to the method introduced in the last chapter.

6.2.1 Design Process

The main requirement of this prototype was the size of the panel. It was intended to construct a large but practical MAP that can be carried by few people and can pass doorframes. For that reason, the width, as the larger dimension, was set to approximately 2.5 m, the height being a reasonable dimension to acquire a landscape aspect ratio. The resulting large MAP prototype dimensions are depicted in Figure 6.2. For comparison, dimensions are shown to scale with respect to the MAP prototypes developed by some of the Carrouso partners, which were introduced in Chapter 2 (Figure 2.6).

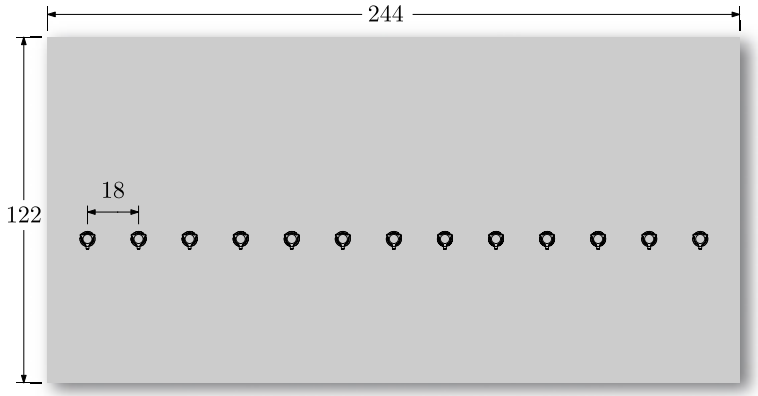

Figure 6.2. Geometric details on the large MAP prototype developed in this thesis. Dimensions in centimeters.

The panel dimensions facilitate the distribution of 13 exciters spaced 18 cm apart, whose distance is the same as the rest of the MAPs of this thesis, and presents an aliasing frequency of approximately 1 kHz. In such a configuration, a secondary source distribution of more than two meters is achieved without intermediate discontinuities that can produce additional undesired aliasing artifacts, as demonstrated in Chapter 3.

As stated in the introduction, the MAP prototype was designed to meet the demands of immersive audio applications. For that purpose, in

addition to the exciter distribution in the horizontal hearing plane, two exciter distributions were implemented above and below the horizontal plane. These are more spaced versions of the central exciter distribution. The total number of exciters in the large panel is 23, which can be driven by typical 24-channel audio cards.

In the building of the prototype, the materials of the housing were chosen to support high structural demands due to the panel size whilst also being as light as possible. This requirement excluded the Medium-Density Fiberboard (MDF), which was used in the smaller prototypes, since its inherent density makes the MAP frame unfeasible. Instead, 19 mm plywood was selected as the engineering wood because of its resistance to twisting, and its high degree of strength. Figure 6.3 shows the back frame in the initial processing steps. An inner crossed rod structure was implemented to enhance the bending resistance and stability both in horizontal and vertical planes, in the same manner as the University of Erlangen prototype [Seuberth, 2003], whose characteristics were presented in Section 2.3.2. To further increase structural stability, wood joints were connected with screws and also glued.

Figure 6.3. Back enclosure of the large MAP in the carpenter's workshop.

The panel is a sandwich of polyester film bonded onto an impregnated paper honeycomb 5 mm thick using a thermoplastic adhesive. The panel relies upon a 4.8 mm honeycomb cell cap resonance for its high frequency performance. Its bending rigidity is 13.4 and 11.7 Nm in the x and y directions respectively and has an areal density of 0.67 kg/m^2. The panel was cut using a sharp knife to the dimensions of Figure 6.2, 122×244 cm. The cutting conditions ensured a smooth, debris-free edge finish.

The exciters were 25 mm diameter dynamic transducers with an eight-foot panel coupling that were attached to the panel in an inertial fashion [Roberts, 1998]. These exciters were chosen due to the smooth frequency spectra they presented in preliminary tests. Although not capable of delivering the electrical power of the ELAC exciters of the Carrouso project prototypes of Section 2.3.2, their 12 W nominal input power is sufficient in a panel driven by such a large number of exciters.

The enclosure was constructed with a clamping mechanism consisting of two frame members, the back enclosure, depicted in Figure 6.3 and the front bezel. These two pieces are forced into pressure contact at the panel edges with two foam strips as edge boundary conditions, as will be explained later. The panel can easily be removed and placed back into the enclosure for fine tunings.

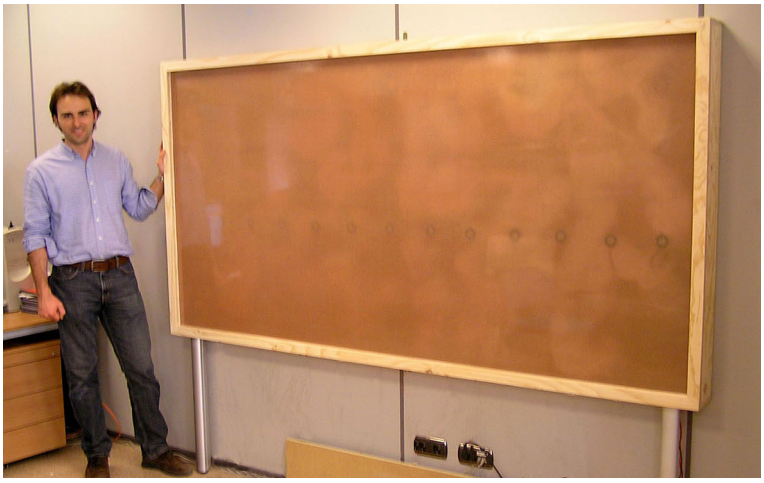

Figure 6.4. Final prototype of the large MAP.

To prevent the formation of standing waves inside the loudspeaker enclosure, the space underneath the panel was lined with a layer of absorbing material. Wiring is channelled through the absorbing material to prevent undesired interaction with the vibrating panel, which would cause a high degree of distortion. Six Speakon 8-Pole connectors were employed due to their robustness which was experienced in early prototypes in the laboratory.

The back enclosure and the front bezel were assembled to obtain the final prototype. Figure 6.4 shows a picture of the presented large MAP with the author of this thesis for comparison purposes.

6.2.2 Edge Boundary Conditions

The clamping mechanism was designed to account for the necessary space required for the absorbing material of the boundary condition. According to the experiments in Chapter 4, elastic boundary type 2 (EB2) provides smooth on-axis responses for mid frequencies and a moderate response in the low frequency region. High frequencies are not governed by the type of edge boundary condition, so no enhancement was expected with the EB2. To achieve such a condition, two foam strips running along the entire perimeter of the enclosure were provided. Figure 6.5 shows a detail of the large MAP front bezel in which the upper foam strip can be observed.

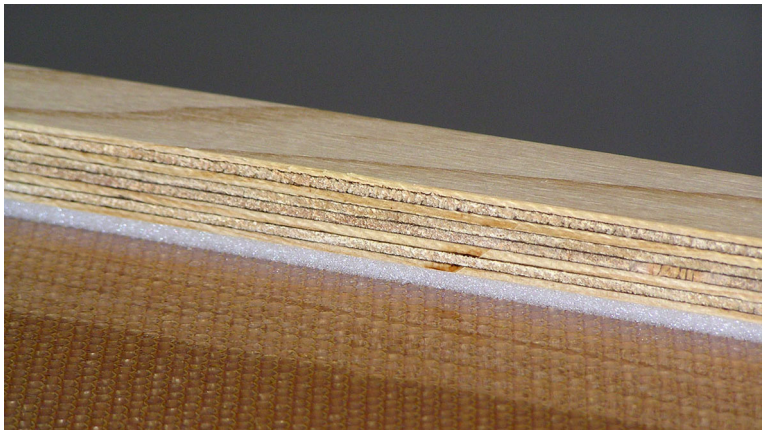

Figure 6.5. Detail of the front bezel showing the EB2 boundary condition with foam.

6.2.3 SOS Filtering

In Chapter 5, the convenience of an efficient spectrum equalization, that takes into account the particular placement of each exciter onto the panel, was stated. This equalization process was applied to the large MAP prototype in order to flatten the exciter responses up to a point where the physical constraints of the panel would counteract the filter process. Due to the positive results on the dedicated exciter equalization, it was decided to perform this process directly.

To that end, all individual exciters were measured on their respective axis. The results showed the same trend observed in the smaller MAPs, consisting of the similarity in the frequency response of symmetrically positioned exciters onto the panel. As discussed in Chapter 5, this feature can be exploited to reduce the number of measurements and filtering processing.

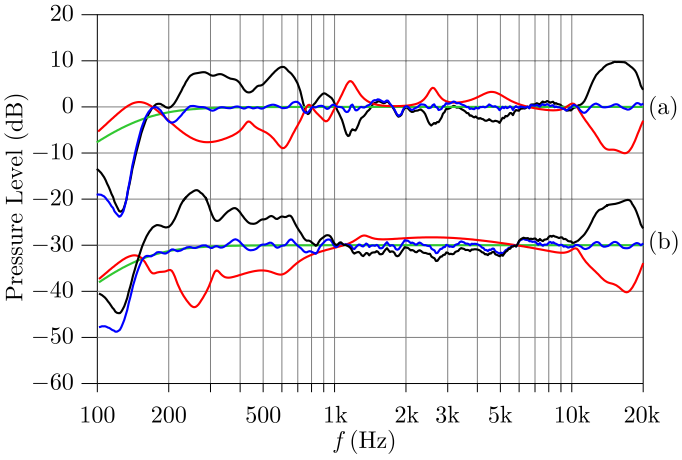

Figure 6.6. Frequency responses of the exciter equalization process for the large MAP. Exciter measurement (black), filter target (green), filter response (red), simulated exciter filtered response (blue). (a) Exciter 1. (b) Exciter 7. Representations are shifted 30 dB in order to maintain clarity.

Figures 6.6(a) and (b) depict two selected measured responses corresponding to the exciter 1, the one closest to the edge, and the exciter 7, which is positioned in the center of the panel, respectively. Due to the enlarged size of the panel, the low cut-off frequency is lower than that of the smaller panels, as expected. The exciter 1 reaches the mid frequency band

at 150 Hz and shows an extended output level from 200 to 800 Hz and from 10 to 20 kHz, the latter being in the region above coincidence frequency. In between, three moderate dips can also be observed. The response of the exciter 7 is slightly extended in the low frequency region to 130 Hz and also presents the same two large peaks, whereas dips are more smoothed. As observed in the figures, the influence of the fact that the exciter is mounted close to the edge is negligible for this large MAP with elastic boundaries.

For these representative responses, all filters are designed with a second-order high-pass Butterworth target at 175 Hz, shown in green in Figure 6.6, and 12 SOS sections. In all cases, from the total number of SOS, one is employed for the second-order high-pass filter. The responses of these filters and the simulated exciter filtered responses are given in Figure 6.6 in red and blue respectively. The rest of the filters are computed in a similar way.

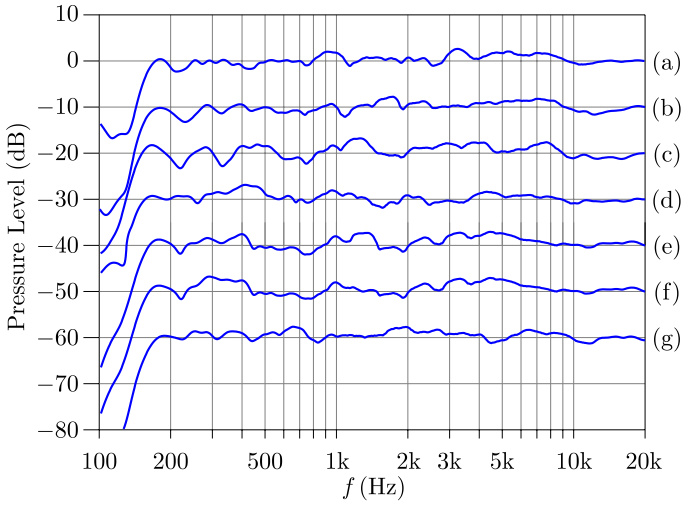

Figure 6.7. Exciter filtered responses of the large MAP. (a) Exciter 1 to (g) Exciter 7. Representations are shifted 10 dB in order to maintain clarity.

By taking advantage of the exciter position symmetry, filters were only calculated for exciters 1 to 6 and for exciter 7. Then, the resulting filters 1 to 6 were applied to the symmetric exciters 8 to 13. These filters were employed in the large MAP and the equalized frequency responses were measured in the laboratory. The resulting frequency responses are depicted in Figure 6.7.

From the above results, the filtering process has equalized the responses considerably, being now almost flat. As expected, some irregularities in the form of partially filtered peaks and dips appear in all the exciters. The physical constraints of the panel played a role by counteracting the filtering process to an extent. However, the filtering process has considerably improved the original uneven responses. To give an objective quality measure of the flatness of responses, the logarithmic standard deviation, introduced in Section 5.4.1, can be calculated. For the filtered responses of Figure 6.7 in the range of the target frequency response (175 Hz to 20 kHz), the resulting logarithmic standard deviation values result in values between 1 and 2 dB.

6.3 Performance

This section will assess the performance of the large MAP by analyzing the sound wavefield created in single exciter operation and by synthesizing a desired source in WFS. The experimental setup for sampling the wave field along a line is similar to that introduced in Section 3.3, but due to the extended horizontal dimension of the MAP, a centered 200 microphone array will be used. For implementing such an array, a single 1/2" electrostatic microphone is driven at 1 cm steps by a linear sliding table. This spacing is sufficiently below the theoretical Nyquist sampling limit of 9 cm. Details of the geometric description of the experimental setup are given in Figure 6.8.

In the following, the results of the experiments on the large MAP are presented and discussed through two case studies, broad aperture radiation and plane waves.

The first case is achieved on programming a WFS axial plane wave (exciting all transducers with the same stimuli) and a 45º plane wave (varying accordingly the phase shift between exciters). The second is obtained on synthesizing a spherical wave in WFS and by means of single exciter operation. To conclude the section, a comparison with smaller MAPs and dynamic loudspeaker arrays working in similar conditions is presented.

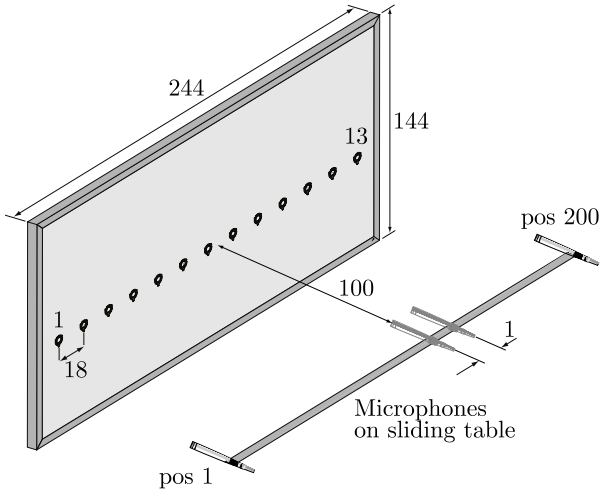

Figure 6.8. Experimental setup geometry for the wavenumber domain analysis. Dimensions in centimeters.

6.3.1 Axial Plane Wave

Figure 6.9 depicts the experimental setup and the responses of the MAP on emitting an axial plane wave ($\theta = 0^{\text{o}}$). Multitrace impulse response shown in Figure 6.9(b) is achieved by representing the impulse responses of each microphone and gives information on the wave front propagating through space. In Figure 6.9(c), a space-time wavenumber domain representation is plotted.

As expected, the multitrace impulse response illustrates some artifacts that can be seen as two edge events, weaker and delayed, that follow the planar wavefront. In the wavenumber domain representation, there are components at zero k_x which are repeated in the spatial axis with periods that depend on the spacing of the transducers in the array [Spors and Rabenstein, 2006]. For such a MAP radiating an axial plane wave and considering 18 cm as the distance between exciters, the maximum spatial frequency without aliasing is k_x=34.9 m^{-1}. In a infinite length loudspeaker array, where radiation occurs at angles reaching $\pm 90^{\text{o}}$, the associated temporal wavenumber would be directly k=34.9 m^{-1} (1.9 kHz). However, the finite size of the MAP causes truncation effects which modify the maximum incoming angle. For the geometry setup, a centered listening point has an angle of $\pm 50^{\text{o}}$ with respect to the array aperture (2.44 m). Then, the

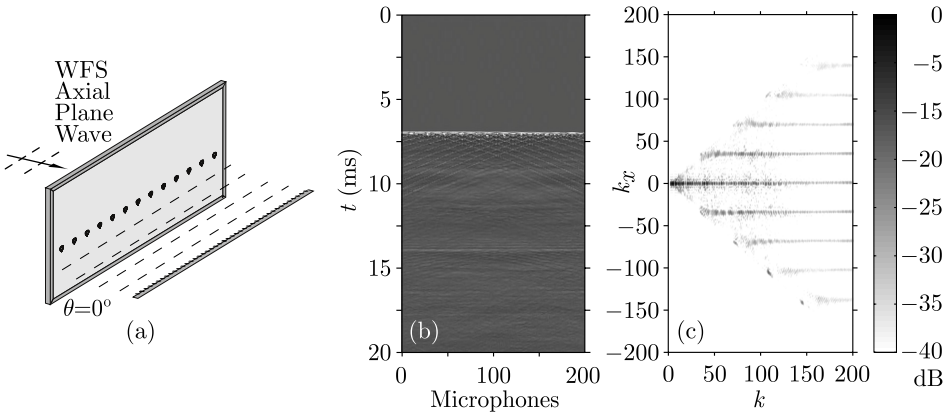

Figure 6.9. Axial plane wave generated by the MAP prototype. (a) Setup. (b) Multitrace impulse response. (c) Wavenumber domain representation.

aliasing spatial frequency of 34.9 m^{-1} matches to k=45 m^{-1}, so the aliasing frequency for axial plane waves in such a particular geometry setup is 2.4 kHz. If other angles are considered, when reaching the maximum plane wave that the MAP is capable of emitting, the aliasing frequency decreases to a minimum of 1.2 kHz. Note that the theoretical aliasing frequency of $c/2\Delta x$, where Δx is the spacing between transducers, is calculated for loudspeaker arrays of infinite length.

6.3.2 45° Plane Wave

For a tilted plane wave, the behavior of the large MAP is presented in Figure 6.10 with the same responses as above. Multitrace impulse response shows again the aliasing artifacts as non-desired curved wavefronts that travel with the tilted planar wavefront. Again, the repetition of spectra in the wavenumber domain representation of Figure 6.10(c) denotes aliased spectra that can be perceived depending on the geometry of the system and the temporal frequency.

On the other hand, the wavenumber domain representation shows that the large MAP is capable of generating the tilted plane wave correctly. The angle with which the spectrum of the desired 45° plane wave is plotted is a measure of the real incoming plane wave angle. It can be computed by taking two coordinates and applying that $\sin\theta = 140/200$, which gives an

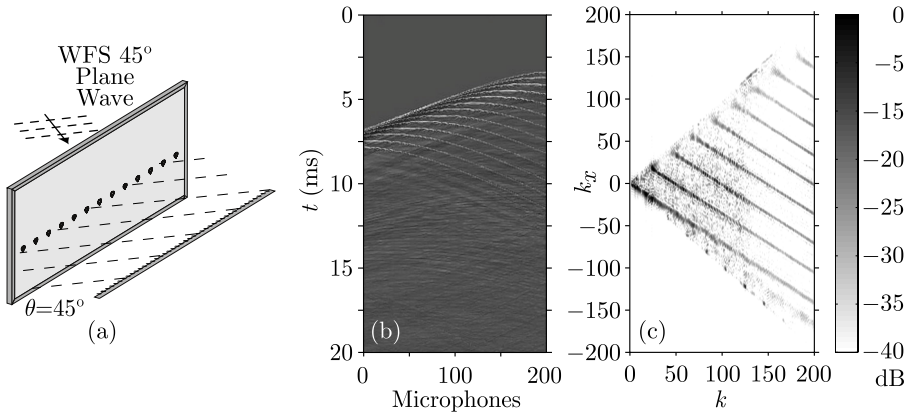

Figure 6.10. 45° plane wave generated by the MAP prototype. (a) Setup. (b) Multitrace impulse response. (c) Wavenumber domain representation.

incoming angle of 44.4°.

6.3.3 Point Source from the Middle Exciter

Once the MAP has been tested with plane waves, the following presents the resulting wavefield on exciting the middle transducer alone (exciter 7). Figure 6.11 shows time and wavenumber domain results of such a configuration. The first consequence of exciting single points is the absence of aliasing artifacts, both in the multitrace impulse response and the wavenumber domain representations. This is due to the fact that no WFS algorithm is present for generating such sound fields. However, the long tail related to the distributed modes of the panel is visible as concentric wavefronts that follow the first impulse. In addition to this ringing, some room reflections can be observed in the multitrace response.

The wavenumber domain representation of Figure 6.11(c) shows a concentric pattern that was also experienced in the latter smaller prototypes of Chapters 3 and 5.

6.3.4 Virtual Point Source

To generate a virtual point source behind the secondary source distribution, a large MAP in this particular case, different amplitude and phase

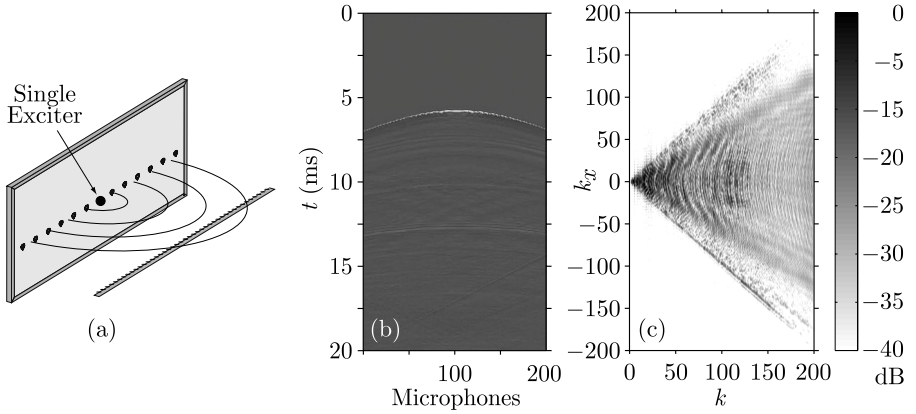

Figure 6.11. Middle Exciter Wave Field generated by the MAP prototype. (a) Setup. (b) Multitrace impulse response. (c) Wavenumber domain representation.

signals must be applied to every exciter. Figure 6.12 shows the experimental setup and responses of a centered virtual source, 30 cm behind the panel. The concave wave fronts that can be observed in the multitrace impulse responses are a sign that the signal is created behind the array. As with plane waves, the multitrace impulse response shows the typical aliasing artifacts that will distort the desired wavefront. The pattern behavior in the wavenumber domain representation of Figure 6.12(c) also indicates that a certain amount of aliasing is present. Such a pattern is the consequence of overlapping spectra in the high frequency region, above the aliasing frequency.

The angle at which a listener would perceive the generated sound field can be studied in the wavenumber domain representation of Figure 6.12(c). To that end, the gray shaded area in this representation has limiting values for k=200 m^{-1} of k_x=$\pm$140 m^{-1}. The angles that can be computed with these values are those formed between the first and last microphone, and the excitation point. For the centered excitation, arcsin 140/200=44°, whereas the experimental angle was 45°.

6.3.5 Virtual Focused Source

Besides generating virtual sources behind the loudspeaker arrays, WFS is also capable of synthesizing virtual sources in front of the array, also known

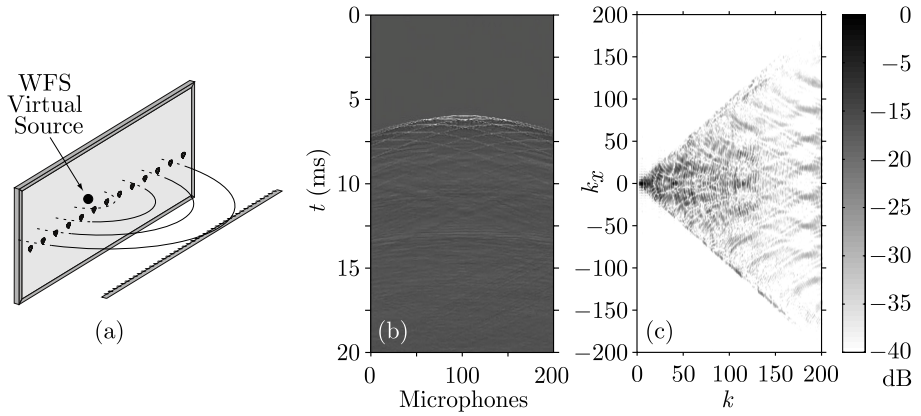

Figure 6.12. Centered spherical wave generated by the MAP prototype. (a) Setup. (b) Multitrace impulse response. (c) Wavenumber domain representation.

as focused sources. Figure 6.13 shows the experimental setup and results of a centered focused source at 50 cm in front of the large MAP.

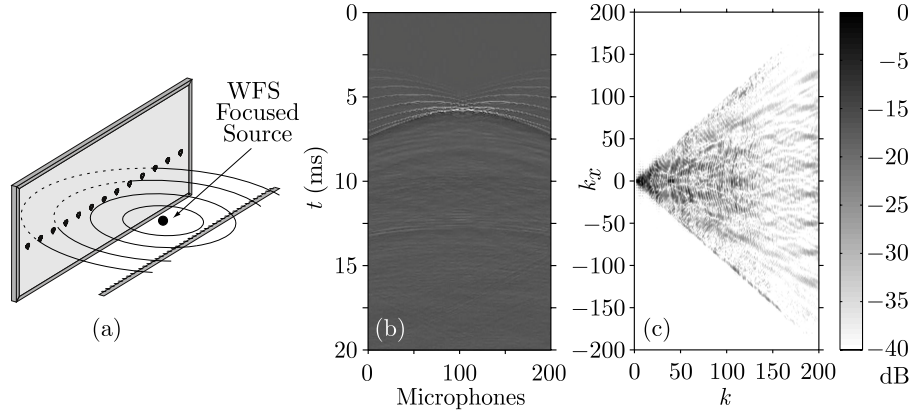

Figure 6.13. Focused source generated by the MAP prototype. (a) Setup. (b) Multitrace impulse response. (c) Wavenumber domain representation.

Contrary to the shape of the wavefronts of sources behind the array, now a convex wave front shape is observed which focuses on a point that will be localized as the position of the focused source. In this case, it is a centered focused point, hence the convex wave front is symmetrically

plotted in Figure 6.13(c) focusing on the 100th microphone position. This figure also shows that the effects of spatial aliasing arrive at the recording line before the synthesized wave front does. Similar results were reported in [van Rooijen, 2001].

The wave field of a focused source diverges after having passed the focus point so a listener positioned in the diverging part of the wave field perceives a virtual source at the position of the focus point. A listener positioned in the converging part of the wave field will experience a confusing perception due to contradictory localization cues [Ahrens and Spors, 2008a]. In this experiment, the focusing point was set to 0.5 m and the measurement was performed at 1 m so as to assure that the sampled wave field was in the diverging part and the localization cues were correct.

6.3.6 Offset Discrete Excitation

In the following, the results on exciting the MAP in offset discrete points via single exciter vibration is presented. Two offset excitation points are measured by exciting the 9th transducer as a slight off-axis point and the 13th transducer, which is the maximum offset value for this MAP. Figure 6.14 shows time and wavenumber domain results of such a configuration. As with a centered transducer excitation, no aliasing artifacts occurred. Comparing the two time responses, a shift in the curvature of the wavefront can be seen, which is consequent with a change in the angle of the incoming wavefront.

The wavenumber domain representations of Figure 6.14(c) and (d) give information about the limiting angles at the microphone sampling line. These angles can be calculated similarly to the centered transducer excitation discussed above by observing the gray shaded area in the wavenumber domain representations. In this case, they show limiting values for k=200 m^{-1} of k_x=(160,−100) m^{-1} for the 9th exciter, and k_x=(175,20) m^{-1} for the 13th exciter. For the 9th exciter, the two resulting limiting angles were arcsin 160/200=53° and arcsin −100/200=−30°, whereas the experimental angles were 50° and −29°. For the 13th exciter, the two calculated angles 61° and 5° matched to the values according to geometry of 61° and 4°.

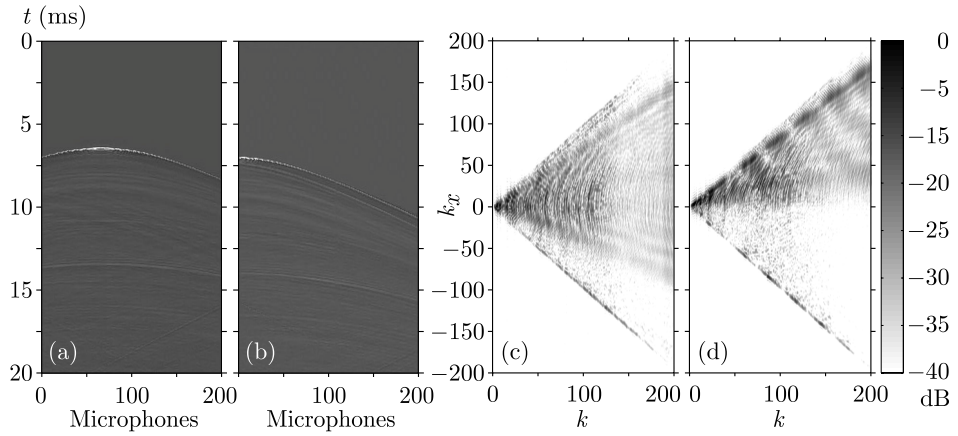

Figure 6.14. Sound field generated by exciting a single transducer in the MAP prototype. Multitrace impulse responses: (a) 9th exciter. (b) 13th exciter. Wavenumber domain representations: (c) 9th exciter. (d) 13th exciter.

6.3.7 Comparison

In this section, the two more representative sources for WFS operation previously discussed, a centered WFS point source and an axial plane wave, will be compared to those of similar prototypes. First, an arrangement of five small MAPs comprising three exciters per panel is considered. Although the panels are substantially smaller, the distance between transducers is the same as the large MAP. Secondly, an array of 5" dynamic loudspeakers, again with similar loudspeaker spacing, is tested with the same stimuli.

Regarding the radiation of small panels, shown in Figures 6.15(a) and (b), the main differences with respect to the large MAP are due to the lack of sufficient mode density in small panels for the low frequency end. This behavior can be seen in the wavenumber domain representation for both plane and spherical wave as a decrease in the energy levels for low frequencies, compared to those of Figures 6.9(c) and 6.12(c). Additionally, the wavenumber domain representation for an axial plane wave of 6.9(c) shows that the desired source, a line at k_x=0 m^{-1}, is more even than with small panels. The same trend occurs for the off-axis plane waves, which are the resulting aliased contributions for the discretization of the secondary source distribution, discussed in detail in Section 3.2.3.

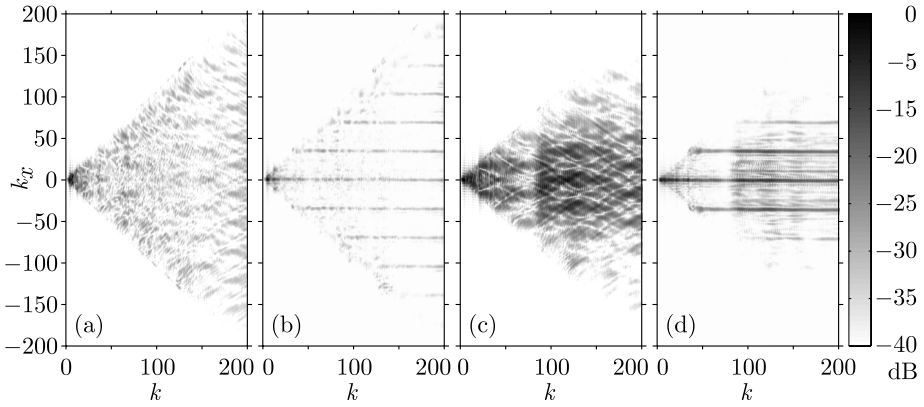

Figure 6.15. Wavenumber domain representations of other loudspeaker systems with similar conditions than the introduced MAP. (a) Small MAP, centered WFS source. (b) Small MAP, axial plane wave. (c) Dynamic loudspeaker array, centered WFS source. (d) Dynamic loudspeaker array, axial plane wave.

Dynamic loudspeaker arrays differ from MAPs in the sound field they create. Piston radiation shows a severe off-axis decrease radiation due to the inherent lobulated pattern for mid and high frequencies, as can be seen in Figure 6.15(c) and (d). Note that only the first replica is emitted by dynamic loudspeakers due to directivity. For the listener, this means that only two additional plane waves, symmetrically distributed with respect to the axial plane wave, are created. Their incoming angles will increase with frequency towards a tangential incidence, which would not be reached at the limit due to directivity and truncation effects. In the case of the large MAP, its broad angle radiation facilitates the reproduction of larger spatial frequencies. Also, if the pattern in the gray shaded area within the wavenumber domain representation of Figure 6.15(c) is analyzed, the typical aliased spectra can be recognized. Subjective evaluation of such artifacts are addressed in [Corteel et al., 2007].

6.4 Conclusion

A large MAP prototype, that has been designed and built to fulfill the demands of immersive audio applications, has been described in this chapter.

The large size screen enhances and improves immersion for a large audience, as pointed out in Section 2.3.4. The low visual profile and the integration of video and audio stimuli of this prototype fulfill the requirements introduced in Section 1.2.

Based on the experiments on early prototypes, the enhancements proposed throughout this thesis have been applied to this large MAP. On the one hand, among the different types of boundary conditions discussed in Chapter 4, the elastic boundary type 2 showed a smooth mid frequency response and a balanced low frequency response. Hence, a boundary condition EB2 built with foam material was employed in the large prototype. On the other hand, exciter equalization has been applied to compensate for the inherent irregular frequency response of MAPs, as introduced in Section 2.5. Due to efficiency with satisfactory results, and the ability of taking advantage of symmetry on the exciter position, the large MAP prototype has been equalized with the IIR filter, structured as a chain of SOS, which was discussed in Chapter 5. The equalization has been performed for the entire frequency band with positive results.

According to the measurements, and the panel behavior explained in Section 2.2, the panel size facilitates a proper mode distribution and density in the mid and low frequency range. This effect is also observed for off-axis radiation directions, which means that wavefronts emanating in broad angles are correctly generated and merged to create the desired wavefield. Also, the large size of the prototype extends the area where truncation effects distort the acoustic signals. In this regard, if several panels are attached to form an array of MAPs, their behavior is not as accurate as with the large MAP, due to new aliasing artifacts caused by the intermediate supporting structures, as discussed in Section 3.5; and their effect is minimized by means of the elastic boundaries discussed in Section 4.5. Results in the form of multitrace impulse responses and wavenumber domain analysis showed that the sound field is properly generated for a wide listening area. The responses between the large MAP and equivalent loudspeaker systems, smaller MAPs and dynamic loudspeakers, have also been compared. The main improvement with respect to smaller MAPs lies in the greater bandwidth for on- and off-axis radiation. However, the use of supporting subwoofers is still advisable for a natural sound reproduction. On the other hand, dynamic loudspeaker arrays showed an irregular energy distribution in space due to their piston-like directivity characteristic.

7 Conclusions

7 Conclusions

The overall aim of this research was to analyze the performance of Multiactuator Panels in the space-time frequency domain to achieve some practical enhancements towards a more accurate Wave Field Synthesis reproduction.

This chapter will revisit the research objectives given int the introductory chapter, summarize the findings of this research work and offer conclusions based on the findings of the remaining chapters. Next, the contribution of this thesis to the enhancement of Multiactuator Panels for Wave Field Synthesis will be listed in another section. Recommendations for future research will be discussed, in terms of how to progress with this research study. Additionally, the final section contains a list of published works occurred during the course of candidature for the degree. The main themes concluded in this thesis are shown in the following section.

7.1 Conclusions

As introduced in Chapter 3 and experimented through the entire thesis, a *methodology for the analysis of sound field radiation in the space-time domain* is an advantageous technique to study wave propagation. The effect

that spatial sampling, both in the reproduction and in the receiving stage, has on the wave field was also addressed with this method. For this purpose, the spatial and temporal frequencies of the wave field are obtained via a linear array of microphones. The resulting multidimensional signal is plotted in a $k_x - k$ graphical representation, where limit spatial frequencies due to the reproduction and receiving sampling spacing can be observed. Moreover, the conditions for evanescent waves and the aliased spectrum can easily be analyzed. The sampling artifacts that spatial aliasing cause and the associated parameters that modify them were also studied. These are, mainly, truncation effects due to geometric arrangement and transducer directivity, which restricts the listening area. This methodology can characterize objectively the frequency region below and above the aliasing frequency depicted in Section 2.3.3 in an graphical manner. Far beyond the simple observation of this graphical representation as a consequence of this multidimensional analysis, this thesis has demonstrated its use as an efficient tool in the analysis of practical loudspeaker setup, with both MAPs and dynamic loudspeaker arrays.

As subsequently explained, some valuable conclusions have been revealed by using this method. The reconstructed wave field at high frequencies presents spatial aliasing artifacts, which are not present in the WFS driving signal. In Section 2.3.3, it was reported that the region above aliasing frequency is characterized by oscillations both in frequency and space. The tool proposed in Chapter 3 characterizes such aliasing artifacts as a superposition of undesired plane waves with different incidence angles at different frequencies. The number of such aliased contributions depends on two parameters when practical implementations are considered: on the one hand, by truncation effects due to the finiteness of the loudspeaker array, on the other hand, by array directivity, as experienced in dynamic loudspeaker arrays and small panels. Both parameters limit the spatial resolution of the arrays. Truncation effects and array directivity also limit the reproduction area and thus, lead to a dependence of the aliasing artifacts on the listener position.

By using the amended tool, another key conclusion arises with significant practical consequences: *in terms of acoustic behavior, large panels are more advisable than small panels for WFS reproduction.* This claim is based on the several findings throughout this thesis pointing towards the use of large-sized panels. First, according to plate radiation introduced

in Section 2.2, large panels show an improved low frequency response since the lowest modes vibrate at frequencies inversely proportional to the largest panel dimension.

Besides, as concluded in Chapter 3, the use of small panels with less exciters, has undesired consequences on the reproduced wave field. Since the contour of the panels presents negligible motion when radiating, new aliasing artifacts, at frequencies below that of larger panels or dynamic loudspeaker arrays, will appear that are a function of the distance between panel centers. Then, for WFS reproduction, it is more convenient to split the panels into the least number of sections possible, in a given reproduction scene.

Nevertheless, a proper election of the edge boundaries, where the panel rests and is held, can minimize the undesired effects on acoustic radiation, as pointed out in the conclusion section of Chapter 4. Edge boundary conditions reducing the replicas of the plane wave field are based on elastic boundaries with soft materials. There are other advantages in employing this sort of boundary condition that will be explained later.

Another consequence of the use of small panels is that the number of exciters near the edges is higher compared to larger panels. In this regard, as an idea introduced in Section 1.2, this thesis has also explored that *the performance of exciters near edges is degraded compared to that of middle positions.* On the one hand, since the driving point is placed in an offset position, the excitation does not generate an even and dense frequency mode pattern. Measurements carried out in Chapter 5 confirmed that a boost in low frequency must be applied to exciters near edges to obtain a comparable response to middle exciters. This lack of low frequency response has been experienced for exciters near edges in all the MAP prototypes of this thesis. However, in regard to the amended idea of the convenience of large MAPs, another point of support is that large panels minimize the impact of boundaries on edge exciters. In Chapter 6, in which a very large panel is built, there is more resemblance between edge exciters and middle exciters. The extension in low frequency and uneven response is similar in all exciters of the panel. In a single MAP, a tapering window that progressively diminishes the level towards edges can minimize this problem but when many MAPs are arranged in landscape orientation to form an extended listening area, the intermediate edges will present such a drawback.

The advantageous response of an edge exciter in the large MAP relies also on the elastic boundary conditions used to hold the panel to the frame. According to the experiments in Chapter 4 and the resulting prototype in Chapter 6, *an elastic boundary condition must be provided to enhance the MAP performance.* This holds not only for the structural behavior of edge exciters but also for acoustic radiation. In general terms, free and clamped conditions boost bass power, at the expense of smoothness compared to elastic boundaries. Wavenumber domain analysis has shown that strong pressure variations would be perceived, both in the frequency response and spatially on moving inside the listening area for these two conditions; this makes them inadvisable in multichannel audio reproduction.

Alternatively, elastic boundaries are a compromise between clamped and free edges, which smooth on-axis responses for mid frequencies, regardless of the elastic material employed. Moderate variations were found in directivity patterns on using clamped and free, but not on elastic boundary types 1 and 2 (one or two elastic materials), where half or the entire part of the support is filled with elastic materials. Both elastic boundary types 1 or type 2 can be used alternatively with similar results for elastic materials with proper flexibility. However, the use of elastic boundary type 3 (simply supported with an elastic material) has no primary advantages over the two other elastic boundaries. Hence, its use is not recommended, considering the problems that will arise on manufacture in a real MAP frame, as mentioned in Section 1.2.

Elastic boundaries can minimize the edge impact to an extent, but moderate irregularities in the spectra of MAP still exist due to the modal nature of the panel. To solve this problem, *an efficient equalization filtering process that accounts for the particular exciter distribution on a panel* has been presented in Chapter 5 and applied to the final prototype in Chapter 6. The filtering method utilizes a very low computational cost, so can be applied to a large multichannel MAP system with affordable hardware processing. Although spectral filtering is generally intended for frequencies above aliasing, the efficiency of this method opens the possibility of also applying equalization for low frequency as a prefiltering process prior to the multichannel room equalization.

As an advantage in laboratory and industry measurements, results in Chapter 5 have confirmed that the similarities in the response of symmetrical exciters on a MAP can be used to reduce considerably the num-

ber of measurement points. Moreover, if several MAPs are manufactured maintaining exciter type and position, panel material and housing, their responses will be similar and thus, the equalization filters can be applied systematically to all panels. To further reduce the computational cost of the process, some subjective tests have confirmed that it is possible to reduce the order of the filter considerably without sacrificing the perceived quality of the equalization. By taking advantage of this filter coefficient reduction, a very large WFS system driven by MAPs can be equalized individually with low hardware requirements.

7.2 Contribution to Knowledge

This section is devoted to how this research work has contributed to the field of Multiactuator Panels for Wave Field Synthesis reproduction. These contributions to that knowledge are listed as follows:

- First, the review of the literature has provided a critical investigation of the state of the art of multi-excited flat panel loudspeaker systems for multichannel audio reproduction. This historic revision has introduced the fundamentals of the distributed mode operation, the early developments to achieve a single exciter panel loudspeaker and the evolution to convert them into multiple exciter systems that can act as loudspeaker arrays for WFS systems. The current MAP systems developed at research centers and in companies have been described in detail. The technical information regarding these MAPs has been gathered from research publications and confirmed by direct communication of the author with the amended centers that designed them.

- A methodology for the analysis of sound field radiation in the space-time domain has been set as an efficient tool for the analysis of loudspeaker arrays, either based on dynamic loudspeakers or MAPs. The tool provides practical information on spatial resolution of the array and characterizes the parameters modifying the aliasing frequency, such as truncation effects and loudspeaker directivity.

- Large panels have proven to be advantageous in many ways for setting a WFS reproduction system. In addition to the lower cut-off

frequency due to the excitation of low frequency modes, large MAPs do not cause extra aliasing artifacts as a consequence of the panel boundaries. Moreover, the effect that edge boundaries cause on exciters positioned close to those edges is substantially lower in large panels, which facilitates the setup of several MAPs in landscape orientation to cover a large listening area without artifacts caused by MAP frame.

- In the manufacture of MAPs, a certain degree of fastening must be provided to hold the panel to the frame. Edge boundary conditions based on elastic boundaries have been successfully tested for that purpose, as a practical alternative to boundary conditions that are either difficult to achieve in a real-world setup or exhibit poor performance. Elastic conditions provide the necessary panel fixing without ruining the MAP acoustic response.

- The spectrum equalization of exciters has been optimized by several means. On the one hand, the symmetrical distribution of exciters on a MAP allows the number of filters to be reduced considerably. This reduction can also be extended to equalize several MAPs in a given setup with a single set of filters, given that the MAPs are manufactured similarly. On the other hand, the efficiency of the filtering method has been augmented by diminishing the number of coefficients with unnoticed consequences under a perceptual point of view.

7.3 Further Work

Following the investigations described in this thesis, the main lines of research that remain open are listed below:

- Panels with a high aspect ratio may share the benefits of absence of additional aliasing artifacts because no discontinuities are present, with an extended low frequency response due to the largest horizontal dimension. This approach would combine the two advantages without excessively enlarging the panel vertically.

- Throughout this thesis, the low frequency extension of large panels has been discussed in detail. However, although the final prototype

is considerably large, the low cut-off frequency is still unsatisfactory compared to dynamic loudspeaker arrays so a subwoofer is advisable. Hence, it would be very interesting to conduct research to enhance the low frequency emission of the panel without recurring external aids.

- Since the filtering method is very efficient, it can be extended to form part of a multichannel room equalization that only accounts for amplitude filtering. Additionally, the measurement procedure can be refined by obtaining each exciter impulse response by considering a type of mean value at some discrete positions around the exciter.

7.4 List of Publications

The following presents a list of published work produced during the course of candidature for the degree. The author of this thesis is the primary author of all the publications and none of these have previously formed a part of another thesis. These publications are listed below:

Journal Articles

- B. Pueo, J.J. López, J. Escolano and S. Bleda, "Analysis of Multiactuator Panels in the Space-Time Wavenumber Domain", *J. Audio Eng. Soc.*, vol. 55, no. 12, pp 1092–1106, Dec. 2007

- B. Pueo, J.J. López and J. Escolano, "Edge Boundary Conditions Impact on the Radiation of Multiactuator Panels for Multichannel Audio Reproduction", *Acta Acust. united with Ac.*, (Accepted)

- B. Pueo, J.J. López, Germán Ramos and J. Escolano, "Efficient Equalization of Multi-Exciter Distributed Mode Loudspeaker", *Appl. Acoust.*, (Submitted)

Conference Papers

- J.J. López, B. Pueo and M. Cobos, "Conventional and Distributed Mode Loudspeaker Arrays for the Application of Wave-Field Synthesis to Videoconference", to be presented at *Int. Workshop on Acoustic Echo and Noise Control*, Seattle, USA, Sept. 2008.

- B. Pueo and J.J. López, "Acoustic Radiation Properties of Dynamic Loudspeaker Arrays versus Multiactuator Panels for Wave Field Synthesis", in *J. Acoust. Soc. Am.*(abstract), vol. 123, no. 5, pp 3202, May 2008.

- B. Pueo, J. Escolano, S. Bleda and J.J. López, "On Large Multiactuator Panels for Wave Field Synthesis Applications", in *124th Conv. Audio Eng. Soc.*, Amsterdam, The Netherlands, May 2008.

- B. Pueo, J. Escolano, J.J. López and S. Bleda, "Analysis of Edge Boundary Conditions on Multiactuator Panels", in *123rd Conv. Audio Eng. Soc.*, New York, USA, Oct. 2007.

- B. Pueo, S. Bleda, J. Escolano and J.J. López, "Analysis of Spatial Resolution of Multiactuator Panels", in *120th Conv. Audio Eng. Soc.*, Paris, France, May 2006.

- B. Pueo, J. Escolano, S. Bleda and J.J. López, "An Approach to High-Powered Wave Field Synthesis Applications", in *118th Conv. Audio Eng. Soc.*, Barcelona, Spain, May 2005.

Wave Field Synthesis

A

Wave Field Synthesis

A

A.1 Introduction

LOOKING BACK IN HISTORY, the development of spatial sound reproduction started at an early stage of loudspeaker technology, as explained in the introductory Chapter 1. In 1953, Snow published an overview of stereophonic techniques and discussed the acoustic curtain as the ideal stereophonic reproduction technique [Snow, 1953]. Figure A.1 shows a reproduction from that article illustrating the desired and implemented stereophonic systems. It was aimed to transport the acoustic of the recording venue to a reproduction room using microphone and loudspeaker arrays. Due to technical constraints at that time, it was not feasible to put his ideas into practice. As a compromise, they applied three-channel stereophony, accepting that the original aim of recreating the real sound field would no longer be fulfilled. Snow described this precursor of WFS in this way: "The myriad loudspeakers of the screen, acting as point sources of sound identical with the sound heard by the microphones, would project a true copy of the original sound into the listening area. The observer would then employ ordinary binaural listening, and his ears would be stimulated by sounds identical to those he would have heard coming from the original sound source".

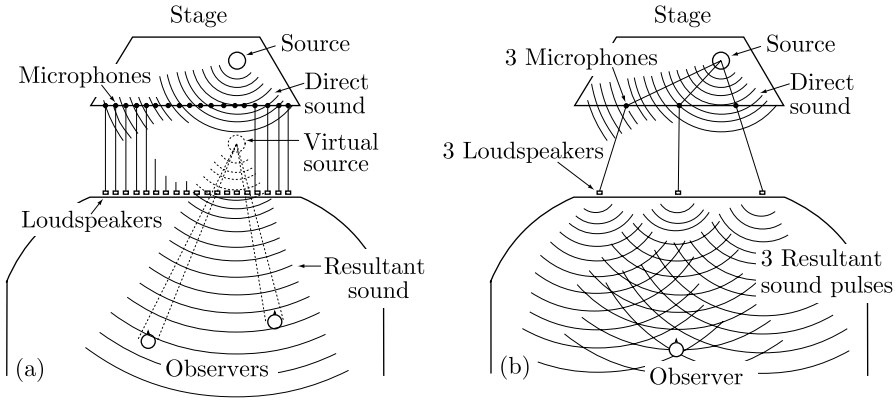

Figure A.1. Acoustic curtain concept. (a) Ideal system. (b) Actual 3-channel stereophonic system due to early technical constrains.

The intuitive acoustic curtain concept was replaced later by a well-founded wave theory. In the late 80s, the Wave Field Synthesis (WFS) concept was introduced by the Technical University of Delft. The origin of this theory was published in "Applied Seismic Wave theory" [Berkhout, 1987] and "A holographic approach to acoustic control" [Berkhout, 1988]. The term "acoustical holography" was used, not yet called WFS, and the system was designed to be the ultimate tool for acoustical control systems in theaters. These publications introduced the physical basis of WFS by applying algorithms known from seismics to the field of acoustics. The basic work on WFS was continued by Berkhout in [Berkhout et al., 1992] and [Berkhout et al., 1993]. Since then, a number of publications have appeared to complement and improve this basic theory. The following sections will describe the WFS concepts.

A.2 Kirchhoff-Helmholtz and Rayleigh Integrals

The theory of WFS is related to Huygens' principle, formulated in 1678. This principle states, that each element of a wave front propagating through a particular medium may be seen as the center of an individual spherical wave. Consequently, the wave front generated by a *primary* sound source can be seen as a series of elementary, *secondary* sources. It is not very practical to position the acoustic sources on the wavefronts for synthesis.

By placing the loudspeakers on an arbitrary fixed curve and by weighting and delaying the driving signals, an acoustic wavefront can be synthesized with a loudspeaker array. Figure A.2(a) illustrates this principle.

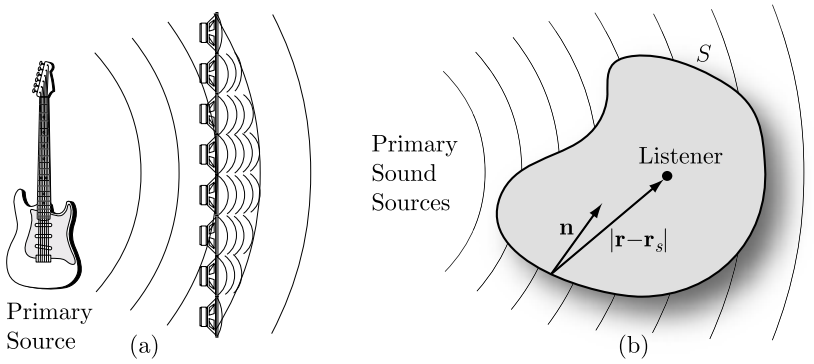

Figure A.2. (a) Basic principle of WFS. (b) Parameters used for the Kirchhoff-Helmholtz integral.

Mathematically, the simple source formulation of the Helmholtz integral investigates the possibility that the pressure inside or outside of the surface could be determined:

$$P(\mathbf{r}) = \iint_S \left[G \frac{\partial P(\mathbf{r})}{\partial n} - P(\mathbf{r}) \frac{\partial G}{\partial n} \right] dS, \tag{A.1}$$

where G is the free space Green function, given by

$$G(\mathbf{r}|\mathbf{r}_s) = \frac{1}{4\pi} \frac{e^{jkR}}{R}, \tag{A.2}$$

and $R = |\mathbf{r} - \mathbf{r}_s|$. Equation (A.1) states, considering the interior problem, that the acoustic field in V generated by the events outside the surface S can be computed uniquely by replacing these events with a distribution of simple monopole surfaces over $P(\mathbf{r})G(\mathbf{r}|\mathbf{r}_s)$ and summing up their contributions over S. Thus, an arbitrary acoustical wave field can be recreated within a source-free volume V by secondary sound sources distributed on a closed boundary surface S. The latter is expressed by the so-called Kirchhoff-Helmholtz integral:

$$P(\mathbf{r},\omega) = \oint_S \frac{1}{4\pi}\left[P(\mathbf{r}_s,\omega)\frac{\partial}{\partial n}\left(\frac{e^{-jk|\mathbf{r}-\mathbf{r}_s|}}{|\mathbf{r}-\mathbf{r}_s|}\right) - \frac{\partial P(\mathbf{r}_s,\omega)}{\partial n}\left(\frac{e^{-jk|\mathbf{r}-\mathbf{r}_s|}}{|\mathbf{r}-\mathbf{r}_s|}\right)\right] dS, \tag{A.3}$$

where $P(\mathbf{r},\omega)$ is the Fourier transform of the sound pressure $p(\mathbf{r},t)$, k is the wave number, $\mathbf{r}$ is the coordinate vector of an observation point and $\mathbf{r}_s$ is the coordinate vector of the integrand functions on the surface S. The underlying geometry is illustrated in Figure A.2(b). The first part of this expression represents a distribution of dipoles with the source strength given by the sound pressure, measured on the surface S. The second term represents a distribution of monopoles, whose strength is given by normal particle velocity component of a sound field, which is proportional to $\partial P/\partial n$.

In practice, the Kirchhoff-Helmholtz integral states that at any listening point within the source-free volume V the sound pressure $P(\mathbf{r},\omega)$ can be calculated if both the sound pressure and its gradient are known on the surface enclosing the volume. This can be used to synthesize a wave field within the surface S by setting the appropriate pressure distribution $P(\mathbf{r}_s,\omega)$. This fact is used for WFS based sound reproduction. If the surface S degenerates to a plane $z = z_1$, separating the listening area from the primary source area, as shown in Figure A.3(a), then Equation (A.3) can be written as the Rayleigh II Integral [Berkhout et al., 1993]:

$$P(\mathbf{r},\omega) = |z - z_1| \int_{S_1} P(\mathbf{r}_s,\omega)\frac{1 + jk|\mathbf{r}-\mathbf{r}_s|}{2\pi|\mathbf{r}-\mathbf{r}_s|^3}\, e^{-j|\mathbf{r}-\mathbf{r}_s|} dS_1. \tag{A.4}$$

An auditorium oriented geometry for (A.4) is shown in Figure A.3(b), where the surfaces S_2, S_3 and $_4$ are fully absorptive. The wave field in the listening area can be generated by a secondary source distribution at z_1, each secondary source represents a dipole, the source signal of which is given by the primary sound pressure at its location.

Hence, it is possible to physically synthesize the wave fronts at any listening point by reradiating the sound pressure, recorded by microphones at $z = z_1$, with loudspeakers having dipole characteristics, as indicated in Figure A.4(a).

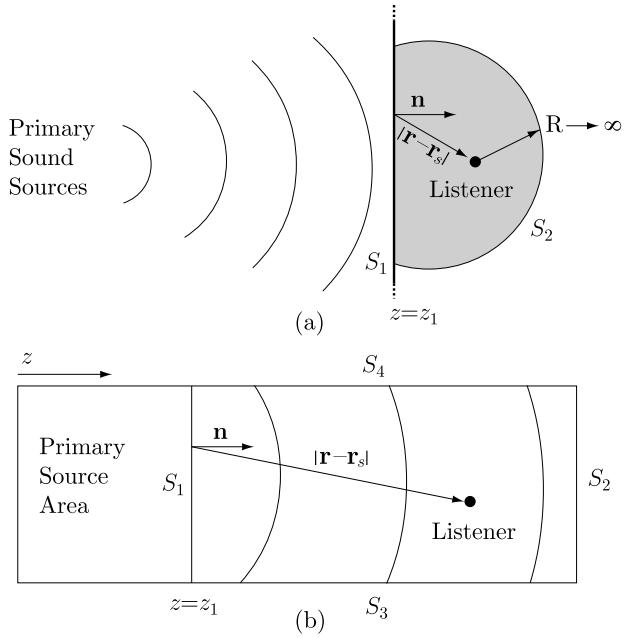

Figure A.3. (a) Simplification of the half-space Kirchhoff-Helmholtz integral. (b) Auditory oriented geometry.

A further step is to place the arrays of transducers used for the recording and synthesizing of the wave fronts in planes with different coordinates z_0 and z_1, respectively, as shown in Figure A.4(b). Then, using Equation (A.4) again, the microphone signals should be transferred to the loudspeakers through a processor simulating the wave front propagation from z_0 to z_1 numerically. This process is the so-called *extrapolation*. In this configuration, loudspeaker positions $\mathbf{r}_n$ at $z = z_1$ act as virtual "listener positions" and thus, the driving signal for each loudspeaker at $z = z_1$, $P(\mathbf{r}_n, \omega)$, is calculated by processing the pressure signals $P(\mathbf{r}_l, \omega)$ recorded by all microphones at $z = z_0$ according to the Rayleigh II integral.

The WFS concept can be compared with optic holography: first, the optical wavefield is recorded over a plane and later, it is recreated by a distribution of light sources, placed on this plane. In sound holography, the acoustic wavefield is recorded over a plane S given by a planar microphone array. Wave field reproduction is then made by secondary sound sources, separately driven loudspeakers. Instead of an ideal continuous distribution

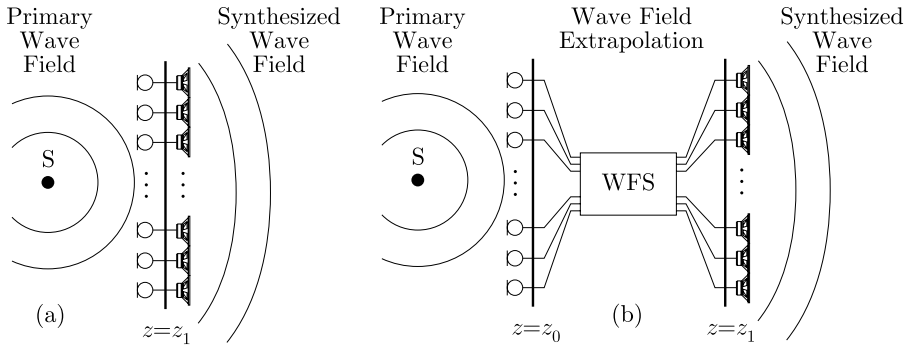

Figure A.4. (a) Illustration of practical WFS according to Equation (A.3). (b) Generalization of the diagram in (a): wave field extrapolation prior to wave field emission.

of secondary sources, discrete distribution is used, which leads to artifacts on the reproduction stage that will be addressed in Section A.4.

A.2.1 First Rayleigh Integral Scheme

The first Rayleigh integral (*Rayleigh I*) states that the wave field in the listening half space can be reconstructed from the original sound field by measuring only the *particle velocity* in the measurement plane and using these measurements as source signals for a distribution of *monopoles* on the reproduction plane [Boone and Verheijen, 1993]:

$$P(\mathbf{r},\omega) = \frac{jk\rho c}{2\pi} \iint_S u_n(\mathbf{r}_s,\omega)\, \frac{e^{-j|\mathbf{r}-\mathbf{r}_s|}}{|\mathbf{r}-\mathbf{r}_s|} dxdy, \tag{A.5}$$

or in its discretized form:

$$P(\mathbf{r},\omega) = \frac{jk\rho c}{2\pi} \sum_n u_n(\mathbf{r}_n,\omega)\, \frac{e^{-j|\mathbf{r}-\mathbf{r}_n|}}{|\mathbf{r}-\mathbf{r}_n|} \Delta x \Delta y, \tag{A.6}$$

where the index n indicates the sampling points in the plane S. The secondary sources can be built with small monopole loudspeakers with volume velocity:

$$U_n(\omega) = u_n(\mathbf{r}_n,\omega)\Delta x \Delta y. \tag{A.7}$$

Notice that for a dynamic loudspeaker, above its resonant frequency, the volume velocity is related to the input voltage $E_n(\omega)$ at its moving coil by

$$U_n(\omega) = \frac{K_m}{j\omega} E_n(\omega), \tag{A.8}$$

where K_m is a constant which depends on the electro-mechanical properties of the loudspeaker systems. From the last two equations,

$$E_n(\omega) = \frac{j\omega}{K_m} \Delta x \Delta y u_n(\mathbf{r}_n, \omega), \tag{A.9}$$

This result shows that the particle velocities in the registration and reconstruction plane must be differentiated (filtered with +6 dB/oct) before being applied to the loudspeakers.

A.2.2 Second Rayleigh Integral Scheme

The second Rayleigh integral (*Rayleigh II*) gives a similar relation between the *sound pressure* in the measurement plane and the distribution of *dipoles* in the reproduction plane:

$$P(\mathbf{r}, \omega) = \frac{jk}{2\pi} \iint_S P(\mathbf{r}_s, \omega) \frac{1 + jk|\mathbf{r} - \mathbf{r}_s|}{jk|\mathbf{r} - \mathbf{r}_s|} \cos\phi \frac{e^{-jk|\mathbf{r}-\mathbf{r}_s|}}{|\mathbf{r} - \mathbf{r}_s|} dxdy, \tag{A.10}$$

with $\cos\phi$ defined as $|z - z_s|/|\mathbf{r} - \mathbf{r}_s|$, where $|z - z_s|$ is the distance between the reproduction plane and the observation point. The discrete form is given by:

$$P(\mathbf{r}, \omega) = \frac{jk}{2\pi} \sum_n P(\mathbf{r}_n, \omega) \frac{1 + jk|\mathbf{r} - \mathbf{r}_n|}{jk|\mathbf{r} - \mathbf{r}_n|} \cos\phi_n \frac{e^{-jk|\mathbf{r}-\mathbf{r}_n|}}{|\mathbf{r} - \mathbf{r}_n|} \Delta x \Delta y. \tag{A.11}$$

In this case, the secondary sources can be built with small unbaffled loudspeakers with volume force:

$$F_n(\omega) = P(\mathbf{r}_n, \omega) \Delta x \Delta y. \tag{A.12}$$

The relation between the volume force and the input voltage above the mechanical resonance frequency is given by:

$$F_n(\omega) = K_d E_n(\omega), \tag{A.13}$$

where K_d is an electro-mechanical constant of the dipole loudspeaker systems. From the last two equations,

$$E_n(\omega) = \frac{1}{K_d} \Delta x \Delta y P(\mathbf{r}_n, \omega). \tag{A.14}$$

Notice that, with respect to the Rayleigh I result, no frequency weighting is needed in this case.

A.3 Derivation of the Driving Signal Function

For the derivation of the loudspeaker driving signal, the geometry shown in Figure A.5 is considered. The pressure field of a virtual source, also known as *notional source* at $\mathbf{r}_m$ in the plane $z = z_0$ should be reconstructed in the horizontal ear plane of a listener located at $\mathbf{r}$ in the plane $z = z$, using a linear array of loudspeakers parallel to the x axis in the plane $z = z_1$. The line connecting source and listener makes an angle θ with the z axis. Note that source, array, and listener are all located in the plane $y = 0$, that is, at the same height. In practice, the loudspeaker array will often be mounted above stage and audience levels. In [Berkhout et al., 1993], it has been shown that the array height y_1 can be neglected when this height is much smaller than the horizontal distances between source and array, and between listener and array, which is often the case.

The derivation given here is a generalized version of that given in [Berkhout et al., 1993]. According to Rayleigh's theorem, the loudspeaker driving signals can be written as a weighted version of the pressure field of the notional source at the array position.

$$Q(\mathbf{r}_n, \omega) = A_n P(\mathbf{r}_n, \omega) = A_n S(\omega) \frac{e^{-jk|\mathbf{r}_n - \mathbf{r}_m|}}{\mathbf{r}_n - \mathbf{r}_m}, \tag{A.15}$$

where A_n is a weighting function, which depends on the lateral position of the nth loudspeaker $A_n = A(x_n, \omega)$. For synthesizing a spherical wavefront,

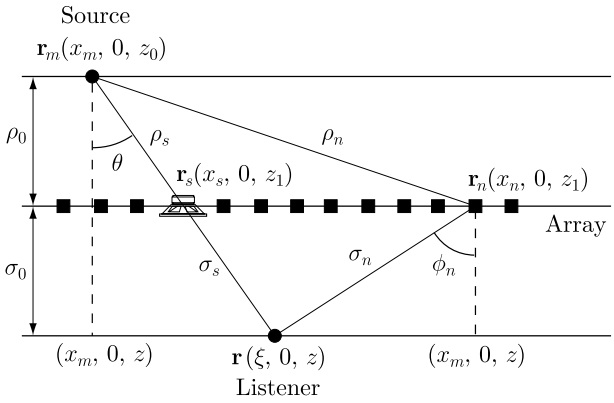

Figure A.5. Configuration for WFS. Loudspeaker array at $z = z_1$ synthesizes wavefield of a source at $\mathbf{r}_m$ in the receiver plane at $z > z_1$.

its mathematical formulation must be considered:

$$P(\mathbf{r},\omega) = S(\omega)\frac{e^{-jk|\mathbf{r}-\mathbf{r}_m|}}{\mathbf{r}-\mathbf{r}_m}, \tag{A.16}$$

where $S(\omega)$ is the spectrum of the notional source. According to the Rayleigh equation, the spherical wavefront can be synthesized as

$$P(\mathbf{r},\omega) = \sum_{n=1}^{N}\left[Q(\mathbf{r}_n,\omega)G(\phi_n,\omega)\frac{e^{-jk|\mathbf{r}-\mathbf{r}_n|}}{|\mathbf{r}-\mathbf{r}_n|}\right]\Delta x, \tag{A.17}$$

where N is the number of loudspeakers in the array, $Q(\mathbf{r}_n,\omega)$ is the driving signal of the nth loudspeaker, ϕ_n is the angle between the main axis of the nth loudspeaker and its connection line to the listener position, and Δx is the spatial interval between the array elements [de Vries, 1996]. Note that the only unknown elements in the synthesis operator are the driving signals of the loudspeakers. Using the geometry of Figure A.5, the latter expression can be written as:

$$\frac{e^{-jkr}}{r} = \sum_{n=1}^{N}\left[A_n G(\phi_n,\omega)\frac{e^{-jk(\rho_n+\sigma_n)}}{\rho_n\sigma_n}\right]\Delta x. \tag{A.18}$$

This discretized integral equation can be approximated by using its

stationary-phase representation [Bleistein, 1984]. Physically this approximation means that the wavefront is synthesized by all loudspeakers of the array together, but a dominant contribution is given by the loudspeaker positioned at the point of stationary phase. After substancial mathematical manipulation, the driving signal $Q(\mathbf{r}_n, \omega)$ of the nth loudspeaker can be found:

$$Q(\mathbf{r}_n, \omega) = S(\omega) \frac{\cos\theta_n}{G(\theta_n, \omega)} \sqrt{\frac{jk}{2\pi}} \sqrt{\frac{|z - z_1|}{|z - z_0|}} \frac{e^{-jk|\mathbf{r}_n - \mathbf{r}_m|}}{\sqrt{|\mathbf{r}_n - \mathbf{r}_m|}}, \tag{A.19}$$

This driving function contains a cylindrical spatial divergence factor $|\mathbf{r}_n - \mathbf{r}_m|^{-1/2}$ and thus, the driving signal of the nth loudspeaker can be interpreted as a weighted version of the sound pressure field at $\mathbf{r}_n$ caused by a notional line source at $\mathbf{r}_m$. The fact that only one horizontal line in the reconstruction plane $z = z_1$ is used in the wavefront synthesis process is "compensated" for by the spatial extension of the notional source from a point to a vertical line. As shown in [de Vries, 1996], any loudspeaker type can be used to form an array for WFS. By adapting the driving signal function according to Equation (A.19) the loudspeaker directivity characteristics are virtually transferred to the notional sources. Recently, in [Spors et al., 2008], the theory of WFS was revisited and a unified theoretical framework covering arbitrarily shaped loudspeaker arrays for two- and three-dimensional reproduction was presented.

Since the formulation of the theoretical framework of WFS, the spatial audio research community has contributed with various research projects, such as the European Carrouso [Carrouso, 2001],[Brix et al., 2001], original work in the technical literature and a number of PhD theses [Vogel, 1993], [Start, 1997], [Verheijen, 1997], [Nicol, 1999], [Hulsebos, 2004], [Corteel, 2006b], [Spors, 2007], [Wittek, 2007], [Gauthier, 2007], [Baalman, 2008].

A.4 Potential and Constrains of WFS

The principle characteristic of WFS is that the acoustic scene remains constant for the entire listening area, that is, the absolute setup of the acoustic scene is independent of the listening position. The relative acoustic perspective as perceived by listeners changes with their movements. This change

involves a realistic change of the sound pressure level when the distance to the virtual source is varied.

The theoretical capabilities of WFS to create a quasi-realistic sound field or to recreate an existing sound field are even larger. For instance, it is possible to simulate a certain directivity characteristic of the virtual source. Furthermore, the location of the secondary sources (loudspeaker array) is no limitation for the creation of virtual sources. WFS theoretically allows the synthesis of virtual sources both in front of and behind the array. In particular, the creation of the so-called focused sources, which are sources in front of the array, makes a significant difference to conventional sound reproduction techniques, as will be shown in Section A.5.2. From a creative point of view, WFS offers an improvement of flexibility: both direction and location stable sources can be reproduced. The design of the acoustic scene is less limited by the constraints of the reproduction technique in comparison to stereo. The simulation of a real acoustic scene is more plausible.

However, since the aim of WFS is the creation of a true copy of a natural sound field, this high aim can only be fulfilled with certain restrictions in practice. Practical implementation of the WFS technique is based on loudspeaker arrays, which act as secondary sound sources. The distribution of these sources is not densely and infinitely continuous, but a finite set of band-limited signals will drive the individual discrete loudspeakers, which in turn, makes the array finite. These two effects limit the performance of real WFS systems:

1. *Spatial Aliasing*
   The distance between transducers Δx defines a spatial sampling frequency for a wavefield at a recording level. Then, the reconstructed wavefield will be physically correct up to the Nyquist frequency:

$$f_{\mathrm{nyq}} < \frac{c}{2\Delta x} \quad \leftrightarrow \quad \Delta x < \frac{\lambda_{\min}}{2}, \tag{A.20}$$

   where $\lambda_{\min}$ is the smallest sound wavelength of concern. Above the Nyquist frequency, together with the correctly reconstructed wave front, additional undesired wave energy will be emitted incorrectly. A description of these aliasing artifacts can be found in Chapter 3 and in [Spors and Rabenstein, 2006], [Corteel, 2006a], [Spors, 2008].

In practice, wave field recreation without spatial aliasing artifacts is possible for frequencies less than the spatial aliasing frequency. This limit frequency is determined by the time difference between two successive loudspeaker signals interfering at the listeners' position. This time difference depends on the spatial sampling interval, that is, the loudspeaker and microphone inter-spacing. Moreover, the maximum wavelength being sampled correctly without spatial aliasing depends on the maximum angle on the microphone side. Accordingly, the maximum wavelength being received correctly without aliasing also depends on the maximal angle on the receiver side. This aliasing frequency is given more generally by

$$f_{\mathrm{al}} = \frac{c}{2\Delta x|\sin\alpha_{\max}|} \tag{A.21}$$

where $\alpha_{\max}$ indicates a maximum angle between an incident plane wave and a microphone array surface. If the angle α is equal to 0^{o}, the wave front is perpendicular to the array surface and the spatial sampling interval Δx can be seen as infinite. In the worst case, when the angle α is equal to 90^{o}, f_{al} will be equal to f_{nyq}. Assuming a loudspeaker spacing Δx=10 cm, the minimum spatial aliasing frequency is f_{al}=1.7 kHz. Regarding the standard audio bandwidth of 20 kHz, spatial aliasing seems to be a problem for practical WFS systems. Fortunately, the human auditory system is not very sensitive to these aliasing artifacts.

When virtual sound sources are recreated by means of WFS, the angle $\alpha_{\max}$ can be set to a certain value. Radiation of plane waves at a wider angle than $\alpha_{\max}$ is then suppressed and spatial aliasing effect can be avoided up to f_{al} frequency. The same technique can be applied for the wave-field recording, where directional microphones will capture waves radiating up to this certain angle.

2. *Truncation Effects*
In theory, the synthesis of the wave field arises from the summation of an infinite number of loudspeaker signals. In practice, however, the loudspeaker array used will always have a finite length. The finite array can be seen as a window, through which the primary or virtual source is either visible, or invisible, to the listener. Hence, an area exists which is "illuminated" by the virtual source, together

with a corresponding "shadow" area [Wittek, 2003]. Applying this analogy, diffraction waves are originated from the edges of the finite loudspeaker array. These error contributions appear as after-echoes for virtual sources and pre-echoes for focused sources. In Chapter 6, two multitrace responses illustrate that the effects of spatial aliasing arrive at the recording line after the synthesized wave for a virtual source in Figure 6.12(b) and before the synthesized wave for a focused source in Figure 6.13(b). Depending on the level and time-offset at the receiver's location of the aliased contributions, it may give rise to colouration. This effect can be successfully minimized if a weighting function is applied to the signals driving the loudspeaker array. At the same time, decreasing the contribution of edge loudspeakers will reduce an area with a correctly reproduced wave field. Thus, the choice of the weighting function will depend on a trade-off between the reduction of diffraction artifacts and the size of the listening area.

A.5 Special Properties of WFS

A.5.1 Localization of Virtual Sources

Through WFS the sound engineer has a powerful tool to design a sound scene. One of the most important properties, with respect to conventional techniques, is its outstanding capability of providing a realistic localization of virtual sources. Typical problems and constraints of a stereophonic image vanish in a WFS sound scene. In contrast to stereophony, WFS can produce a number of source stimuli, based on virtual sources and plane waves. These sources are localized on the same position throughout the entire listening area so listeners can move without losing their localization. In Figure A.6, the arrows indicate the directions of the auditory events when virtual point sources and plane waves are reproduced.

WFS can enhance the localization of virtual sources and the sense of presence and envelopment through a realistic reproduction of the amplitude distribution of a virtual source. In practice, this means that when the listener is approaching the location of a virtual source the amplitude increases in a realistic way. Accordingly, the amplitude of a plane wave, which can be seen as a source in infinite distance, changes least in different listener positions. Subjective experiments on sound localization, correspondence of

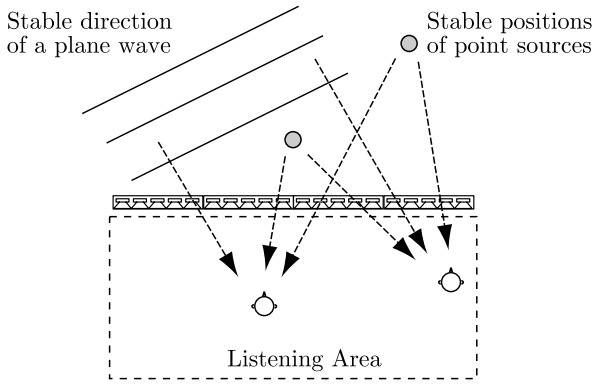

Figure A.6. WFS is capable of reproducing both the stable positions of point sources and the stable direction of a plane wave.

perceived auditory and visual source direction can be found in [de Brujin and Boone, 2003].

These properties enable the synthesis of complex sound scenes which can be experienced by the listener while moving around within the listening area. Figure A.6 illustrates the way in which the sound image changes at different listening positions. This feature can be made use of deliberately by the sound engineer to realize new spatial sound design ideas [Thiele et al., 2003]. Moreover, it has been shown that the enhanced resolution of the localization compared with stereophony enables the listener to easily distinguish between different virtual sources, which makes the sound scene significantly more transparent.

Typical implementations of sound field reproduction systems do not take the Doppler Effect into account. However, the Doppler Effect, both for moving virtual sound sources and inherently also for moving listeners, can be accurately reproduced in WFS [Franck et al., 2007], [Ahrens and Spors, 2008b].

A.5.2 Virtual Sources in Front of the Loudspeaker Array

Figures A.7(a) and (b) show the wave fronts of a point source behind the array and in front of the array, respectively, in a simulation. The concave wave fronts of Figure A.7(a) achieve the synthesis of the signal of a virtual source behind the array. However, WFS is also capable of synthesizing

a virtual source in front of the array. Therefore, the WFS array emits convex wave fronts which focus on a point that will be the "focused source", illustrated in Figure A.7(b). Naturally, the localization will not be correct for listening positions between the focus point and the array because the sound emission of the virtual source occurs here reversely.

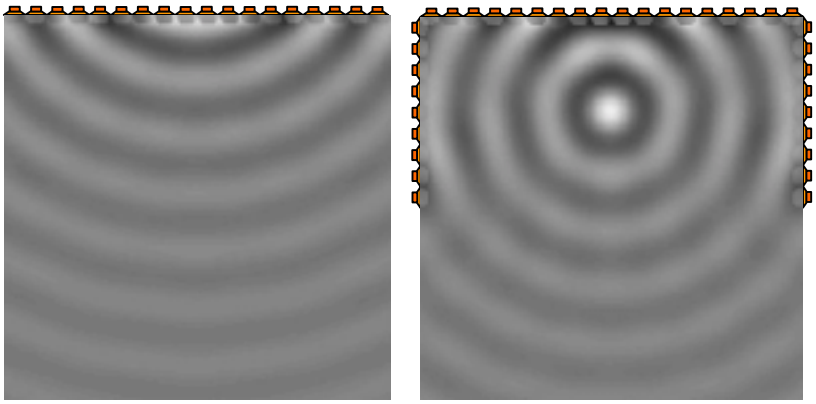

Figure A.7. (a) Virtual source behind the array. (b) Virtual source in front of the array, also known as focused source.

For practical application, it is an enormous progress that virtual sound sources can be created in the field between the listener and the loudspeakers can be created. Sound engineers can be offered completely new tools for spatial sound design. Moreover, the reproduction of focused sources with directional characteristics is also possible but with a limited listening area [Spors et al., 2008], [Ahrens and Spors, 2008b].

Bibliography

This chapter contains an alphabetical listing of the sources referred to in this thesis. The Harvard system of referencing [author, date] is used.

J. Ahrens and S. Spors. Notes on Rendering Focused Directional Virtual Sound Sources in Wave Field Synthesis. In *Proceedings of the Annual German Conference on Acoustics (DAGA)*, Mar. 2008a.

J. Ahrens and S. Spors. Reproduction of Moving Virtual Sound Sources with Special Attention to the Doppler Effect. In *124th Conv. Audio Eng. Soc.*, Amsterdam, The Netherlands, May 2008b.

J. A. Angus. Distributed Mode Loudspeaker Radiation Mechanisms. In *108th Conv. Audio Eng. Soc.*, number 5164, Paris, France, Sept. 2000a.

J. A. Angus. Distributed Mode Loudspeaker Resonance Structures. In *109th Conv. Audio Eng. Soc.*, number 5217, Los Angeles, USA, Sept. 2000b.

J. A. Angus. Distributed mode loudspeaker polar patterns. In *107th Conv. Audio Eng. Soc.*, number 5065, New York, USA, Sept. 1999.

H. Azima and N. Harris. Boundary Interaction of Diffuse Field Distributed-Mode Radiators. In *103rd Conv. Audio Eng. Soc.*, number 4635, New York, USA, Sept. 1997.

H. Azima and J. W. Panzer. Distributed-Mode Loudspeakers (DML) in Small Enclosures. In *106th Conv. Audio Eng. Soc.*, number 4987, Munich, Germany, May 1999.

H. Azima, N. Harris, and M. Colloms. *Acoustic Device*, 1997. International Patent Application WO 98/26630.

M. Baalman. *On Wave Field Synthesis and Electro-Acoustic Music, with Particular Focus on the Reproduction of Arbitrarily Shaped Sound Sources*. PhD Thesis, Technische Universität Berlin, Germany, 2008.

M. R. Bai and T. Huang. Development of Panel Loudspeaker System: Design, Evaluation and Enhancement. *J. Acoust. Soc. America*, 109(6): 2751–2761, June 2001.

M. R. Bai and B. Liu. Determination of Optimal Exciter Deployment for Panel Speakers Using the Genetic Algorithm. *J. Sound Vibration*, 269: 727–743, Jan. 2004.

G. Bank. The Intrinsic Scalability of the Distributed-Mode Loudspeaker. In *104th Conv. Audio Eng. Soc.*, number 4742, Amsterdam, The Netherlands, May 1998.

L. L. Beranek. *Acoustics*. McGraw-Hill, 1954.

A. Berkhout. A Holographic Approach to Acoustic Control. *J. Audio Eng. Soc.*, 36(12):977–995, Dec. 1988.

A. Berkhout, D. de Vries, and P. Vogel. Wave Front Synthesis: a New Direction in Electro-Acoustics. In *93th Conv. Audio Eng. Soc.*, number 3379, San Francisco, USA, Mar. 1992.

A. Berkhout, D. de Vries, and P. Vogel. Acoustic Control by Wave Field Synthesis. *J. Acoust. Soc. America*, 93(5):2764–2778, May 1993.

A. J. Berkhout. *Applied Seismic Wave Theory*. Elsevier Science, 1987.

N. Bleistein. *Mathematical Methods for Wave Phenomena*. Academic Press, 1984.

H. Bonhoff. Optimization of Vibrating Panel Loudspeakers. Master's Thesis, Chalmers University of Technology, Götegorb, Sweden, 2005.

M. Boone. Multi-Actuator Panels (MAPs) as Loudspeaker Arrays for Wave Field Synthesis. *J. Audio Eng. Soc.*, 52(7–8):712–723, July 2004.

M. Boone and W. de Brujin. On the Applicability of Distributed Mode Loudspeaker Panels for Wave Field Synthesis Based Sound Reproduction. In *108th Conv. Audio Eng. Soc.*, Paris, France, Feb. 2000.

M. Boone and E. N. G. Verheijen. Multichannel Sound Reproduction Based on Wave Field Synthesis. In *95th Conv. Audio Eng. Soc.*, number 3719, New York, USA, Oct. 1993.

M. Boone, W. de Bruijn, and W. van Rooijen. Recent Developments on WFS for High Quality Spatial Sound Reproduction. In *110th Conv. Audio Eng. Soc.*, number 5370, Amsterdam, The Netherlands, May 2001.

J. Borwick. *Loudspeaker and Headphone Handbook*. Focal Press, 3rd edition, 2001.

S. Brix, T. Sporer, and J. Plogsties. Carrouso - An European Approach to 3D-Audio. In *110th Conv. Audio Eng. Soc.*, number 5314, Amsterdam, The Netherlands, May 2001.

M. E. Brown. *Introduction to Thermal Analysis. Techniques and Applications*. Springer, 2nd edition, 2001.

H. Buchner, S. Spors, and R. Rabenstein. Efficient Active Listening Room Compensation for Wave Field Synthesis. In *116th Conv. Audio Eng. Soc.*, number 6119, Berlin, Germany, May 2004.

Carrouso. Creating, Assessing and Rendering in Real Time of High Quality Audio-Visual Environments in MPEG-4 Context, (IST, EU). http://cordis.europa.eu/ist/ka3/iaf/projects/carrouso.htm. Last seen on may 2008.

K. Chiao, N. Harris, and C. Kyriakakis. A New Approach to Speaker/Room Equalization. In *109th Conv. Audio Eng. Soc.*, number 5221, Los Angeles, USA, Sept. 2000.

D. Clark. High-Resolution Subjective Testing Using a Double-Blind Comparator. *J. Audio Eng. Soc.*, 30(5):330–338, May 1982.

L. Copley, T. Cox, and M. Avis. Distributed Mode Loudspeakers Arrays. In *112th Conv. Audio Eng. Soc.*, number 5610, Munich, Germany, May 2002.

E. Corteel. Equalization in an Extended Area Using Multichannel Inversion and Wave Field Synthesis. *J. Audio Eng. Soc.*, 54(12):1140–1161, Dec. 2006a.

E. Corteel. Synthesis of Directional Sources Using Wave Field Synthesis, Possibilities, and Limitations. *EURASIP J. Appl. Signal Process.*, 2007 (1):1–18, 2007.

E. Corteel. *Caractérisation et extensions de la Wave Field Synthesis en conditions réelles*. PhD Thesis, Université Paris VI, France, 2006b.

E. Corteel and R. Nicol. Listening Room Compensation for Wave Field Synthesis. What Can Be Done? In *Proceedings of the AES 23th Int. Conf. on Signal Processing in Audio Recording and Reproduction*, Helsingør, Denmark, May 2003.

E. Corteel, U. Horbach, and R. Pellegrini. Multichannel Inverse Filtering of Multiexciter Distributed Mode Loudspeakers for Wave Field Synthesis. In *112th Conv. Audio Eng. Soc.*, number 5611, Munich, Germany, May 2002.

E. Corteel, K.-V. Nguyen, O. Warusfel, T. Caulkins, and R. Pellegrini. Objective and subjective comparison of electrodynamic and map loudspeakers for wave field synthesis. In *AES 30th Int. Conf.*, Saariselkä, Finland, Mar. 2007.

L. Cremer, M. Heckl, and B. A. Petersson. *Structure Borne Sound: Structural Vibrations and Sound Radiation at Audio Frequencies*. Springer, 3rd edition, 2005.

J. Dattorro. The Implementation of Digital Filters for High Fidelity Audio. In *AES 7th Int. Conf. on Audio in Digital Times*, Toronto, Canada, May 1989.

W. de Brujin and M. Boone. Application of Wave Field Synthesis in Life-Size Videoconferencing. In *114th Conv. Audio Eng. Soc.*, number 5801, Amsterdam, The Netherlands, Mar. 2003.

D. de Vries. Sound Reinforcement by Wave Field Synthesis: Adaptation of the Synthesis Operator to the Loudspeaker Directivity Characteristics. *J. Audio Eng. Soc.*, 44(12):1120–1131, Dec. 1996.

F. Fahy and P. Gardonio. *Sound and Structural Vibration*. Academic Press, 2nd edition, 2007.

B. Fazenda, M. Avis, and J. Davies. Low Frequency Room Excitation Using Distributed Mode Loudspeakers. In *AES 21st Int. Conf. on Architectural Acoustics & Sound Reinforcement*, number 90, St. Petersburg, Russia, June 2002.

A. Franck, A. Gräfe, T. Korn, and M. Strauß. Reproduction of Moving Virtual Sound Sources by Wave Field Synthesis: An Analysis of Artifacts. In *32nd Int. Conf. on Multichannel Audio: DSP for Loudspeakers*, Hillerød, Denmark, Sept. 2007.

B. Friedlander and B. Porat. The Modified Yule-Walker Method of ARMA Spectral Estimation. *IEEE Trans. Aerosp. Electron. Syst.*, 20(2):158–173, Mar. 1984.

L. Fuster, J. J. López, A. González, and P. Faus. Time and Frequency Domain Room Compensation Applied to Wave Field Synthesis. In *Proc. of the 8th Int. Conference on Digital Audio Effects (DAFx05)*, Madrid, Spain, Sept. 2005a.

L. Fuster, J. J. López, A. González, and P. Zuccarello. Room Compensation Using Multichannel Inverse Filters for Wave Field Synthesis Systems. In *118th Conv. Audio Eng. Soc.*, number 6401, Barcelona, Spain, May 2005b.

P.-A. Gauthier. *Synthèse de Champs Donores Adaptative*. PhD Thesis, Université de Sherbrooke, Canada, 2007.

P.-A. Gauthier and A. Berry. Objective Evaluation of Room Effects on Wave Field Synthesis. *Acta Acust. united Ac.*, 93(5):824–836, Sep/Oct 2007.

M. Gerzon. Periphony: With-Height Sound Reproduction. *J. Audio Eng. Soc.*, 21(1):2–10, Dec. 1973.

V. Gontcharov and N. Hill. Diffusivity Properties of Distributed Mode Loudspeakers. In *108th Conv. Audio Eng. Soc.*, number 5095, Paris, France, Sept. 2000.

V. Gontcharov, R. Hill, and J. Taylor. Measurement Aspects of Distributed-Mode Loudspeakers. In *106th Conv. Audio Eng. Soc.*, number 4970, Munich, Germany, May 1999.

S. A. Hambric. Structural Acoustic Tutorial, Part 1: Vibrations in Structures. *Acoustics Today*, 2(4):21–33, Oct. 2006.

N. Harris. Spatial Bandwidth of Diffuse Radiation in Distributed-Mode Loudspeakers. In *111th Conv. Audio Eng. Soc.*, number 5412, Nov. 2001.

N. Harris. Modelling Acoustic Room Interaction for Pistonic and Distributed-Mode Loudspeakers in the Correlation Domain. In *117th Conv. Audio Eng. Soc.*, number 6180, Oct. 2004.

N. Harris and M. Hawksford. Modelling room interaction effects for pistonic and distributed-mode loudspeakers in both the frequency and time domains. In *114th Conv. Audio Eng. Soc.*, number 5732, Amsterdam, The Netherlands, Mar. 2003.

N. Harris and M. O. Hawksford. The Distributed-Mode Loudspeaker (DML) as a Broad-Band Acoustic Radiator. In *103rd Conv. Audio Eng. Soc.*, number 4526, New York, USA, Sept. 1997.

N. Harris, S. Flanagan, and M. Hawksford. Stereophonic Localization in the Presence of Boundary Reflections, Comparing Specular and Diffuse Acoustic Radiators. In *104th Conv. Audio Eng. Soc.*, number 4684, Amsterdam, The Netherlands, May 1998a.

N. Harris, S. Flanagan, and M. O. Hawksford. Stereophonic Localization in Rooms, Comparing Conventional and Distributed-Mode Loudspeakers. In *105th Conv. Audio Eng. Soc.*, number 4794, Sept. 1998b.

N. Harris, V. Gontcharov, and M. Hawksford. Measurment and Simulation Results Comparing the Acoustic of Various Direct Radiators in the Presence of a Dominant Specular Reflection. In *109th Conv. Audio Eng. Soc.*, number 5215, Los Angeles, USA, Sept. 2000.

K. Heron. *Panel-Form Loudspeaker*, 2000. US Patent No. 6,058,196.

K. Heron. *Panel-Form Loudspeaker*, 1998. International Patent Application WO 98/26630.

K. Heron. *Panel Form Loudspeaker*. Defense Research Agency, DRA, Farnborough, 1991.

U. Horbach, E. Corteel, and D. de Vries. Spatial Audio Reproduction Using Distributed Mode Loudspeaker Arrays. In *AES 21st Int. Conf. on Architectural Acoustics & Sound Reinforcement*, St. Petersburg, Russia, June 2002.

L. Hörchens and D. de Vries. Retrieval of a Model for the Removal of Dispersion From Wave Fields in Plates. In *Proc. of the 19th Int. Congress on Acous. (ICA07)*, Madrid, Spain, Sept. 2007.

E. Hulsebos. *Auralization Using Wave Field Synthesis*. PhD Thesis, Delft University of Technology, The Netherlands, 2004.

E. Hulsebos, D. de Vries, and E. Bourdillat. Improved Microphone Array Configurations for Auralization of Sound Fields by Wave Field Synthesis. *J. Audio Eng. Soc.*, 50(10):779–790, Oct. 2002.

M. Karjalainen, E. Piirilä, A. Järvinen, and J. Huopaniemi. Comparison of Loudspeaker Equalization Methods Based on DSP Techniques. *J. Audio Eng. Soc.*, 47(1/2):14–31, Feb. 1999.

O. Kirkeby, P. A. Nelson, H. Hamada, and F. Orduña. Fast Deconvolution of Multichannel Systems Using Regularization. *IEEE Trans. Speech Audio Proc.*, 6(2):189–194, Mar. 1998.

M. Kuster, D. de Vries, D. Beer, and S. Brik. Structural and Acoustic Analysis of Multiactuator Panels. *J. Audio Eng. Soc.*, 54(11):1065–1076, Nov. 2006.

A. W. Leissa. *Vibration of Plates*. Acoustical Society of America, 1999.

R. M. Lerner and R. C. Waag. Wave Space Interpretation of Scattered Ultrasound. *Ultrasound in Medicine and Biology*, 14(2):97–102, 1988.

E. C. Levi. Complex-Curve Fitting. *IRE Trans. Automat. Contr.*, 4:37–44, 1959.

J. J. López, A. González, and L. Fuster. Room Compensation in Wave Field Synthesis by Means Of Multichannel Inversion. In *IEEE Workshop on Appl. of Sig. Proc. to. Audio and Acoust. (WASPAA'05)*, New Paltz, NY, USA, Oct. 2005.

P. A. Nelson, F. Orduña, and H. Hamada. Multichannel Signal Processing Techniques in the Reproduction of Sound. *J. Audio Eng. Soc.*, 44:973–989, Nov. 1996.

R. Nicol. *Restitution Sonore Spatialisé sur une Zone Étendue*. PhD Thesis, Université du Maine, France, 1999.

A. Oppenheim, R. Schafer, and J. R. Buck. *Discrete-Time Signal Processing*. Prentice Hall, 2nd edition, 1999.

J. W. Panzer and N. Harris. Distributed-Mode Loudspeaker Radiation Simulation. In *105th Conv. Audio Eng. Soc.*, number 4783, San Francisco, USA, Sept. 1998.

T. W. Parks and S. Burrus. *Digital Filter Design*. John Wiley & Sons, 1987.

J. G. Proakis and D. G. Manolakis. *Digital Signal Processing. Principles, Algorithms and Applications*. Prentice Hall, 1998.

E. Prokofieva. Effect of Porous Material on the Diffusivity of an Unbaffled DML Panel. In *114th Conv. Audio Eng. Soc.*, number 5735, Munich, Germany, Mar. 2003.

E. Prokofieva, V. Horoshenkov, and N. Harris. Intensity Measurements of the Acoustic Emission from a DML Panel. In *112th Conv. Audio Eng. Soc.*, number 5609, Munich, Germany, May 2002a.

E. Y. Prokofieva, K. V. Horoshenkova, and N. Harris. The Acoustic Emission of a Distributed Mode Loudspeaker Near a Porous Layer. *J. Acoust. Soc. America*, 111(6):2665–2670, June 2002b.

R. Rabenstein, P. Steffen, and S. Spors. Representation of Two-Dimensional Wave Fields by Multidimensional Signals. *Signal Processing*, 86(6):1341–1351, June 2006.

B. Rafaely. Plane-Wave Decomposition of the Sound Field on a Sphere by Spherical Convolution. *J. Acoust. Soc. America*, 116(4):2149–2157, Oct. 2004.

D. R. Raichel. *The Science and Applications of Acoustics*. Springer, 2006.

G. Ramos and J. J. López. Filter Design Method for Loudspeaker Equalization Based on IIR Parametric Filters. *J. Audio Eng. Soc.*, 54(12): 1162–1178, Dec. 2006.

K. Renji. On the Effect of Boundaries on Radiation Resistance of Plates. *J. Acoust. Soc. America*, 110(3):1253–1255, Sept. 2001. (Letter to the editor).

K. Renji, P. Nair, and S. Narayanan. On Acoustic Radiation Resistance of Plates. *J. Sound Vib.*, 212(4):583–598, May 1998.

M. Roberts. Exciter Design for Distributed-Mode Loudspeakers. In *104th Conv. Audio Eng. Soc.*, number 4743, Amsterdam, The Netherlands, May 1998.

F. Rumsey and A. Naqvi. Active Listening Room Simulator: Part 1. In *110nd Conv. Audio Eng. Soc.*, number 5385, Amsterdam, The Netherlands, May 2001a.

F. Rumsey and A. Naqvi. The Active Listening Room Simulator: Part 2. In *111nd Conv. Audio Eng. Soc.*, number 5425, Amsterdam, The Netherlands, Nov. 2001b.

D. Seuberth. Kompensation von Flachlautsprechern für ein Wellenfeldsynthesesystem. Master's Thesis, Multimedia Communications and Signal Processing, University of Erlangen-Nuremberg, Germany, 2003.

G. Sherman. Integral-Transform Formulation of Diffraction Theory. *J. Opt. Soc. America*, 57(12):1490–1498, Dec. 1967.

J. Shewell and E. Wolf. Inverse diffraction and a new reciprocity theorem. *J. Opt. Soc. America*, 58(12):1596–1603, 1968.

W. Snow. Basic Principles of Stereophonic Sound. *J. SMPTE*, 61(2):922–940, Mar. 1953.

S. Spors. Investigation of Spatial Aliasing Artifacts of Wave Field Synthesis in the Temporal Domain. In *Proceedings of the Annual German Conference on Acoustics (DAGA)*, Mar. 2008.

S. Spors. *Active Listening Room Compensation for Spatial Sound Reproduction Systems*. PhD Thesis, University of Erlangen-Nuremberg, Germany, 2007.

S. Spors and R. Rabenstein. Spatial Aliasing Artifacts Produced by Linear and Circular Loudspeaker Arrays Used for Wave Field Synthesis. In *120th Conv. Audio Eng. Soc.*, number 6711, Paris, France, May 2006.

S. Spors, A. Kuntz, and R. Rabenstein. Approach to Listening Room Compensation with Wave Field Synthesis. In *Proceedings Audio Engineering Society 24th Int. Conf. on Multichannel Audio*, Alberta, Canada, June 2003.

S. Spors, M. Renk, and R. Rabenstein. Limiting Effects of Active Room Compensation Using Wave Field Synthesis. In *118th Conv. Audio Eng. Soc.Effects of Active Room Compensation Using Wave Field*, number 6400, Barcelona, Spain, May 2005a.

S. Spors, D. Seuberth, and R. Rabenstein. Multi-Exciter Panel Compensation for Wave Field Synthesis. In *Proceedings of the Annual German Conference on Acoustics (DAGA)*, Mar. 2005b.

S. Spors, H. Buchner, R. Rabenstein, and W. Herbordt. Active Listening Room Compensation for Massive Multichannel Sound Reproduction Systems Using Wave-Domain Adaptive Filtering. *J. Acoust. Soc. Am.*, 122(1):354–369, July 2007.

S. Spors, R. Rabenstein, and J. Ahrens. The Theory of Wave Field Synthesis Revisited. In *124th Conv. Audio Eng. Soc.*, number 7358, Amsterdam, The Netherlands, May 2008.

E. Start. *Direct Sound Enhancement by Wave Field Synthesis*. PhD Thesis, Delft University of Technology, The Netherlands, 1997.

E. W. Start, V. G. Valstar, and D. de Vries. Application of Spatial Bandwidth Reduction in Wave Field Synthesis. In *98th Conv. Audio Eng. Soc.*, number 3972, Paris, France, Feb. 1995.

K. Steiglitz and L. E. McBride. A Technique for the Identification of Linear Systems. *IEEE Trans. Automat. Contr.*, 10(4):461–464, 1965.

H. Teutsch and W. Kellermann. Acoustic Source Detection and Localization Based on Wavefield Decomposition Using Circular Microphone Arrays. *J. Acoust. Soc. America*, 120(5):2724–2736, Nov. 2006.

G. Thiele, H. Wittek, and M. Reisinger. Potential Wavefield Synthesis Applications in the Multichannel Stereophonic World. In *Proceedings of the AES 24th Int. Conf. on Multichannel Audio*, Banff, Canada, June 2003.

S. P. Timoshenko and S. Woinowsky-Krieger. *Theory of Plates and Shells*. Mc Graw Hill, 2nd edition, 1959.

A. C. Ugural. *Stresses in Plates and Shells*. Mc Graw Hill, 2nd edition, 1999.

J. van Dorp. Wave Field Synthesis Using Multi Actuator Panel Loudspeakers: Design and Application of Various Digital Filtering Algorithms. Master's Thesis, Faculty of Applied Science, TU Delft, The Netherlands, 2005.

J. van Dorp and D. de Vries. Wave Field Synthesis Using Multi-Actuator Panel: Further Steps to Optimal Performance. In *Proceedings of the AES 28th Int. Conf. on Multichannel Audio*, Piteå, Sweeden, June 2006.

W. van Rooijen. Distributed Mode Loudspeakes for Wave Field Synthesis. Master's Thesis, Faculty of Applied Science, TU Delft, The Netherlands, 2001.

R. van Zon, E. Corteel, D. de Vries, and O. Warusfel. Multi-Actuator Panel (MAP) Loudspeakers: How to Compensate for Their Mutual Reflections? In *116th Conv. Audio Eng. Soc.*, number 6052, Berlin, Germany, May 2004.

J. Vanderkooy. Aspects of MLS Measuring Systems. *J. Audio Eng. Soc.*, 42(4):219–231, Apr. 1994.

E. Verheijen. *Sound Reproduction by Wave Field Synthesis*. PhD Thesis, Delft University of Technology, The Netherlands, 1997.

E. Verheijen, P. van Tol, and M. Boone. Evaluation of Loudspeaker Arrays for Wave Field Synthesis in Audio Reproduction. In *98th Conv. Audio Eng. Soc.*, number 3974, Paris, France, Feb. 1995.

P. Vogel. *Application of Wave Field Synthesis in Room Acoustics.* PhD Thesis, Delft University of Technology, The Netherlands, 1993.

E. G. Williams. *Fourier Acoustics. Sound Radiation and Nearfield Acoustic Holography.* Academic Press, 1999.

R. Wilson. Filter Topologies. *J. Audio Eng. Soc.*, 41(9):667–678, Sept. 1993.

H. Wittek. Perception of Spatially Synthesized Sound Fields, 2003.

H. Wittek. *Perceptual Differences between Wave Field Synthesis and Stereophony.* PhD Thesis, University of Surrey, United Kingdom, 2007.

S. Zhang, Y. Shen, X. Shen, and J. Zhou. Model Optimization of Distributed-Mode Loudspeaker Using Attached Masses. *J. Audio Eng. Soc.*, 54(4):295–305, Apr. 2006.

H. Zhu, R. Rajamani, J. Dudney, and K. Stelson. Active Noise Control Using a Distributed Mode Flat Panel Loudspeaker. *ISA Transactions*, 42(3):475–484, July 2003.

U. Zölzer. *Digital Audio Signal Processing.* John Wiley & Sons, 1997.